Investigation of Ultrasonically Powered Implantable Microdevices for Wireless Tissue Impedance Measurements

by

Dmitrijs Celinskis

A Thesis Presented in Partial Fulfillment
of the Requirements for the Degree
Master of Science

Approved November 2014 by the
Graduate Supervisory Committee:

Bruce Towe, Chair
Rosalind Sadleir
Bradley Greger

ARIZONA STATE UNIVERSITY

May 2015

ABSTRACT

Bioimpedance measurements have been long used for monitoring tissue ischemia and blood flow. This research employs implantable microelectronic devices to measure impedance chronically as a potential way to monitor the progress of peripheral vascular disease (PVD). Ultrasonically powered implantable microdevices previously developed for the purposes of neuroelectric vasodilation for therapeutic treatment of PVD were found to also allow a secondary function of tissue bioimpedance monitoring. Having no structural differences between devices used for neurostimulation and impedance measurements, there is a potential for double functionality and closed loop control of the neurostimulation performed by these types of microimplants. The proposed technique involves actuation of the implantable microdevices using a frequency-swept amplitude modulated continuous waveform ultrasound and remote monitoring of induced tissue current. The design has been investigated using simulations, *ex vivo* testing, and preliminary animal experiments. Obtained results have demonstrated the ability of ultrasonically powered neurostimulators to be sensitive to the impedance changes of tissue surrounding the device and wirelessly report impedance spectra. Present work suggests the potential feasibility of wireless tissue impedance measurements for PVD applications as a complement to neurostimulation.

DEDICATION

To my family, notably to my brother

ACKNOWLEDGMENTS

This Thesis would never have come into life without the continuous guidance and support from my mentor and supervisor Professor Bruce Towe.

I also would like to express gratitude to my committee members, Dr. Bradley Greger and Dr. Rosalind Sadleir, for their time and mentorship.

I would like to thank Daniel W. Gulick for many valuable discussions, advising, and both technical and moral support all the way along my Master studies.

Special gratitude must be addressed to my family. This work would not be possible without their support and patience.

TABLE OF CONTENTS

Page

LIST OF FIGURES

Figure Page

CHAPTER 1

INTRODUCTION

At the present state of technology, tissue electrical bioimpedance measurements are performed using wired systems by placing surface electrodes on the tissue of interest for current injection and voltage measurements. In case of conventional non-invasive bioimpedance measurements, the system is sensitive to the greatest extent to impedance changes occurring near the surface of the skin, whereas deeper tissues can be of the greater interest. From the practical point of view, presently available and clinically used bioimpedance measurement systems are bulky and are not meant to be used for chronic measurements outside the clinic by untrained users.

Present work entertains the idea of chronic, wireless impedance measurements by means of ultrasonically powered implantable neurostimulation devices. Whereas proposed microimplant's based approach is invasive by its nature, tissue damage and patient discomfort would be reduced to the minimum by device miniaturization and simplification of the implantation procedure. Injection is considered as one of the envisioned methods of implantation. The benefits of the investigated approach involve ability to measure impedance chronically at the point of interest, i.e. in the area of tissue exposed to the greatest physiological alternations and being of the greatest clinical relevance.

The devices of the type used in this work previously have been investigated only for neurostimulatory applications. One of the major applications envisioned for the proposed impedance measurement technique involves monitoring of tissue perfusion. Though, the more ambitious goal is to apply this technique for indirect monitoring of neural activity by measuring the transient resistance changes occurring during neural events. This relates to the idea of closed-loop functionality and bidirectional communication with the nervous system, allowing feedback control of device operation.

The most common way of performing neural stimulation is by using implantable battery-powered pacemaker-like devices. Recently, these types of devices have been equipped also with neural recording functionality. Still, despite the dramatic improvements of the quality of life

delivered to the patients suffering from such disorders as epilepsy or Parkinson's disease, this type of technology is associated with significant discomfort of the user. This discomfort is caused by the relatively big dimensions of commonly used devices surgically placed beneath the skin. Moreover, these devices require regular inductive recharging of the batteries, as well as recurrent surgery once every 3-5 years to replace the batteries.

In case of neural recording performed for research purposes or control of the prostheses, the state of the art technology involves placement of the tethered electrodes into nervous tissue with lead wires tunneled through the skin. This leads to even more severe limitations of this technology compared to the previously described implantable pacemaker-like devices. In this case, transcutaneous wires introduce significant risk of infection. Furthermore, tethering causes additional damage to the tissue, as well as degrades the quality of the neural recording over time.

Consequently, the notion of wireless power delivery and wireless communication gained increased interest in the recent years. A lot of work has been done in the attempt of developing wirelessly powered implantable neural devices serving either for monitoring or therapeutic purposes. Such novel types of devices can be characterized by a range of clinically relevant advantages over presently available technologies. These potential advantages include:

- reduced risk of infection as a consequence of elimination of the transcutaneous wires;
- reduced patient discomfort associated with tethering of the lead wires tunneled beneath the skin, increased patient mobility and overall quality of life;
- reduced injury and post-surgical recovery after implantation;
- simplified implantation procedure;
- reduced dimensions can allow more dense and chronic stimulation or recording from multiple sites;
- reduced degradation of performance over time and improved quality of recording or stimulation.

Wireless powering can involve utilization of electromagnetic waves, acoustic waves, and harvesting of body motion, thermal or chemical (blood glucose) energy. All these modalities will

be addressed in the review of background literature, but the key emphasis in the present work is on the power transfer by means of acoustical waves.

One of the potential applications for the investigated technique is related to the condition called Peripheral Vascular Disease (PVD). PVD is a serious healthcare burden caused by the atherosclerosis of the limb arterial circulation, accounting for about 3 billion dollars of healthcare expenditures and around 60,000 lower limb amputations each year in the United States alone [39]. This disease is severed by the increased danger of limb loss and pain [40-41]. During the progress of PVD tissue perfusion becomes decreased, causing tissues ischemia and hypoxia. In turn, previous studies have demonstrated high sensitivity of tissue bioimpedance measurements to ischemia and hypoxia [42-43],[45-47],[50-51], making it a potential indicator of tissue condition, treatment efficacy, and stage of the disease.

Although, results of the studies demonstrating impedance sensitivity to tissue perfusion are widely available, any attempts to use impedance measurement technique for monitoring of tissue perfusion with PVD have not been reported, adding extra value to present study. Furthermore, investigated technique has one more highly significant advantage, which follows from the fact that devices of the same type as used in the present work are capable of inducing vasodilation and increasing tissue perfusion [2]. This in turn can be used as a treatment of PVD. Consequently, the ultimate medical solution envisioned in this work involves closed-loop system capable of both treatment and monitoring of PVD. The envisioned idea and principle of work are summarized on Fig. 1.

Taking into consideration all said above, the main goal of the present work was to investigate the possibility of wireless impedance measurements using ultrasonically powered microdevices. This question is addressed by means of the simulations, benchtop testing and animal experiments, involving the assessment of the ability of system to provide spectral characterization of the samples and differentiation between tested samples. This study is a first step in assessment of the applicability and feasibility of proposed technique, forming a bridge to the ultimate goal of development of the multi-functional wireless microdevices.

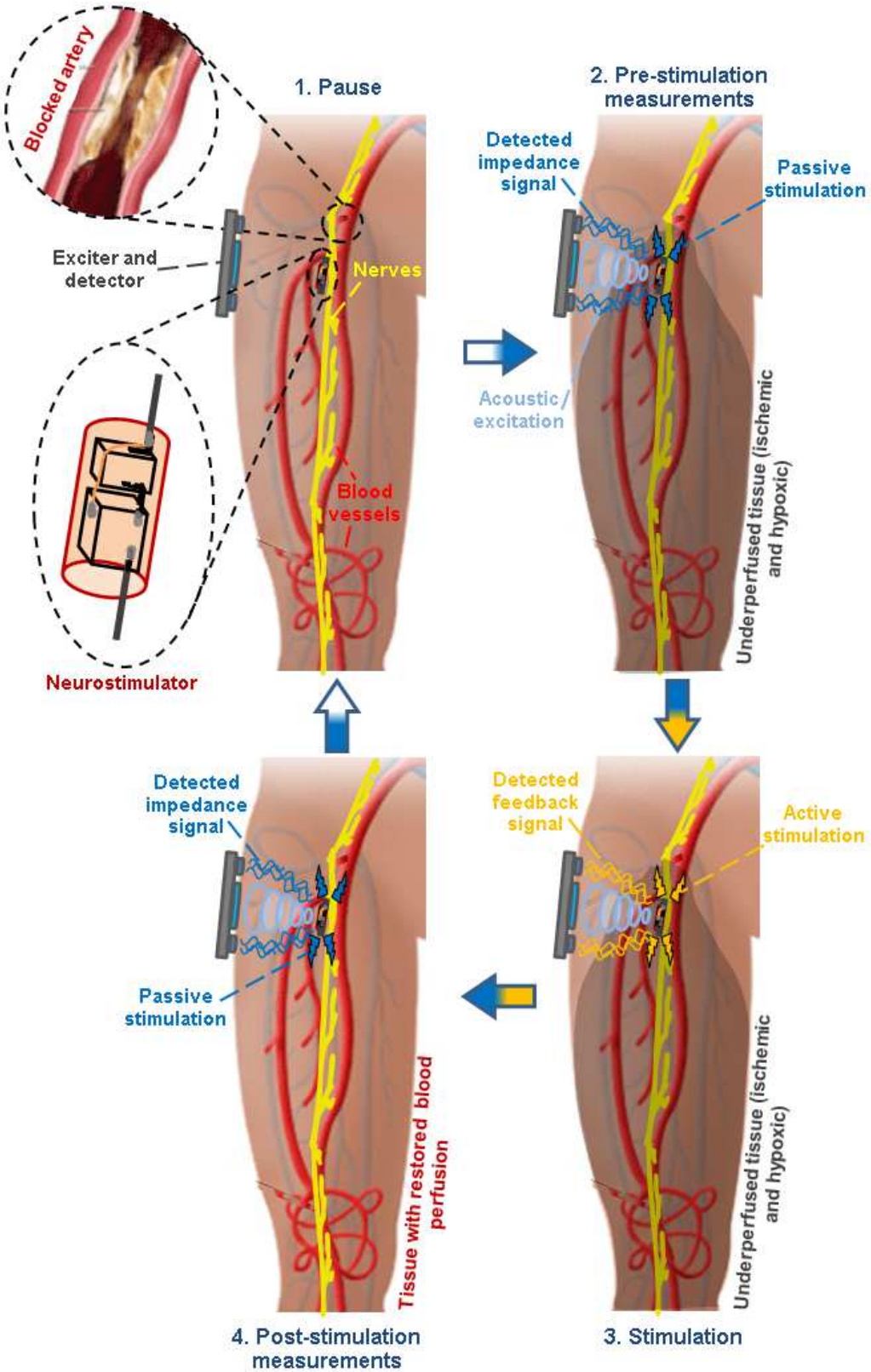

Fig. 1. Illustration of the overall idea behind envisioned application of wireless microdevices for monitoring of tissue ischemia.

CHAPTER 2

BACKGROUND AND LITERATURE REVIEW

Implantable microdevices

From [10-11], [13], [17-19] it is possible to identify some common most desirable characteristics of implantable devices: small sizes (10-100 μm), significantly reduced or eliminated risk of infection, no degradation of performance over time, elimination of tethering, high density, simple implantation, no limitations for mobility of the patient. To meet these requirements microscale implants must be characterized by low power consumption. In order to successfully address all these requirements, conventional powering using transcutaneous wires or bulky pacemaker batteries with restricted lifespan cannot be used. Wirelessly powered passive devices investigated in the present work can be considered as the potential solution addressing these needs.

Wireless power transfer

Wireless powering and communication plays a major role in the process of further advancement of the existing implantable technologies. Wireless, passive and implantable microelectronic devices of millimeter and sub-millimeter size can be realized and a number of different approaches have been proposed. These include wireless powering by light, microwaves, epidermically applied high frequency currents, or ultrasound [1-27], [29-32]. The smallest of these can pass through a syringe needle, so minimizing trauma of insertion. Alternatively, some work has been done on the energy harvesting from the host organism itself [19],[33-34]. Examples of such systems include piezoelectric energy harvesting of internal tissue motion, thermoelectricity based batteries and glucose bio-fuel batteries utilizing glucose from the blood. The general review of the majority of environmental and human energy harvesting techniques is given in [18-19]. In turn, the review of the wireless powering paradigms is given in [20] and [21].

Methodologically four main types of wireless energy transfer can be identified, proposed to be applicable for medical implantable devices: optical powering, volume conducted high frequency currents, acoustic powering, and radiofrequency (RF) or microwave powering.

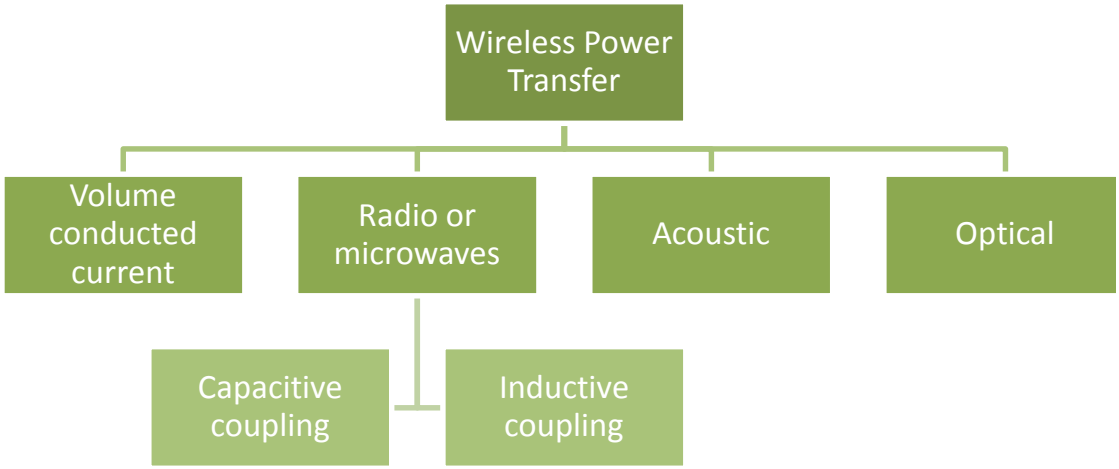

Fig. 2. Wireless power transfer modalities.

Radio and microwave powering can be sub-divided into power transfer trough capacitive and inductive coupling (Fig. 2).

Optically powered microdevices can be made utilizing near-infrared (NIR) spectrum light for wireless power transfer. The choice of this part of the spectrum follows from relatively low absorption and scattering of the NIR light by tissue. Effective light conversion into electric currents can be achieved by employing semiconductors. In [29] authors have reported the ability to produce muscle activation via stimulation of the rat's spinal cord gray matter using floating light-activated microelectrical stimulators (FLAMES). The smallest tested device had the size of 140 μm x 500 μm and thickness of about 100 μm. The device was implanted approximately 2.35 mm below the dorsal pial surface into rat's spinal cord. The largest forces produced by rat's upper limb were around 1.08 N. Despite lower attenuation of NIR light by tissue compared to visible light, in their latter work [30] authors demonstrated that the intensity was reduced to 1.85% of the subdural intensity after passing through 1 mm of tissue and to 0.15% at 2 mm. In addition to the low penetration depth, this technique is associated with significant temperature increase near the surface where the photons enter the tissue.

Utilization of the epidermically applied *volume conducted high frequency currents* has not received much support due to the concerns associated with direct tissue exposure to electrical currents, and apparent problems associated with achieving sufficient power density at the target

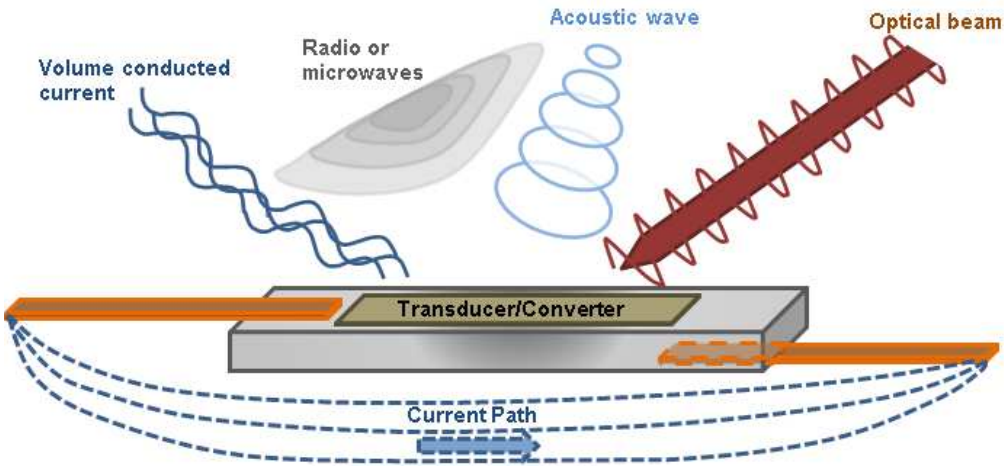

Fig. 3. Illustration of wireless microdevice with different modalities of wireless energy delivery.

area of tissue, as well as difficulties with ensuring multi-channel operation. This technique relies on the utilization of the innocuous high frequency currents conductively supplied to the tissue to power up the implants and produce low frequency currents [32].

Capacitive coupling is the form of electromagnetic powering used for energy and data telemetry (purely electric near field coupling) [19], [26]. In its basic form, described in [26], approach is based on two parallel aligned plates that behave as capacitor. Capacitive link ensures information or energy transfer via electrical fields through the skin, which acts as a dielectric media between two capacitive plates. This approach is characterized by a good confinement of the electromagnetic flux, but very restricted powering distance. In [26] the radio frequency (up to 18 MHz) range waves were used to analyze the powering efficiency through 1 mm of tissue. Authors demonstrated that by using 25 mm x 25 mm plates it is possible to induce wirelessly up to 2 V DC voltage. Methodologically different approach involving capacitive powering was proposed in [3]. Instead of the capacitor's plates-like antennas, proposed devices were made in the form of small dipoles with a length of about 1 cm and 800 μm or less in diameter, activated using sub-GHz frequencies. Dipole-like devices are capacitively coupled to a body surface dipole antenna through electric fields. The implant incorporates low-threshold Schottky diode to produce rectification of the high-frequency radiowave and turn it into high-frequency pulsating DC applicable for neural stimulation. The ability to cause motor response in rat was demonstrated with external antenna located as far as 7 cm away in the air.

Inductive power transfer (purely magnetic near field coupling) [13], [16-19], [27], [31], [35]. This is the simplest powering scheme employing two mutually-coupled coils: radio frequency electromagnetic field is carried from the external source coil to the receiving coil on the implant side (in most studies frequencies below 20 MHz are utilized). The key difference from the capacitive coupling is that inductive powering depends primarily on the magnetic field component of the EM wave and not as much on the electric component. Since tissue loss is negligible at low frequencies, the power transfer efficiency depends only on the properties of coils - the sizes and the distance between them (this distance is typically restricted to the near field of the source being equal or less than the wavelength). The closer and bigger is receiver coil, the greater is power transfer efficiency. This powering modality for long time has been considered as the most promising and effective one, until recently more miniscule devices became highly desirable. One of the reasons for wide-spread of this technique is the fact that involved magnetic fields do not interact with biological matter, although induced Eddy currents still can have heating effects.

Furthermore, tissue absorption increases with frequency, resulting in exponential decay of the electromagnetic fields inside tissue. This observation led to the conclusion that low MHz-range is most optimally suited for electromagnetic powering. Cochlear implants can be mentioned as the most common system utilizing this powering modality [35]. In the recent years, low GHz-range electromagnetic wave powering became the target for intensive investigations [22-25]. The important conclusion was made suggesting that for the sub-millimeter size devices the optimal frequency is about 2 orders of magnitude higher than the commonly used range of low-MHz frequencies. The optimal frequency was concluded to be in the GHz-range when the dimensions of the transmit antenna are much smaller than a wavelength. Simulations performed in [25] demonstrated that transition to high frequencies can allow reduction in the dimensions of the receiver by 100 times, while maintaining the same power transfer efficiency. Besides that, authors highlight reduced displacement and orientation sensitivity with high frequency powering mode. In [25] the technique called midfield wireless powering was proposed, which employs electromagnetic induction coupling without exponential decay. The key difference realized in this technique lies in the design of external coil. Instead of the usual coil of wire, they used a

patterned metal plate with 4 ports. This plate is driven by much higher power than conventional inductive powering wire coils, but 4 port antenna design allows cancellation of the side lobes of the electromagnetic waves in tissue, allowing only central portion of the beam to reach the implant. This can be considered as a form of electromagnetic focusing, producing higher power density in the area of interest and reduced amount of power dissipated in the tissue. This helps to maintain delivered radiation levels within the FDA limits. Additional benefit of this technique relates to the ability of beam steering by controlling the powering of the excitation coil. At this point, 2 mm big pacemaker device with 6 mm by 6 mm external excitation coil was tested in the rabbits, demonstrating 0.1 percent power transfer efficiency, which is sufficient for typical pacemaker applications.

The idea of *acoustic powering* received a lot of attention in the last decade [1-2], [4], [6], [10-13], [15]. In the past this technique was overlooked due to the fact that electromagnetic powering demonstrates more superior performance for short range powering using big aperture antennas. Only upon scaling of the implantable devices down to sub-millimeter sizes the high potential of acoustic power transfer became evident. This approach relies on energy transmission between two piezoelectric transducers through acoustically coupling medium. Piezoelectric materials can convert ultrasound to electric power at efficiencies on the order of 10% under good conditions. The benefits of ultrasonic powering lies in the fact that the speed of acoustic waves in tissue (in soft tissues on average 1540 m/s) is much smaller than speed of electromagnetic waves ($3x10^8$ m/s), allowing the utilization of ultrasound waves with much lower frequencies. Additionally, acoustic waves can be easily focused, reducing the amount of dissipated power and increasing the energy density delivered to the specific spot in the tissue. This potentially allows separate activation of the multiple implants through beamforming techniques [12], which is important for multichannel functionality. The benefits of the ultrasound are manifested by the fact that FDA defined limit for the spatial-peak temporal-average intensity (I_{SPTA}) of the ultrasound is 72 times greater (720 mW/cm^2) [36-37] than approved limit for electromagnetic waves (10 mW/cm^2) [10]. Finally, tissue attenuation of the ultrasound is significantly lower than attenuation of the high frequency EM waves. Path losses of ultrasound as it passes through tissue vary

depending on the frequency and the tissue type, but typical losses might be on the order of 1-5 dB/cm. For instance, as was shown in [10], by passing through 2 mm of brain tissue, the attenuation of 10 MHz ultrasound waves is on the order of 1 dB, whereas for 10 GHz electromagnetic waves it is on the order of 20 dB.

Ultrasound energy at medical diagnostic frequencies in the range of 1-10 MHz is strongly attenuated by air and bone, and thus, like ultrasound imaging, is limited to the specific parts of the body. Lower frequencies in the range of 500 kHz - 1MHz are generally more suited to powering implanted devices where bones may interfere such as the skull. The tradeoff is that lower sound frequencies carry a lower energy density and they cannot be focused to the implant location as finely as higher frequencies.

In the literature only two actual attempts of building acoustically powered implantable microdevices could be identified. The first one dates to 2003 [1] when utilization of the ultrasound powering for implantable devices was proposed and later demonstrated direct conversion of ultrasound energy to neurostimulation pulses. Since then, only recently in 2013 the team from UC Berkeley proposed so called “neural dust” system. This idea attracted a lot of attention due to the huge interest and clinical need for proposed wireless 100 μm neural devices capable of fully chronic and highly dense recordings. The key problem associated with this proposal is the fact that this idea still resides at the modelling stage and only results of the unsuccessful attempts of acoustic data transfer were recently presented in 2014 [11]. Still, this modality of wireless powering exhibits a lot of promise for neural applications.

Electrical bioimpedance measurements

Wirelessly powered implantable microdevices are most commonly considered only for neurostimulation and neural recording applications. Present work entertains the idea of the new potential application for wirelessly powered implants – electrical impedance measurements. Therefore, a brief review of the electrical bioimpedance measurement principles and applications is provided.

The simplest way how tissue electrical impedance can be measured relies on utilization of two surface electrodes serving for both constant current injection and voltage measurements. Alternatively, constant voltage can be applied to the tissue and resulting currents measured for impedance estimation, but this alternative is not supported due to the safety concerns associated with application of the currents of not constant magnitude. The bipolar measurement technique is especially sensitive to the changes in electrode-tissue interface, making so called tetrapolar impedance measurement technique more appropriate. This technique involves utilization of two pairs of electrodes for current injection and voltage measurements. In reported work on impedance measurements [42-52] applied subthreshold current is in the range of 10-500 microamperes, but typical value is considered to be 1 mA/cm^2. This range is so broad due to the fact that the majority of applications involve current application through the skin associated with the skin resistance as high as hundreds of kOhms (depending on humidity, cleanliness, etc.) and thus requiring much higher currents, whereas applications involving electrode placement directly to the exposed tissues require smaller currents.

Effective tissue characterization typically requires multiple frequency impedance measurements (impedance spectroscopy), which allows differentiation between different tissue types and conditions based on the impedance spectra. Impedance spectra are known to have four dispersions associated with contributions of the certain tissue forming elements (e.g. α dispersion in frequency range below ~100 Hz is considered to be contributed by nucleic acids, surface charged vesicles, cell tubular system, surface charge and membrane relaxation) [50-51]. Single frequency measurements have also been used, but they allow only monitoring of the trends of impedance changes and not the estimation of absolute impedance values. This is due to the fact that a large number of variables can affect the single frequency tissue impedance.

The most successful applications of tissue bioimpedance measurements are impedance cardiography and body composition analysis [48], but many other physiologic parameters and conditions have been under investigation [52]:

- non-invasive blood glucose level estimation [28];
- blood flow (e.g. impedance plethysmography, impedance phlebography);

- eye movements;
- muscular contractions;
- vascular impairments (e.g. estimation of the pulse transit time by means of the impedance and ECG measurements as an indicator of the condition of vascular system [55]);
- body fluid shifts (pulmonary oedema or intrathoracic fluid, blood volume changes);
- respiratory function;
- cancer (especially breast and skin cancers) [49];
- cerebral monitoring (attempts are made to detect epilepsy onset or determine significance of stroke damage [44], as well as to monitor neural activity non-invasively through measurements of resistance changes during neuronal depolarization in the brain [56-57]);
- guidance of the physical intervention (impedance measurements were proposed for needle guidance by determining what type of tissue needle is passing through) [54];
- tissue ischemia and hypoxia (this includes tissue ischemia and hypoxia assessment in the various parts of the body from the brain to the heart) [42-43], [46-47], [50-51];
- neurostimulation (study was done trying to utilize impedance measurements to determine current threshold required for stimulation) [53].

It is important to highlight that the key problem of impedance measurements is associated with non-specificity of impedance variations, i.e. different causes can produce absolutely the same impedance changes (e.g. temperature changes, changes in electrode contact or polarization). This fact significantly limits the ability of impedance measurements to give quantitative repeatable results and clinical applicability of this technique.

Tissue ischemia monitoring

Following the previous studies done in our lab, one potential application for impedance measurement technique investigated in the present work is peripheral vascular disease (PVD). This condition involves reduction in tissue perfusion. For the purpose of this work tissue ischemia monitoring techniques are reviewed.

Ischemia is condition of reduced oxygen (hypoxia) and nutrient supply to the tissue due to the constriction or obstruction of blood vessels. Tissue hypoxia is directly related to ischemia in the way that ischemia always results in hypoxia, but hypoxia can be present also in the case of fully functional cardiovascular system due to the problems with pulmonary system.

The review of the available tissue ischemia monitoring techniques is given in [51]. Some examples of these techniques are laser Doppler, pH measurements, angioscopy, MRI diffusion mapping and ankle-brachial index estimation. In [50] and [51] authors reviewed the characteristics of ideal ischemia monitor. The best fulfillment of these requirements demonstrated pH measurements based technique. In [50] and [51] the correlation between impedance and pH measurements was investigated, and correlation was demonstrated to be as high as 0.93. This result highlights high feasibility of impedance technique for ischemia monitoring.

Several researchers have demonstrated apparent impedance correlation to ischemia and hypoxia. The only difficulty with interpretation of these observations lies in the fact that different studies involve different system setups and parameters, leading to different results. More importantly, none of these measurements involved electrodes similar to the ones used within present work, making the comparison of the tissue impedance values difficult.

In [43] evolution of the transencephalic cerebral resistance was demonstrated in seven asphyxiated piglets at 50 kHz using four silver rod rough surface electrodes of 2.5 mm diameter drilled into skull. The resulting impedance magnitude change after 50 minutes of hypoxia was as high as 120 percent with the mean resistance value of 56.2 Ω. In [46] the needle-type impedance and pH sensor was designed to measure impedance in rat kidney at 1 kHz during the occlusion period of 60 min. During whole period of occlusion impedance was gradually increasing and resulting change was again as high as 120 percent, but the baseline impedance in this case was

on the order of 1500 Ω. In [50] authors performed correlative study involving pH and impedance measurements. This study involved 29 rabbits, whose leg perfusion was controlled by a vascular occluder, placed over a femoral artery and vein. Impedance measurements were done using needle electrodes and spectra were recorded at 27 frequencies, allowing estimation of the various impedance related parameters. One of the estimated parameters was instantaneous resistivity at zero frequency (R_o), which in the typical experiment after 108 min long occlusion changed by about 16%. This is the only reported case when observed changes were so small, but in contrast to previous cases, R_o was estimated, not measured, and its mean value was determined to be around 60 Ω. The important conclusion of this work was that ischemia can be detected even more accurately using tissue impedance measurements than by measuring pH. In [51] Songer et al. demonstrated direct correlation of tissue pH measured invasively with impedance measured externally using disposable wet gel ECG electrodes (the selection of the electrodes was supported by their low noise level ≤5% in the frequency range of interest between 1 kHz and 100 kHz). These data were obtained from 15 bloodless human surgeries of the lower limbs. Again, estimated baseline average R_o was shown to be around 60 Ω, and although authors have not produced excessive ischemia cases themselves, literature survey performed by the authors indicated that ischemia causes the resistivity of the muscle tissue to increase by as much as 30% almost immediately after the onset of ischemia.

The cellular changes underlying discussed increase trends were concluded to involve the shifts of fluid volume within tissue from extracellular to intracellular space. Cell membranes act as capacitors, meaning that low frequency currents are dependent only on extracellular current pathways. Cell swelling leads to the narrowing of the extracellular conducting pathways and consequent increase in low frequency electrical impedance [51].

Background work

An extensive work has been done in our lab exploring applicability of acoustically powered devices for neural stimulation [1-2], [4], [6], [8]. Additionally, as it has been discussed before, microwave powered devices have also been proposed by our lab [3], [5], [7] with potential

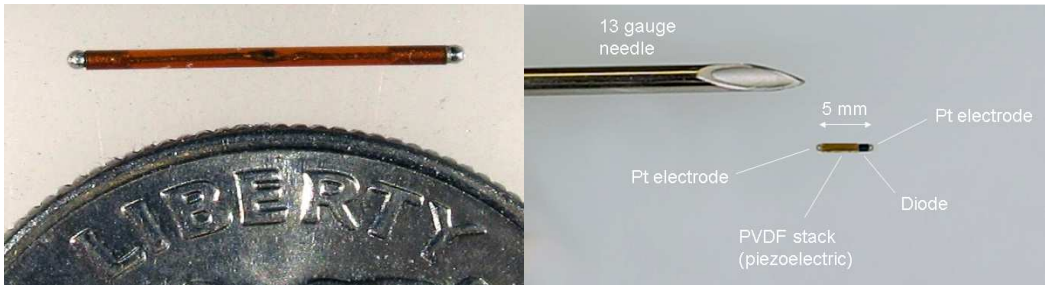

Fig. 4. Microwave powered dipole devices [3].

applications both in neural recording and stimulation. Still, as it was demonstrated previously, microwave and acoustic powering involve different advantages and disadvantages (e.g., ultrasound is greater attenuated by bone, but microwaves by soft tissues), and final conclusions about applicability of one technique over another for specific applications are still to be formulated.

For the purposes of neurostimulation both types of devices have demonstrated the ability to produce currents on the milliampere order:

- *acoustically powered device* made of PZT-5A, with a 1.3 mm diameter and about 10 mm length was shown as capable of producing milliampere order currents in Sprague-Dawley rat. Device was placed next to the sciatic nerve about 10 mm deep in the tissue and it was actuated using average ultrasound power levels between 10 mW/cm^2 and 100 mW/cm^2 [2]. Used power level was significantly lower than FDA approved safety limit (average power limit is 720 mW/cm^2), suggesting possibility of further scaling down of the device dimensions by utilizing higher power levels;
- *microwave powered device* with dimensions on the order of 0.8 mm in diameter and 1.5 cm length driven at 915 MHz demonstrated the capability to produce milliampere-order currents at 7 cm tissue depths when pulsed at 10 W peak power [3].

From these results it can be seen that both powering modalities allow achieving sufficient current levels for impedance measurements. Still, there is a number of considerations related to these two powering modalities, which have led to our favoring of the acoustically powered devices. One of the advantages of microwave powering is absence of requirement for physical coupling of antenna with tissue. The second advantage is a much weaker directional sensitivity,

which to certain extent is present in all powering modalities. If we consider the actual way how microwave powered system would be used, it seems attractive to have an ability to perform patient treatment without being required to maintain a stable physical coupling with the patient. Still, if these devices are expected to be used chronically then we would need to mount the excitation antenna with all supporting circuitry to the body of the patient anyway. This consideration minimizes all potential gains from the first advantage of microwave powered devices. Moreover, there is a set of disadvantages associated with devices relying on microwave energy transfer:

- the safety concerns associated with tissue exposure to electromagnetic waves (the main of which usually relates to the heating effects) are much greater than for the acoustic waves. As it was mentioned earlier, the power density limit for the microwaves is 10 mW/cm^2, whereas for ultrasound it is 720 mW/cm^2;
- another observed issue was related to the interference of the powering signal with surrounding telecommunication systems, particularly commonly used wireless communication channel of 2.45 GHz (although in our devices 915 MHz frequency was used, wireless routers were still able to pick up test signals due to the imperfections in their construction);
- at this point it seems to be much more difficult to achieve effective multichannel operation of microwave powered devices. The most straightforward approach would be tuning of the devices to certain frequency, which in reality is significantly complicated by the damping of the Q of the devices by the tissue. In case of acoustic powering, fine focusing capabilities potentially allow to utilize beamsteering to activate devices separately;
- presently, the lowest achievable dimensions of microwave powered devices seem to be on the higher end than for the ultrasonically powered devices. The energy transfer efficacy is higher at wavelengths comparable to device dimensions, favoring the much shorter ultrasound wavelengths in tissue. This also relates to the additional benefit of ultrasound involving much more effective focusing capabilities;

— battery drain for the powering of external exciter was observed to be much greater in case of the microwave system, which can become a serious problem in continuous everyday applications.

All these considerations switched the focus of the present work to ultrasonically powered devices. Although, in theory the same technique investigated in this work potentially can be realized using microwave powered devices.

One of the potential applications of wirelessly powered devices was reported by our lab in [2]. It was shown that these types of devices are able to produce modulation of the blood flow at sub-motor activation current levels applied to the rat's sciatic nerve of the lower limb. In [2] two trials were made right after the implantation and two weeks after the implantation, resulting in 25.1% and 13.8% changes in perfusion, respectively. These changes can be even greater in case of longer stimulation, as well as in cases of diseased subjects. These observations allowed authors to conclude the feasibility of acoustically powered devices for treatment of peripheral vascular disease.

Preceding work formed the basis for potential application of the presently investigated technique of wireless impedance measurements for monitoring of the peripheral vascular disease, as well as potential feedback control of the neurostimulatory treatment of this condition. The idea of dual functionality and feedback control seems to be feasible due to the fact that there are no structural differences between microdevices used for neurostimulation and impedance measurements. The only difference is associated with device actuation, output signal measurements and analysis.

In this work we find that a variant of our previously reported ultrasound powered neurostimulator allows, with appropriate supporting external circuitry, the measurement of the magnitude and phase of impedances. This approach involves microdevice actuation with baseband frequency swept AM carrier ultrasound and consequent generation of demodulated current proportional to tissue impedance. Volume conduction is then used for signal detection and extraction of impedance information.

CHAPTER 3

METHODS AND MATERIALS

Construction of acoustically powered microdevices

Photographs of some of the devices built in the process of this work are shown on Fig. 5. Fig. 6 shows the basic assembly of components in three different structures considered within present work. Implantable neurostimulators were constructed using Magni-Focuser (power of 3.50 X; Edroy Products Co., Inc) to assemble the electronic components, and then inserted and encapsulated in polyimide tubing. Tubing was filled with the medical grade epoxy (353ND, Epoxy Technology). In all cases device contained piezoelectric element PZT-5A and two wire-type platinum iridium (PtIr) electrodes. All interconnections of the components were made using conductive silver epoxy. For the longer distances golden wires were used. For the purposes of rectification and demodulation of the electrical current produced by piezoelectric element, three different types of rectifiers were used:

- the Schottky diode (e.g., CDC7630, Skyworks Solutions, Inc.). It has a low threshold voltage and a small SC-79 package;
- the full bridge rectifier diode (e.g., Bridge Quad HSMS-2818-TRIG; forward threshold voltage of 410 mV and reverse breakdown voltage of 20 V; dimensions 3 mm x 1 mm x 2.5 mm). It can be characterized by a higher threshold voltage caused by the fact that it incorporates four diodes (in contrast to one in the previous case), which are interconnected in a bridge circuit configuration. The idea is that such arrangement provides the same polarity of output for either polarity of input (performs full-wave rectification). Consequently, as this configuration incorporates four diodes it is associated

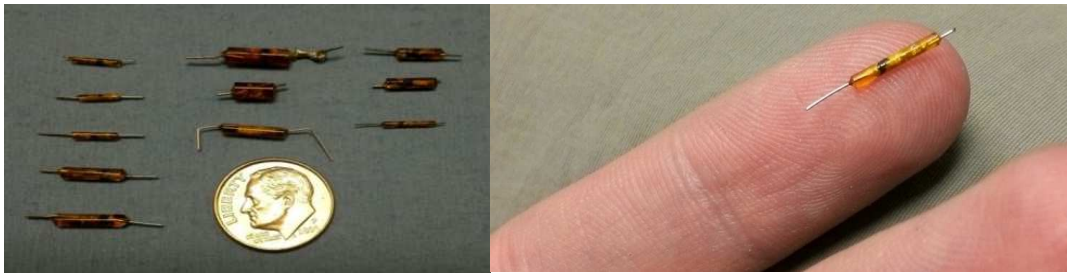

Fig. 5. Photographs of the acoustically powered microdevices.

with the greatest dimensions;

- the variable capacitance (i.e., varactor or varicap) diode (e.g., 5mV 1240-074LTF, Skyworks Solutions, Inc.; capacitance of 54.6 pF). The capacitance of this diode varies as a function of the voltage applied across its terminals. The type of the varactor used within present work incorporates two diodes connected back-to-back, providing it the medium dimensions between two previous types of rectifiers.

The reasoning behind considering these types of rectifiers, as well as an overview of performance of the devices incorporating these configurations, is provided within the results and discussion sections on system characterization.

Some details regarding construction and operation of the Schottky diode based devices are available in [1-2], [4] and [6].

It is important to emphasize that devices constructed and used within present work are bigger than potentially achievable device dimensions. This is related to the fact that the goal of this work does not involve development of the final optimal clinically applicable system. Instead, present work is focused on proving and demonstrating the ability of proposed technique to detect impedance changes. All further system sophistication and optimization is the aim for future work. Within the framework of this work, the smallest constructed device was 6.35 mm in length (plus the length of the electrodes 2.50 mm) and 1.14 mm in diameter. The smallest PZT-5A crystal tested within this work had the dimensions of 350 μm x 300 μm x 127 μm, which in case of being driven by continuous waveform with acoustic power density around 190 mW/cm^2

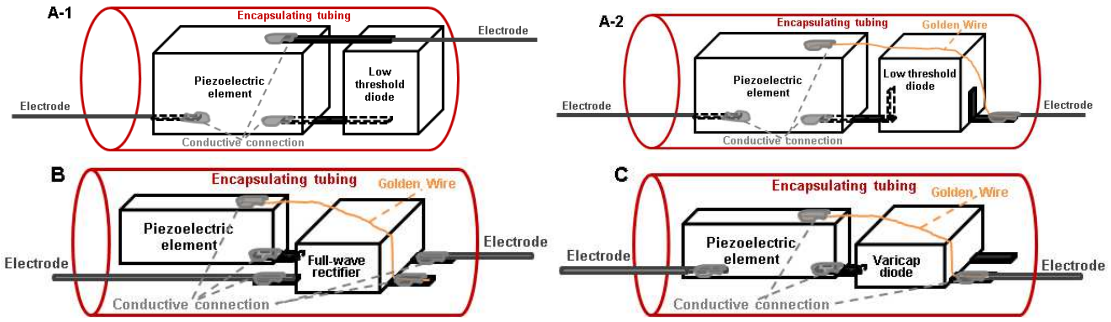

Fig. 6. Schematics of microdevices. A-1 and A-2 – variations of the single diode based device, B – full-wave rectifier based device, C – varicap diode based device.

generated voltages on the order of 110 mV (details of these measurements are not further discussed within this work).

Principle behind wireless impedance measurements

The main idea behind the proposed impedance measurement technique investigated within present work is summarized on Figure 7A. Full sequence of the physical processes involved in the measurement procedure can be divided into six main steps:

1. Conversion of the externally supplied amplified amplitude modulated (AM) electrical driving signal (carrier) into ultrasound waves using piezoelectric transducer. Ideally, generated acoustic waves have equivalent waveform and spectral characteristics to those of the electrical driving signal.
2. Ultrasound propagation through the tissue and coupling with an implant.
3. Conversion of the acoustic waves back into electrical current.
4. Rectification and demodulation of the current by the rectifier.
5. Volume conduction of rectified currents through the tissue. The magnitude and phase characteristics of the current depend on tissue impedance. Additionally, the sensitivity of the device is greatest in the areas of the highest current density, i.e., in the proximity to the device. Volume of the highest sensitivity can be estimated using principles discussed in [52].
6. Detection of volume conducted current, and extraction of the magnitude and phase characteristics of the baseband signal component.

Additionally, Fig. 7B describes the principle of neural stimulation realized using the same type of device. The key difference between impedance measurements and neural stimulation lies within the differences of the waveforms used for driving an ultrasound exciter. In the case of impedance measurements, this signal is continuous, but in the case of neural stimulation the train of pulses is used. Pulse excitation allows boosting of the spatial peak of acoustic power, which results in the consequent increase of the generated stimulatory current. Such optimization is important due to the existing regulatory limits restricting the acoustic power levels

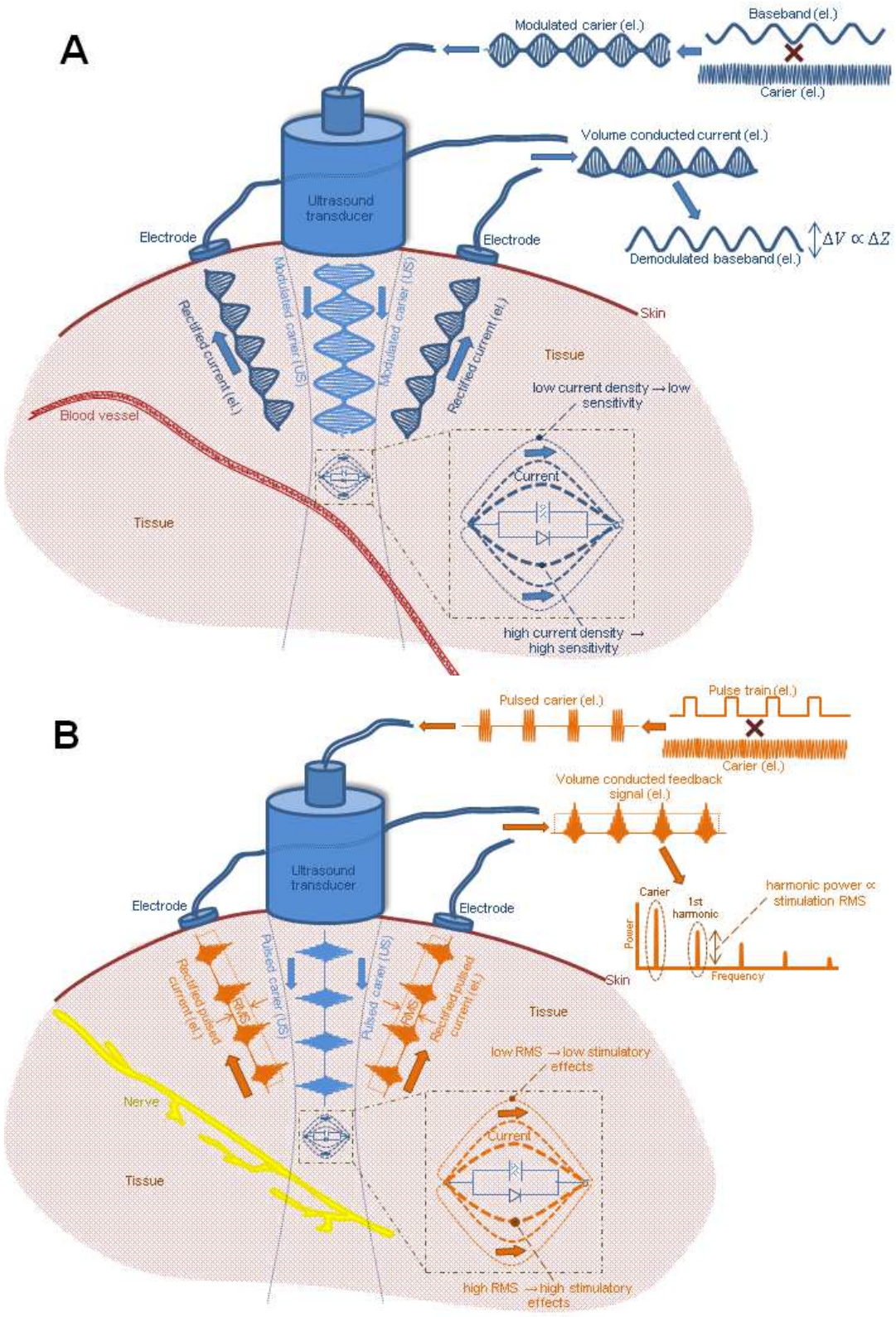

Fig. 7. Schematic of the principle of wireless impedance measurement technique and neural stimulation using acoustically powered devices. (A) Impedance measurement principle, (B) neural stimulation principle. Acoustic signals are marked as “US”, electrical signals as “el.”

dissipated in the tissue and consequently limiting the maximal achievable current. Overall, this form of powering leads to the increased ability of the system in reaching neural stimulation threshold, which depends on variety of factors, such as tissue and output port impedance of the device, and device position relative to the targeted nerve (e.g., extrafascicular vs. intrafascicular stimulation).

Additional difference between microimplant's based wireless stimulation and impedance recording lies within the role of rectifier. In case of neural stimulation, the role of the rectifier involves rectification of the high frequency carrier. This is due to the observation made in our lab that nerves do not respond to the high frequency (in our case low-MHz range) alternating currents, but instead they respond to the RMS value of rectified monophasic applied stimulus. Consequently, the rectifier converts biphasic signal with RMS = 0 into semi or fully rectified signal with much higher RMS. In turn, in the case of impedance measurements, the stimulatory effects are highly undesirable, but rectifier still plays an important role in signal demodulation, i.e., separation of the baseband signal from the carrier. This baseband signal is required for tissue interrogation because it lies within the low-kHz frequency range, which corresponds to α and β electrical dispersions of biological matter. Without demodulator, tissue would be interrogated only by the high frequency carrier and not by the baseband signal. The principles of rectification and demodulation will be discussed to the greater extent in the following section on device characterization.

Fig. 7 also introduces the idea of utilization of the surface electrodes used for feedback control of neural stimulation and for impedance measurements. In [8-9] authors introduced the idea of localization of implanted piezoelectric crystals by measuring the electrical potentials using surface electrodes. This proposal involved utilization of the volume conducted fields for estimation of the currents generated by the implant. In the ultimate clinical application, current control would be very critical because we cannot rely on the "blind" stimulation, having only physiological response as a form of feedback. Proposed approach of current estimation relies on the extraction of carrier harmonics from the detected volume conducted currents. As it will be discussed later, harmonic generation is an intrinsic quality of the rectifiers, which potentially can be useful for

separation of the signal produced by the device from initial excitation signals. Initially the idea of this form of current control was introduced for microwave powered devices and was demonstrated to be feasible through benchtop experiments, but it can become useful also for the applications involving ultrasound devices.

System structure and experimental setup

The basic structure of the system used to perform the majority of experiments within this work is shown on Fig. 8A. Specific system components used to execute the experiments are shown on Fig. 8B. In majority of experiments, the setup contained a baseband signal generator (Stanford Research Systems DS345 30 MHz), carrier signal generator (Philips PM5138), driver amplifier (OPHIR GRF 3032), ultrasound transducer (varied for different experiments, both

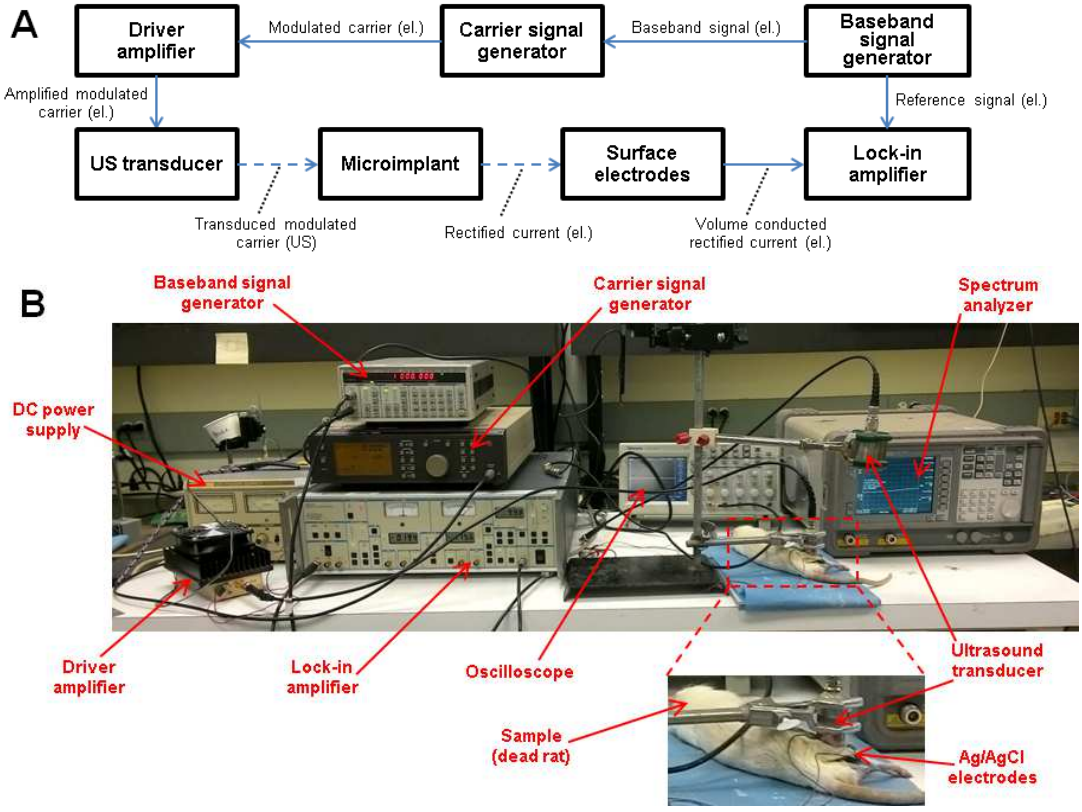

Fig. 8. Block diagram of the impedance measurement system (A) and photograph of the system setup (B). In (A) solid arrows denote wired connections, but dashed arrows – wireless coupling through the tissue (acoustical (US) or electrical (el.) coupling).

commercial and self-made transducers were used; an example of the structure of self-made transducer is shown on Fig. 9), sample under investigation, acoustically powered microimplant, surface electrodes (Ag/AgCl) and lock-in amplifier (Stanford Research Systems SR530). Additionally, on the Fig. 8B spectrum analyzer (Hewlett Packard ESA-L1500A 9kHz-1.5GHz) and the oscilloscope (Tektronix TDS 2024 200 MHz) are shown, which were used for the characterization of system performance, but are not the essential components of the measurement system.

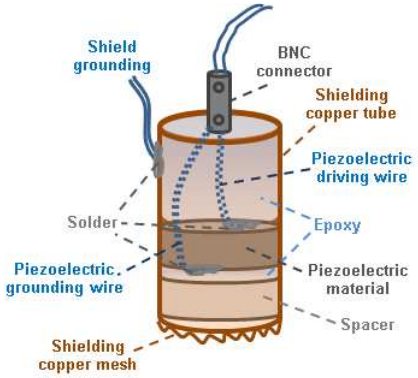

Fig. 9. Structure of the custom-made unfocused shielded and grounded ultrasound transducer.

Carrier signal generator provides a high frequency sinusoidal signal (in the frequency range from 0.5 MHz – 2 MHz, which depends on the resonance frequencies of the ultrasound exciter and receiver), required to power ultrasound transducer. Baseband signal generator outputs a low frequency (in the range of 10 Hz up to 100 kHz) sinusoidal baseband signal. This low frequency signal is used to amplitude modulate (AM) the high frequency carrier, which then through the amplifier is applied to the transducer. Amplification is required in order to achieve sufficiently high acoustic power output from the ultrasound exciter. For impedance measurements typical voltages used to power ultrasound transducers were in the range of 30-60 V. Control of this voltage allows control of the current output from the implant, and in addition to the control over other waveform parameters, this essentially allows us to switch between stimulation and impedance measurement modes of operation of the microdevice. By changing powering parameters different stimulation regimens can be achieved – stimulation at nerve motor subthreshold or above threshold levels, resulting in such effects as blood perfusion modulation or pain relief and motor response respectively (as discussed in [2]).

After supplying amplified voltage to the ultrasound transducer, it reproduces the same AM modulated signal in acoustic form, which then propagates through the tissue in the form of compression-rarefaction wave and couples to the implant. The piezoelectric crystal of the device (in our case PZT-5A) then generates an AM modulated waveform in the form of an electrical

current, which essentially replicates the external driving waveform (as it could be noted from the Fig. 7B, this is not absolutely true in case of the pulsed powering due to the fact that we are working with damped ultrasound transducers). Next, the rectifier of the microimplant rectifies (demodulates) AM modulated current, causing tissue interrogation by both low frequency baseband signal and high frequency carrier (additionally, tissue becomes interrogated by all the harmonics produced as result of rectification process). The magnitude of the current passing through the tissue depends on tissue impedance. This impedance in turn has a frequency dependent nature, which allows spectral characterization of the electrical properties of this tissue. In our system this is done by sweeping the baseband signal and making measurements at every baseband frequency. The skin potential generated by the device current flow is remotely detected via surface bioelectrodes. The amplitude and phase of detected current are recorded as a function of ultrasound modulation frequency. In the present work, phase and magnitude (RMS value) information were extracted from the detected surface potentials using lock-in amplifier. This amplifier is fed with the baseband reference signal, which essentially allows locking into specific frequency of interest and extraction of the signal at this frequency even out of the very complex and noisy waveform (extracted signals can be on the order of nanovolts).

It is worth noting that some of the further discussed experiments involved direct wired connection of the implant by clip leads to the measurement equipment. Though, in the ultimate clinically applicable system such measurements would not involve any wired coupling to the device.

Simulations and experiments

I. System simulations

Performance of the system involving low-MHz carrier modulation by low-kHz baseband signal with consequent signal demodulation using low-threshold voltage diode was analyzed using PSpice simulations (PSpice Student Version 9.1 OrCAD Inc.). Layouts of the simulated electrical circuits are shown on Fig. 10 and 11.

Circuits shown on Fig. 10 were used to analyze the applicability of demodulated AM carrier for extraction of the impedance information from the sample. These circuits compare four possible scenarios: sample interrogation using the baseband signal applied directly from the generator (Fig. 10A), sample interrogation using AM modulated carrier (Fig. 10B), sample interrogation using demodulated AM carrier with impedance data extraction at baseband, carrier sidebands and carrier harmonic sidebands (Fig. 10C and 10D). Additionally, circuit performance

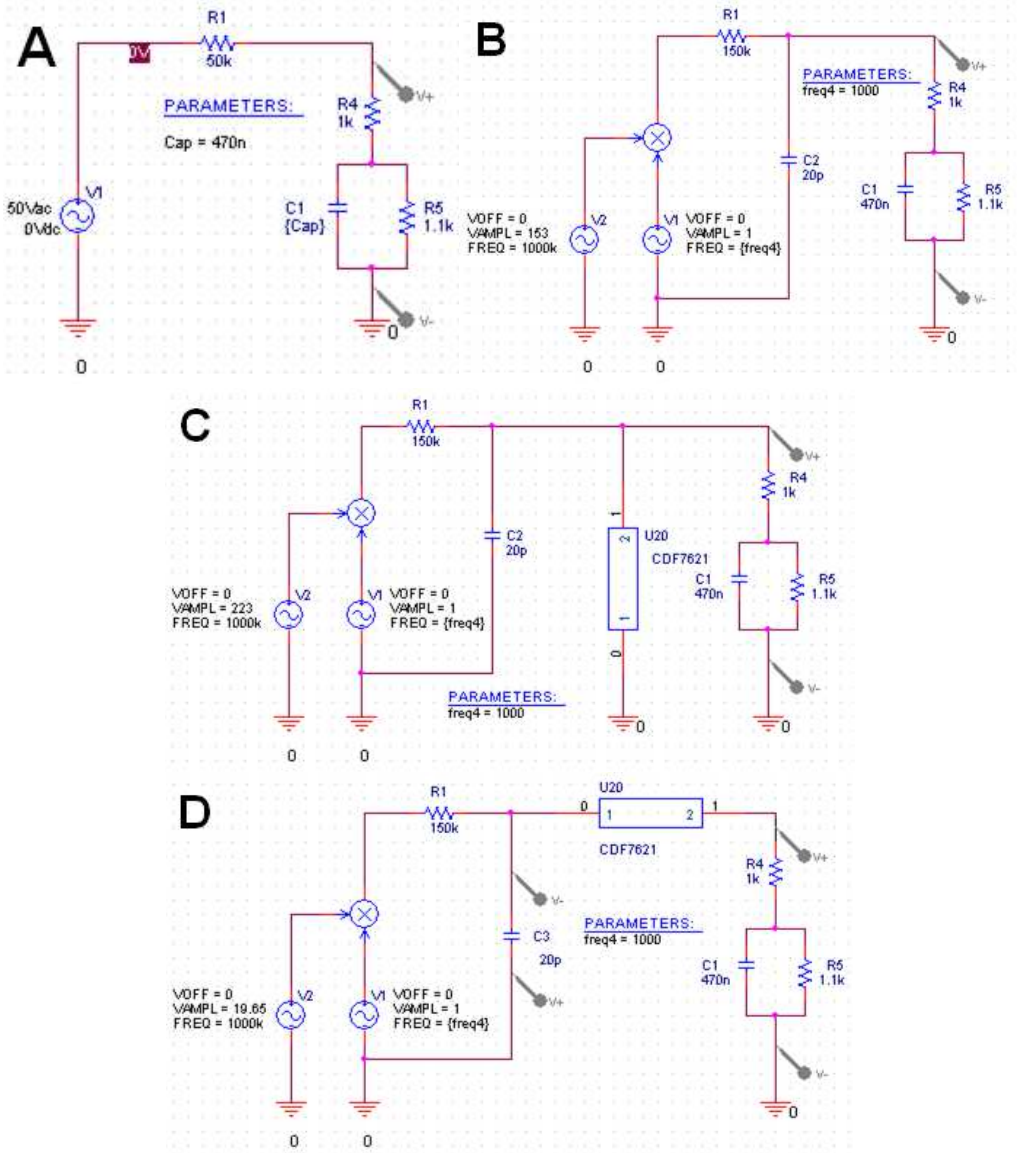

Fig. 10. Layouts of the circuits used for PSpice simulations of impedance analysis of the RC circuit. (A) Circuit for impedance measurements using direct output from the baseband signal generator. (B) Circuit for impedance measurements using modulated carrier. (C), (D) Circuits with diode in parallel (C) and series (D) connection for impedance measurements using demodulated AM carrier.

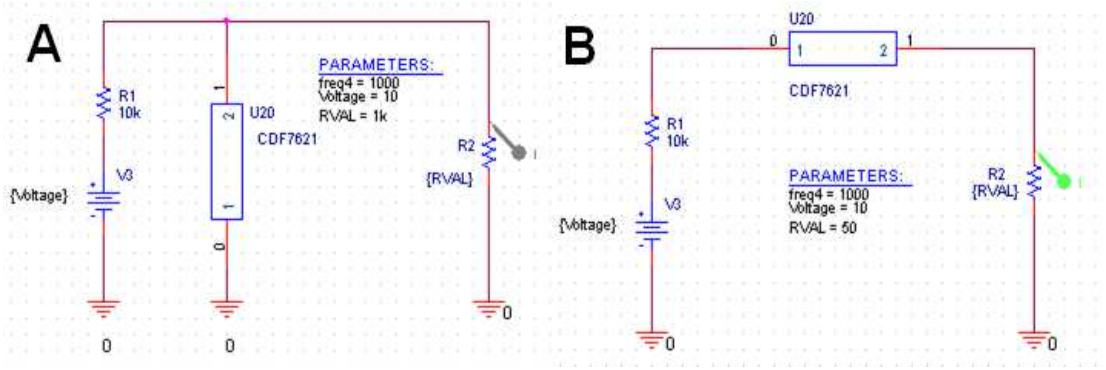

Fig. 11. Layouts of the PSpice circuits used for the analysis of I-V characteristic curves of the diode in two different connections. (A) Parallel diode configuration, (B) series diode configuration.

is assessed for two cases involving different diode connection configurations (Fig. 10C and 10D).

In the circuits shown on Fig. 10B, 10C and 10D, modulation was achieved using multiplication of the outputs of two signal generators. 20 pF capacitor in parallel to the generators mimics a piezoelectric voltage source, whereas 150 kΩ resistor mimics leakage resistance of the piezoelectric crystal. Modulated carrier (1MHz) was then applied through the diode and 1 kΩ electrode resistance to the parallel RC circuit mimicking our sample. Resistance value of RC circuit has not been changed, whereas capacitance was varied (100 nF to 470 nF) to introduce impedance changes.

Analysis of the effects of diode connection configuration on the system performance involved simulations of the diode's I-V characteristic curves. For this purpose circuits shown on Fig. 11 were used, which involved DC voltage application to the diode and consequent current measurements across the load.

In all simulations a CDF7621 (Skyworks, Inc.) Schottky diode was used. This type of diode suits well our application. It is characterized by low threshold voltage (270-350 mV at 1 mA) and diode die dimensions as low as 0.241 mm x 0.241 mm x 0.165 mm (Package 571-006).

II. System performance characterization

The typical setup used for the system performance characterization on the benchtop is shown on Fig. 12A and 12B. Basically, experiments with the bigger transducers (diameter ≥ 40 mm, as shown on Fig. 12A) involved attachment of the water bath to the transducer for acoustic coupling.

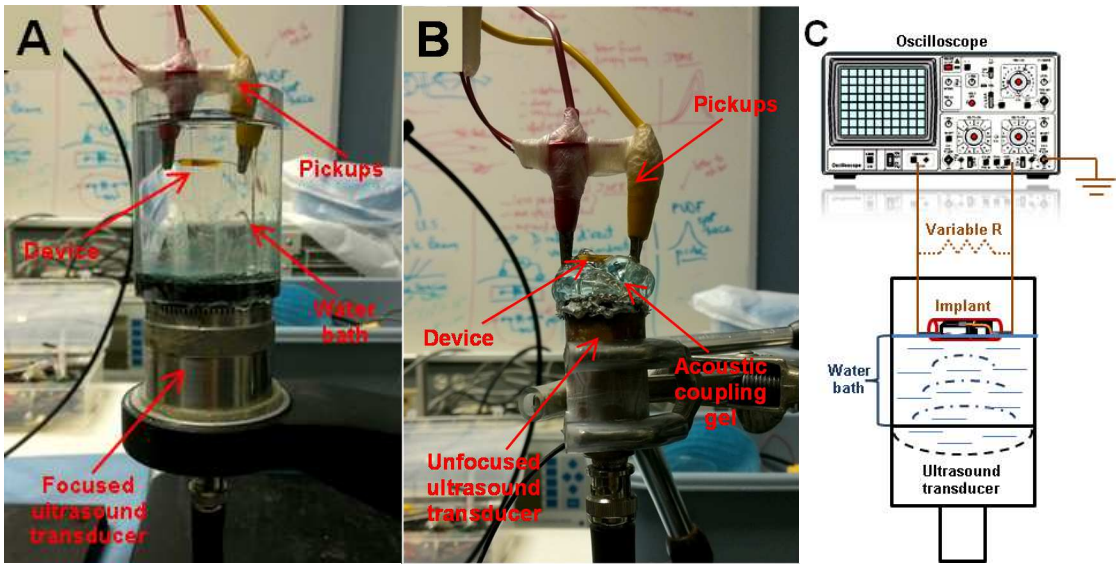

Fig. 12. Photographs and schematic of the device and transducer testing setups. (A) Example of the testing involving big diameter (38 mm) focused transducer. (B) Example of the testing involving small (20 mm) unfocused self-made transducer. (C) Example of setup for estimation of the implant output port impedance and its behavior with different loads.

Device then could be placed into water bath using the electrical pickups for signal detection and for holding the device in place. Alternatively, as it will be discussed later, device could be maintained stationary in the water bath using some self-made holders with signal detection using the remote electrodes. In addition, in case of the self-made transducers of the type shown on Fig. 9, instead of attaching the water bath to the transducer, ultrasound coupling gel could be placed on top of the face of the transducer to ensure the coupling. For instance, such types of the setups were used in order to analyze the dependence of the output voltage of device on load (as shown on Fig. 12C; results are shown on Fig. 32 and 33). The same setup shown on Fig. 12C was also used to determine the output port impedance of the devices by finding the resistive load, which causes output voltage drop by a half.

The same setups were also used to obtain waveforms and spectra shown on Fig. 31, having water bath filled with the saline solution of conductivity equivalent to the muscle tissue (880 μS/cm). The device response shown on Fig. 30 was obtained using the same principle as shown on Fig. 12, but instead of the two generators and amplifier to drive the transducer, the pulser/receiver (Computer controlled pulser/receiver, Model 5800, Parametrics, Inc.) was used.

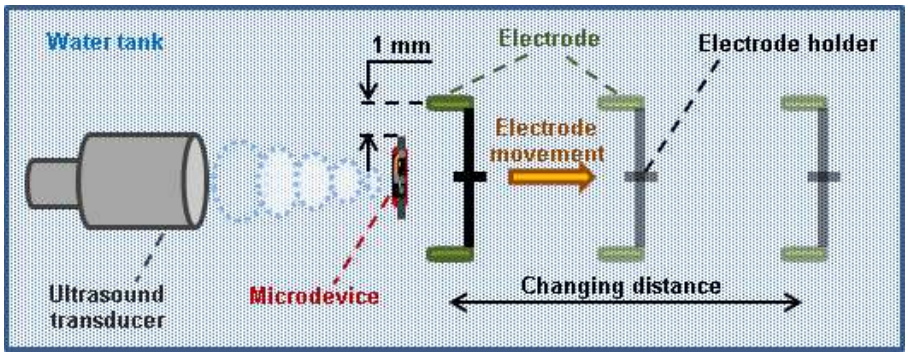

Fig. 13. Schematic of the experiment for the analysis of wirelessly measured output voltage dependence on the distance between the electrodes and device.

Results presented on Fig. 27B were obtained using the setup similar to the setup shown on Fig. 12A, only instead of the pickups, Ag/AgCl electrodes were used for wireless detection. In turn, plot of the phase and RMS variation with time for the bridge based device shown on Fig. 28B was obtained from the device placed in the cadaveric rat following the principles discussed in the further chapters on tissue sample interrogation experiments.

Furthermore, the dependence of the wirelessly detected output voltage on the distance between the device and the electrodes was analyzed using the setup sketched on Fig. 13. For these measurements solution with conductivity of 1950 μS/cm was used. Focused commercial transducer (Ø40 mm, Panametrics, Inc.) driven at the carrier of 1.4 MHz modulated by 1 kHz was immersed into water tank. The acoustic power density in the focus used for this experiment was ~ 43 mW/cm^2, which is more than 15 times smaller than approved FDA limit. Such low level acoustic power was used to prevent overdrive and consequent overheating of the driving amplifier and transducer itself, as well as to reduce the problems with crosstalk.

It must be noted that in all cases of wireless measurements signals were measured using the lock-in amplifier, whereas in cases of the measurements done using the pickups signals were typically analyzed using the oscilloscope. If not stated otherwise, all plots in the Results section having RMS voltages on the ordinate axis, are based on the measurements done using the lock-in amplifier, whereas the peak-to-peak (Pk-Pk) voltages were measured using the oscilloscope.

FDA limits for the ultrasound are defined as acoustic power density, but when we are driving the ultrasound transducer the only known parameter is the driving voltage used to power

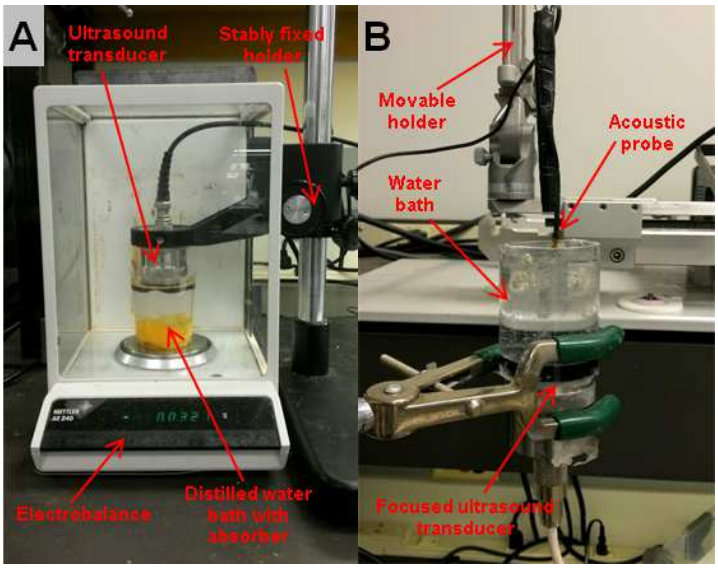

Fig. 14. Photographs of the acoustic power output measurements. (A) Acoustic radiation force caused weight deviation measurements using electrobalance. (B) Measurement of the focal spot size for focused transducer.

the transducer. Therefore, to be able to compare the acoustic energies used in the experiments to FDA limits it was necessary to convert driving voltages into acoustic power density. This was achieved using the electrobalance method shown on Fig. 14A, which involves measurements of the ultrasound pressure. For these measurements water bath with highly absorbent material at the bottom was used. The cup with absorber and solution was placed on the highly sensitive scales (METTLER AE240, sensitivity = 0.1 mg). Face of the transducer stably fixed by the holder was immersed into water bath. Before starting the measurements, the setup was left at least for 30 minutes to let it settle down and prevent any drift during measurements. Next, for every given driving voltage the apparent mass increase was recorded. Obtained mass was converted into acoustic power using the following equation:

$$P = \frac{\Delta m \cdot g \cdot c}{1+R^2} \qquad (1)$$

where Δm is the deviated weight caused by the radiation force, g is the gravity, c is velocity of ultrasound waves in water and R is the reflection coefficient of the target. In our case, the target is made out of sponge and is considered to be 100% absorptive, resulting in R = 0.

To translate acoustic power into acoustic power density, in case of the focused transducer the acoustic power was divided by the size of the focal spot, whereas for the

unfocused transducer the acoustic power was divided by the surface area of the face of the transducer itself. In order to determine the size of the focal spot, the setup shown on Fig. 14B was used. The acoustic probe made of PZT-5A with dimensions of 1.016 mm x 0.102 mm x 0.635 mm was moved around the acoustic field of the transducer and peak-to-peak voltages were recorded from the scope. The focal spot is defined as the area of full width half maximum, i.e., the area in which transducer output is within the half of the peak output. For the commercial focused transducer shown on Fig. 12A and 14, used to perform the majority of measurements, the focal spot was estimated to be 0.38 mm^2 by examining the plot of the output voltages from the acoustic probe. Acoustic power density dependence on the driving voltage for two of the transducers used within present study is shown on Fig. 27A.

Consequently, using the setup shown on Fig. 12A and 12B, the dependence of the wirelessly detected output voltage on the estimated acoustic power density was determined (results shown on Fig. 27B).

III. Wired characterization of RC circuits

First experiment involving impedance measurements was basically equivalent to the PSpice simulation involving parallel diode configuration with interrogation of the RC circuit (Fig. 10C). In the experiment shown on Fig. 15A, three different capacitance values were used: 100 nF, 220 nF, 470 nF (the same as in the simulations). In this experiment the Schottky based device was placed on top of distilled water bath (with conductivity of 5 μS/cm) to provide acoustic coupling of ultrasound transducer with the implant. Electrodes of the device were covered with clay for the isolation to prevent loading of the device by solution.

Experiment also involved several additional conditions. The output of the device was also recorded in the case of absence of the capacitor, allowing analysis of the device performance at different baseband frequencies just with the resistive load. As it is discussed in the conference proceeding [59] written based on some of the results presented here, one of the experiments involved interrogation of RC circuit having 10 kΩ in series with the device. This was done to make the device act as a constant current source instead of the constant voltage source (as in

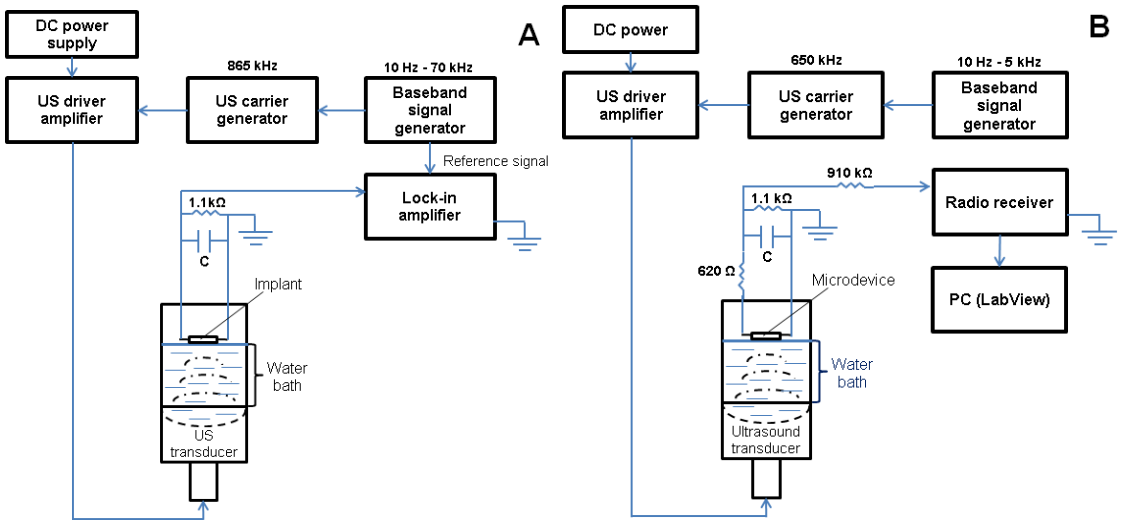

Fig. 15. Schematics of the RC circuit impedance wired measurement experiments. (A) Measurements using lock-in amplifier, (B) measurements using radio-receiver.

case of the layout shown on Fig. 15A). Constant current sources are often used in conventional impedance measurements to limit the current and prevent any damage caused to the tissue under investigation. These experiments involved the baseband frequency sweeping and consequent phase and voltage RMS recording at different frequencies.

An additional experiment shown on Fig. 15B was done to investigate impedance measurement approach involving detection of the carrier sideband signals. This approach was also tested using simulations and will be discussed in the Simulations Discussion section. In the experiment the detection was achieved using radio receiver (WinRadio G305e). Measured signals were fed into computer, which allowed data analysis using LabView SignalExpress by creating a WinRadio virtual sound card. Further, impedance spectra were recorded by looking at the magnitude of the baseband signal in FFT spectra. The input stage of the radio receiver incorporated 910 kΩ resistance to prevent overloading of the receiver. Basically, with such input resistance only very small fraction of the signal could pass through and the bulk of the signal could be radio-transmitted from the device to the receiver. Presence of the wired connection essentially ensured stable coupling of the radio receiver to the signal source between the trials, eliminating any extra variability associated with slight deviations of antenna placement relative to the source.

IV. Wired and wireless characterization of saline solutions

In the transition process from the experiments involving absolutely non biological samples (e.g., RC circuits) to the experiments utilizing actual tissue samples and ultimately the live subjects, system ability to detect impedance changes was tested by performing the experiments with saline solutions. The solutions were made by adding salt to distilled water. Conductivities were chosen to be equivalent to conductivities of different tissue types.

The experiment shown on Fig. 16A was done using the solutions with conductivities of 2.5, 335, 1800 and 4400 μS/cm. For the experiment shown on Fig. 16B the solutions with conductivities of 170, 1300, 2000, 2200 μS/cm have been used. Consequently, in the first case measurements were done by having the clip-leads attached to the device, whereas in the second case measurements were done totally wirelessly using the Ag/AgCl electrodes immersed into solution. As in this case the solutions themselves have been used as the samples under investigation, the device was fully immersed into solutions (in contrast to the experiments with RC circuits, where device with isolated electrodes was placed just on the surface of the solution without touching the solution).

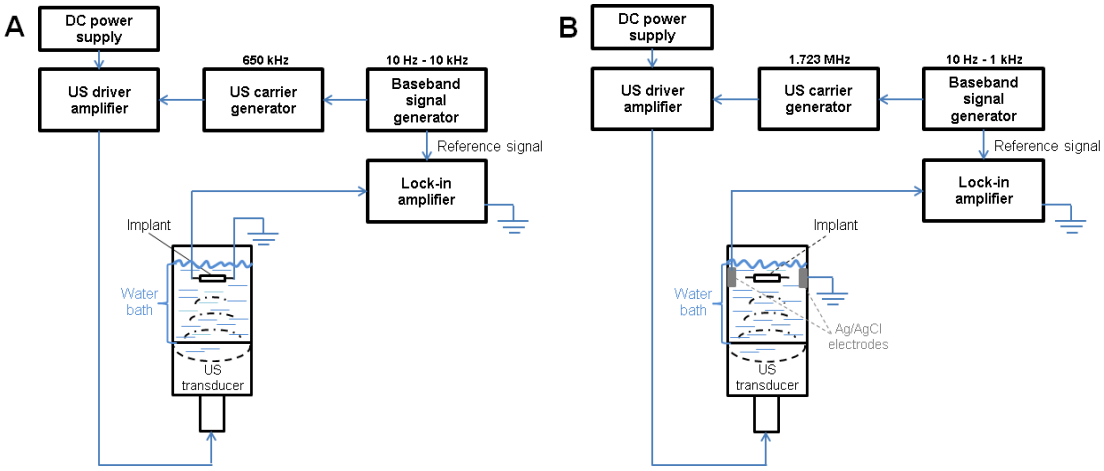

Fig. 16. Schematics of the saline solution interrogation experiments. (A) Wired measurements with signal measurements using clip leads, (B) wireless measurements using Ag/AgCl electrodes.

V. Wired and wireless characterization of tissue samples

Next set of experiments was done with tissue samples, involving measurements using slices of beef stacked into water bath and measurements using devices placed into cadaveric rats. For wired and wireless impedance measurements of beef samples the setup shown on Fig. 17A was used. The only difference in case of the wired measurements involved attachment of the clip-leads to the device for signal detection instead of the Ag/AgCl electrodes used for wireless signal detection (as shown on Fig. 17A). In both cases the implant was placed on top of the stack of beef (40 mm high) with its electrodes inserted into meat sample and device body having good contact with meat surface to ensure acoustic coupling. In case of the remote signal detection, the output of the implant was detected using Ag/AgCl surface electrodes, placed at the same height as implant's electrodes and 15 mm away from the implant's electrodes in the horizontal plane. In both cases of wired and wireless measurements the impedance changes were induced by adding drops (~ 0.1 ml) of saline solution (~ 1500 μS/cm) to the sample.

In case of the experiment shown on Fig. 17B, which involved device placement into cadaveric rat's muscle pocket of the lower limb in vicinity of femoral artery (approximately the same location where it was placed in the live rat in this study and in [2]), the impedance changes were induced by injecting (~0.1 ml) the saline solution (~1500 μS/cm) into the area around the device.

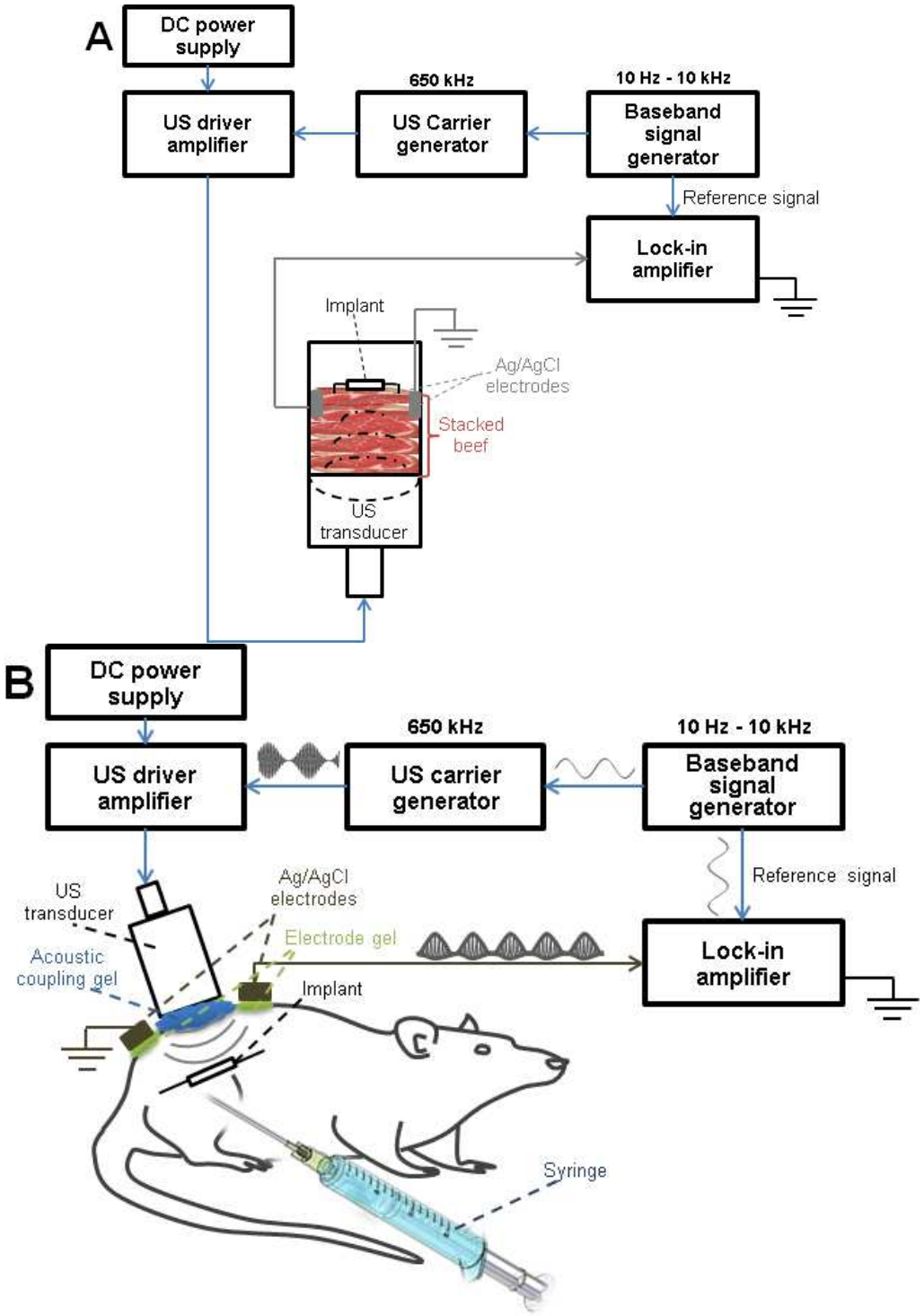

Fig. 17. Schematics of the wireless impedance measurement experiments of tissue samples. (A) Experiment with device placed on top of the stacked beef, involving induction of the impedance changes by adding the drops of saline solution. (B) Experiment with device placed into muscle pocket in the lower limb of cadaveric rat. Impedance changes were induced through injection of saline solution (in both experiments 0.1 ml, 1500 μS/cm).

VI. Live animal experiments

The bridge rectifier based device was implanted into female Sprague Dawley rat (mass 289 g., DOB 03.18.2014) on May 8, 2014. The device was implanted into the lower left limb in the muscle pocket in vicinity to femoral artery. The pocket between the muscles was entered in the location shown on Fig. 18A and device was pushed down into pocket along a femoral artery. It was attempted to place the device as low as possible in the limb. This was done because, as it will be discussed later, the planned live animal experiment involved occlusion of the femoral artery at the base of the limb (in the region of hip joint) to cause the reactive hyperaemia, detectable using the laser Doppler flowmeter.

The surgery was approximately an hour long; rat was anesthetized using the isoflurane. After the surgery, having the rat placed back into cage, rat removed the simple-interrupted braided suture within approximately an hour, leading to the repeated suturing of the wound using the intradermal pattern. Rat was further left for 5 days to heal and within these days rat was administered with subcutaneous injections of the following drugs: Baytril, Buprenorphine, Meloxicam (detailed information can be found on the approved protocol #1270).

The implanted device was of the type shown on Fig. 6B. The device was 6 mm long and 3 mm in diameter (1.8 mm long electrodes with diameter of 0.5 mm; the dimensions of the used PZT-5A are 1.6 mm x 1.0 mm x 0.8 mm).

Five days after the implantation the experiment similar to what is shown on Fig. 19A was

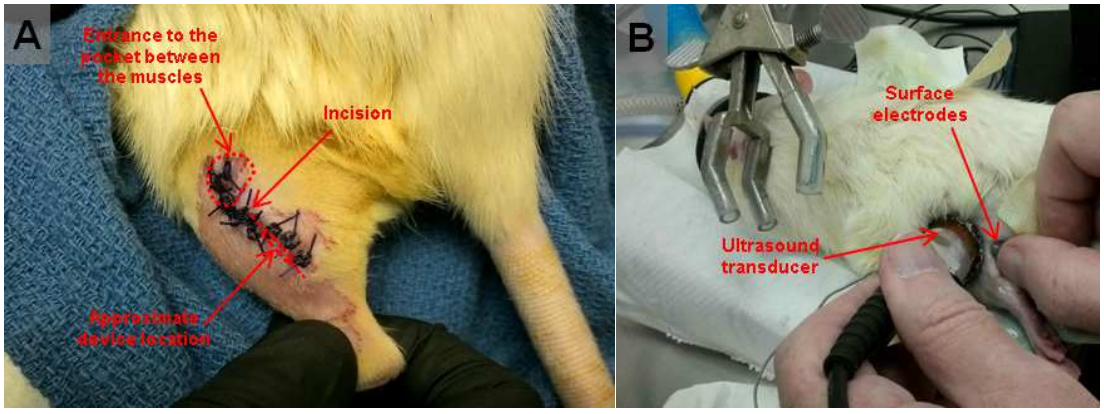

Fig. 18. Photographs of the live rat during the experiments. (A) Post-surgical photograph of the incision site, (B) photograph of the impedance measurement experiment.

performed aiming at identifying if the implant can be excited and produce signals detectable from the surface of the skin. The first trials of the experiment, in contrast to that is shown on Fig. 19A, involved measurements done using just a pair of the electrodes and ungrounded highly-focused commercial transducer (Ø38 mm). Commercial transducers are characterized by much better shielding than our custom-made transducers and consequently weaker crosstalk. Therefore, transducer could be driven using maximally achievable voltages – 60 V, which produced 315 mW/cm^2 of acoustic power density in the focal spot. During this experiment the lower limbs of the rat were restrained using the surgical tape, as well as the Ag/AgCl electrodes were secured to remain stationary by fixating them using the tape. Rat was held under the isoflurane for a whole duration of each experiment. The photograph of the typical trial showing the transducer and electrode placement is shown on Fig. 18B.

The trials performed at later stages of this work were done following the measurement principles shown on Fig. 19. Fig. 19A shows the idea behind the differential impedance measurement experiments, whereas Fig. 19B shows the principle of the shock excitation of the implant, which provides higher spatial peak power. Basically, the system shown on Fig. 19A incorporates such additional components as extra electrode, as well as shielding and grounding of the self-made transducer (Fig. 9). All of these measures were gradually introduced to reduce the level of crosstalk, which showed to be a mild problem during the experiments with cadaveric rats and were observed to be magnified during the first trials with a live rat. Additionally, the transducer has shown to play an important role, therefore in the latter trials six different transducers have been tested (4 commercial and 2 self-made ones), mainly having different focusing, shielding, bandwidth and resonant frequencies.

The measurement system shown on Fig. 19B did not involve differential measurements using three electrodes because the time delay between the interference and actual signal was providing the immunity against crosstalk. Moreover, in this case the ultrasound pulser/receiver was not only used to drive the transducer with 180 V, but also to detect the signals from the device, providing 60 dB gain for detected signals.

All animal experiments were approved by institutional IACUC.

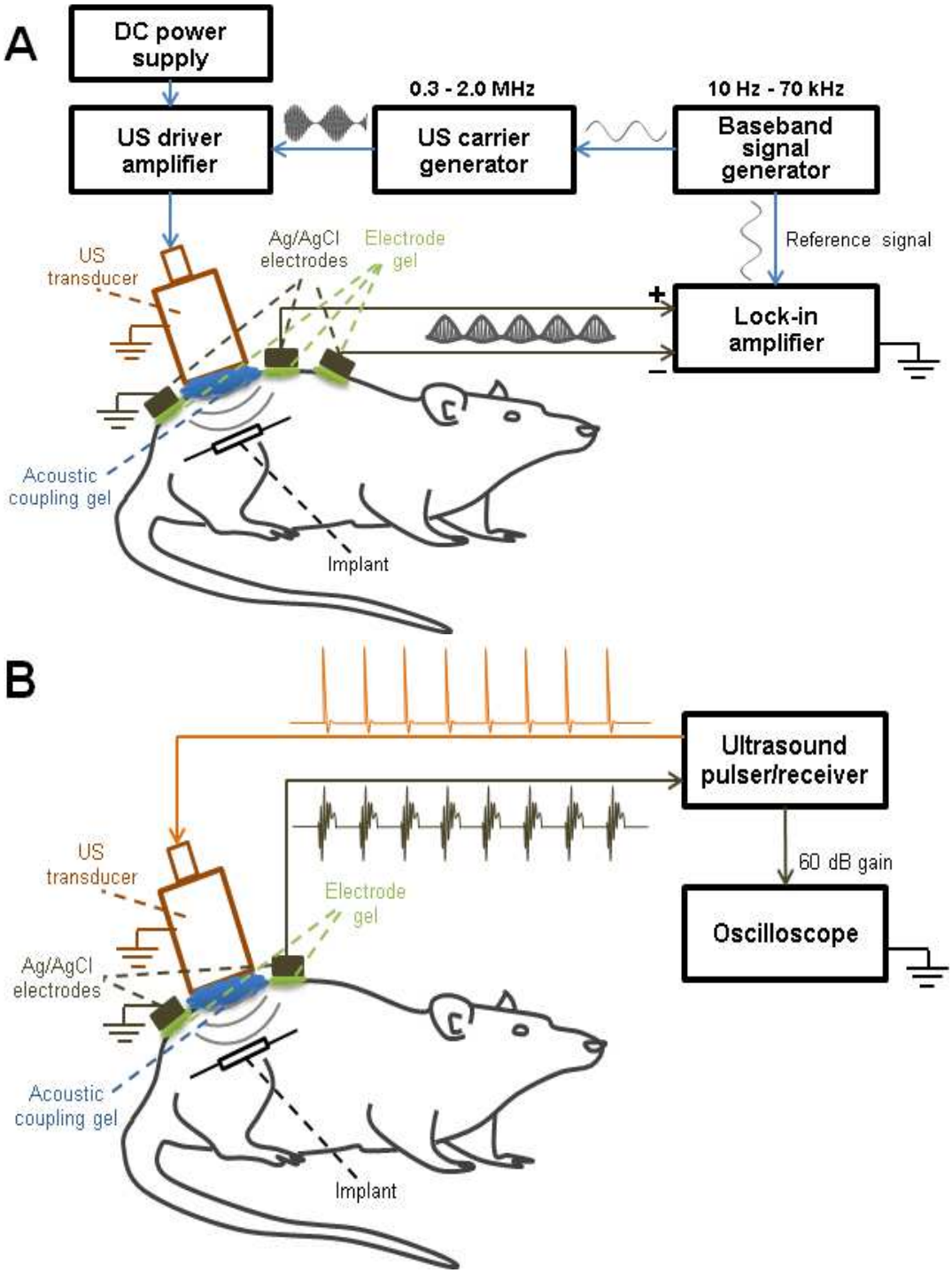

Fig. 19. Schematics of the live rat experiments. (A) Schematic of the impedance measurement experiment, (B) schematic of the experiment testing the magnitude of the wirelessly detected signal produced by the tone burst excitation.

CHAPTER 4

RESULTS

I. System simulations

As result of the simulations based on the circuits shown on Fig. 10 and 11, the plots shown on Fig. 20 through 26 have been obtained.

Plots shown on Fig. 20 and 21 demonstrate the shapes of the waveforms and spectra of the voltages produced by the circuits shown on Fig. 10C and 10D, respectively. The purpose of the analysis of these circuits involves identification of the best diode configuration (although, potentially other types of rectifiers could be used) in the implants, allowing most efficient

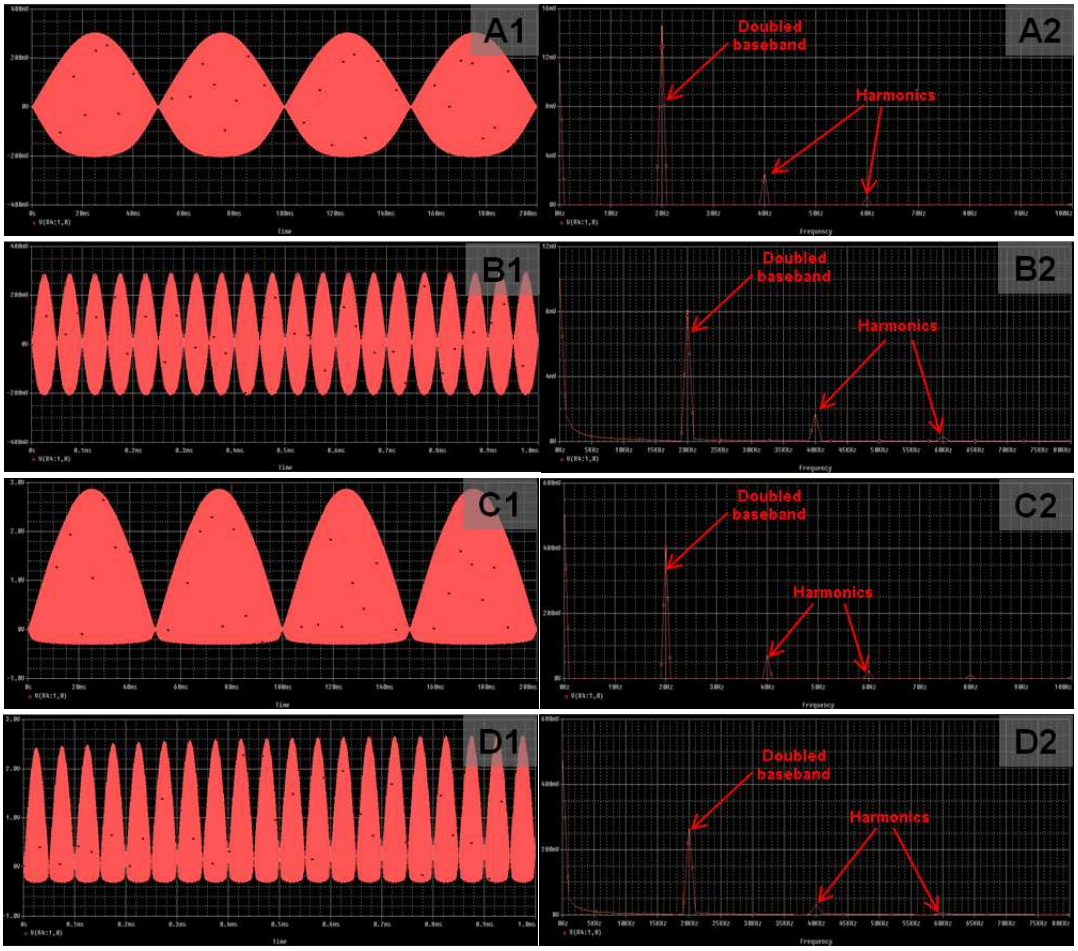

Fig. 20. Waveforms and Fourier spectra of the rectified AM voltage produced in the case of parallel diode configuration (Fig. 10C). (A) 10 Hz baseband with 0.5 V drive, (B) 10 kHz baseband with 0.5 V drive, (C) 10 Hz baseband with 3 V drive, (D) 10 kHz baseband with 3 V drive.

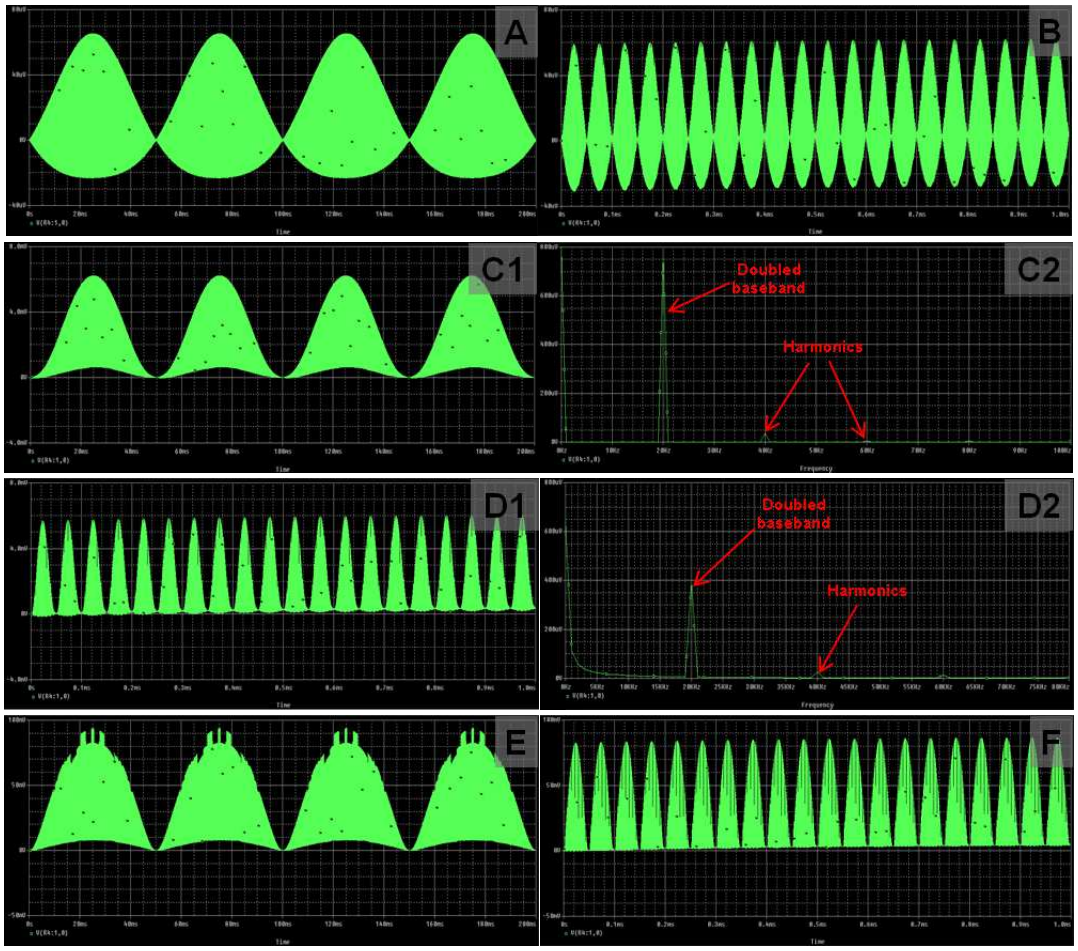

Fig. 21. Waveforms and Fourier spectra of the rectified AM voltage produced in the case of diode connection in series (Fig. 10D). (A) 10 Hz baseband with 0.05 V drive, (B) 10 kHz baseband with 0.05 V drive, (C) 10 Hz baseband with 0.5 V drive, (D) 10 kHz baseband with 0.5 V drive, (E) 10 Hz baseband with 3 V drive, (F) 10 kHz baseband with 3 V drive.

impedance measurements and neurostimulation. The key further addressed features of these waveforms and spectra include: the level of rectification, presence or absence of DC offset, harmonic production in the spectral domain, level of the carrier versus baseband signal, and diode performance dependence on the driving voltage.

Fig. 22 shows the I-V characteristic curves for the Schottky diodes for the circuits shown on Fig. 11. These curves were obtained for three different loads and they provide further insights into circuit behavior with two different diode configurations.

Next, Fig. 23 and 24 provide actual RC circuit interrogation results for four circuits shown on Fig. 10. These results are shown in the form of frequency spectra of the output voltages

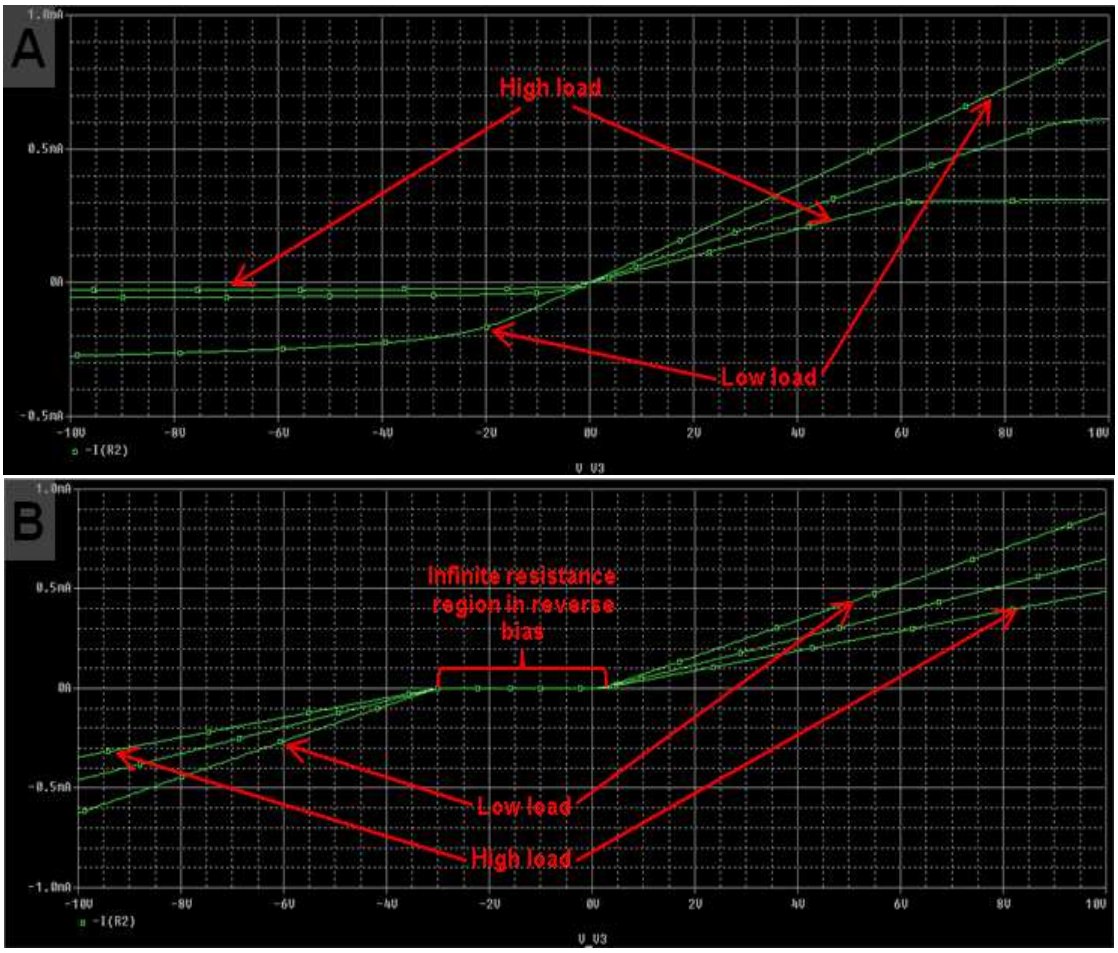

Fig. 22. I-V characteristic curves of the Schottky diode in two different configurations for three different loads – 1 kΩ, 5 kΩ and 10 kΩ. (A) Parallel diode connection (Fig. 10C), (B) diode connection in series (Fig. 10D).

across the RC circuit for the frequency range between 10 Hz and 50 kHz (this frequency range follows from the frequencies achievable using our experimental setup). Output voltages were obtained at the baseband frequencies from the Fourier spectra (as shown on Fig. 20 and 21). In reality, the harmonic frequencies of the baseband were used for getting these plots, as will be discussed further in the discussion section, because as it can be seen from the spectra on Fig. 20 and 21, the actual baseband signals were not present after the demodulation. Instead, only the harmonics were present with the main power at double-baseband frequency. For all the plots on Fig. 23 output voltages were maintained to be 2 V across the piezoelectric voltage source (20 pF capacitor) by adjusting driving voltages for every circuit configuration.

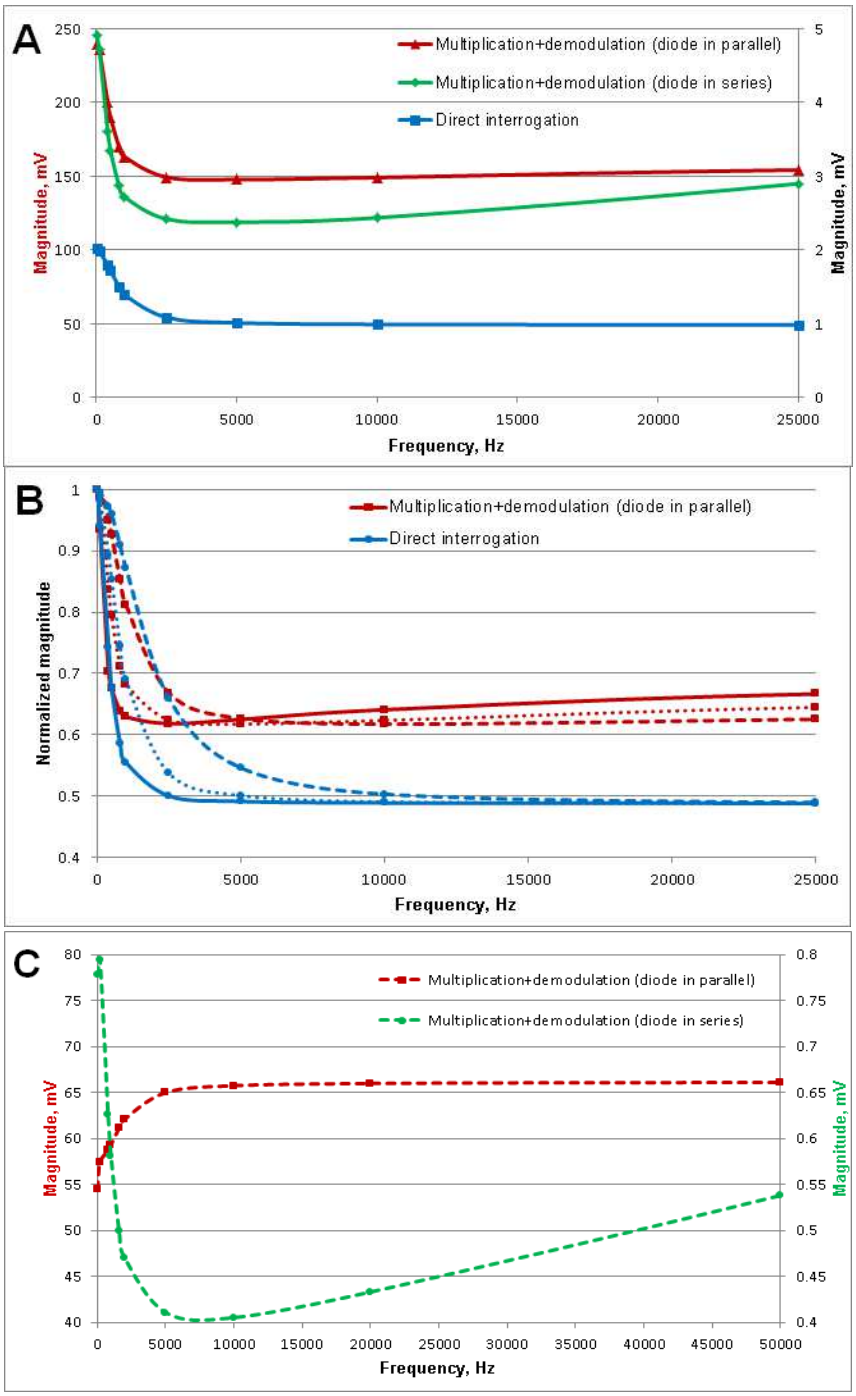

Fig. 23. Impedance analysis plots from PSpice simulations based on the circuits shown on Fig. 10A, 10C and 10D. (A) Comparison of the three interrogation cases: using demodulated AM voltage for series diode configuration (Fig. 10D), using demodulated AM voltage for parallel diode configuration (Fig. 10C), and using baseband voltage directly from the generator (Fig. 10A). (B) Comparison of the RC circuit characterizing curves obtained using AM demodulated voltage from parallel configuration and direct circuit interrogation using the baseband generator. (C) RC circuit impedance spectra obtained using 2nd harmonic produced by the diode. In (A) and (B) solid lines denote RC circuit with C = 470 nF, in (B) and (C) dashed lines denote RC circuit with C = 100 nF, in (B) dotted lines denote RC circuit with C = 220 nF.

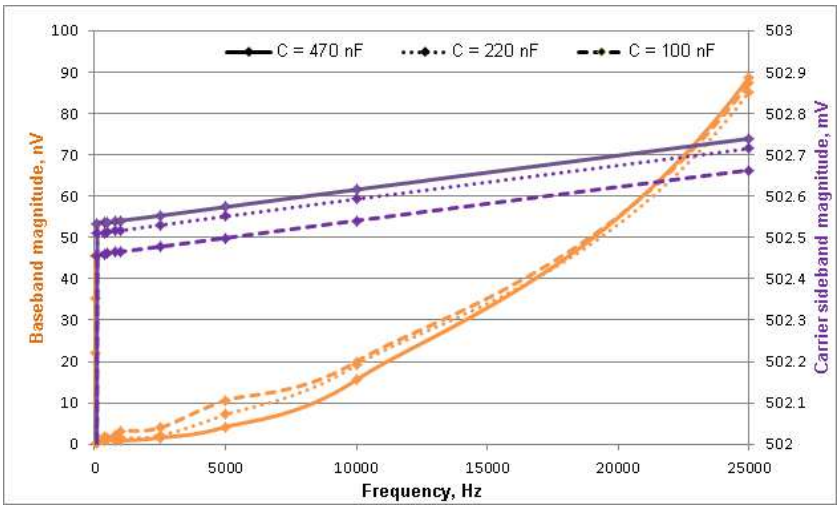

Fig. 24. RC circuit impedance plots resulting from interrogations using AM modulated carrier without demodulation (based on the circuit shown on Fig. 10B). Orange traces correspond to the signal value at baseband frequency, purple – at carrier sideband frequency ($F_{CARRIER}$ + $F_{BASEBAND}$).

Fig. 23A provides voltage spectra comparison of the three circuit layouts shown on Fig. 10A, 10C and 10D for the RC circuit with capacitance of 470 nF. Fig. 23B provides RC circuit interrogation results for the circuits shown on Fig. 10A and 10C with capacitance values of 100 nF, 220 nF and 470 nF. Fig. 23C shows voltage spectra obtained using demodulated carrier from two different diode configurations as before, only in this case a second harmonic of the baseband signal was used (3x frequency of the baseband). This was done to identify whether one of the configurations allows sample interrogation using simultaneously multiple frequencies having

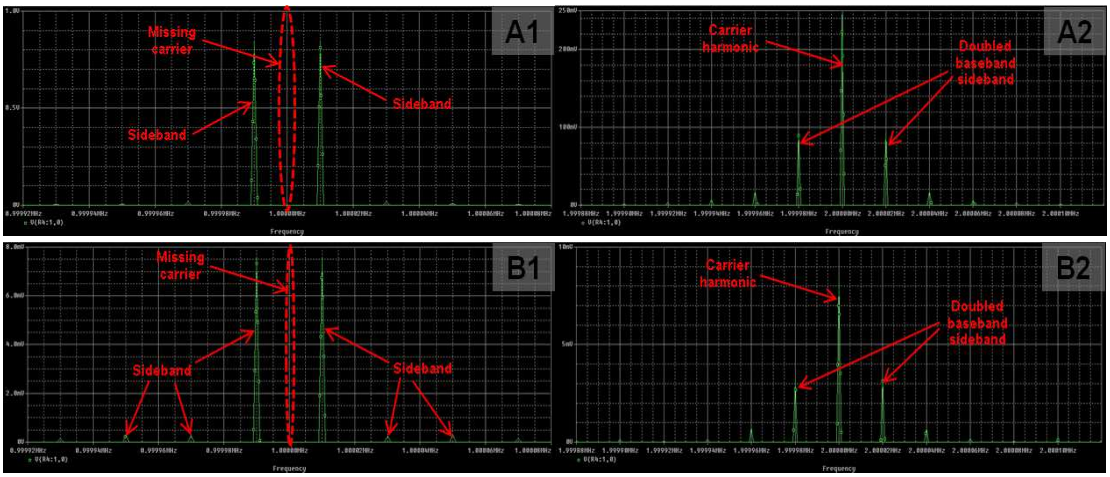

Fig. 25. Fourier spectra of the carrier and carrier harmonic frequency ranges (modulation at 10 Hz). Carrier frequency for parallel (A1) and series (B1) diode configuration, carrier harmonics for parallel (A2) and series (B2) configuration.

harmonic relationships. These harmonics represent the bi-product of the process of demodulation and it would be beneficial not to waste this power, and use it to interrogate the sample simultaneously at multiple frequencies, as will be discussed further.

Furthermore, Fig. 24 presents the results of the RC circuit interrogation using AM modulated carrier without demodulation (based on the circuit shown on Fig. 10B).

Finally, Fig. 25 presents the high frequency-range spectra for two diode configurations. Fig. 25 includes spectra of the both sidebands of the carrier itself, as well as spectra showing the harmonics of the carrier with sidebands of the doubled baseband frequency.

The spectral components shown at Fig. 25 were used to produce impedance spectra shown on Fig. 24 and 26. As will be discussed later, this type of analysis was done in order to investigate the potential of impedance data collection using the radio receiver with antenna, instead of the surface electrodes. These spectra were made by using voltage magnitude values from Fourier spectra obtained for different modulation frequencies. The following spectral components have been investigated (Fig. 26A1 and 26B1):

- peaks at frequencies $f_{carrier}$ -/+ $f_{baseband}$;
- peaks at frequencies $2fc_{arrier}$ -/+ $2f_{baseband}$;
- peak at harmonic frequency $2f_{carrier}$.

After identifying the spectral component exhibiting the trend characteristic for impedance frequency dependent nature, specific spectral components were selected to investigate their sensitivity to impedance changes (Fig. 26A2 and 26B2). Impedance changes were made the same way as before, by changing the capacitance value of the RC circuit.

To obtain Fourier spectra and impedance spectra shown on Fig. 24, 25 and 26, respectively, the circuits shown on Fig. 10B, 10C and 10D have been used.

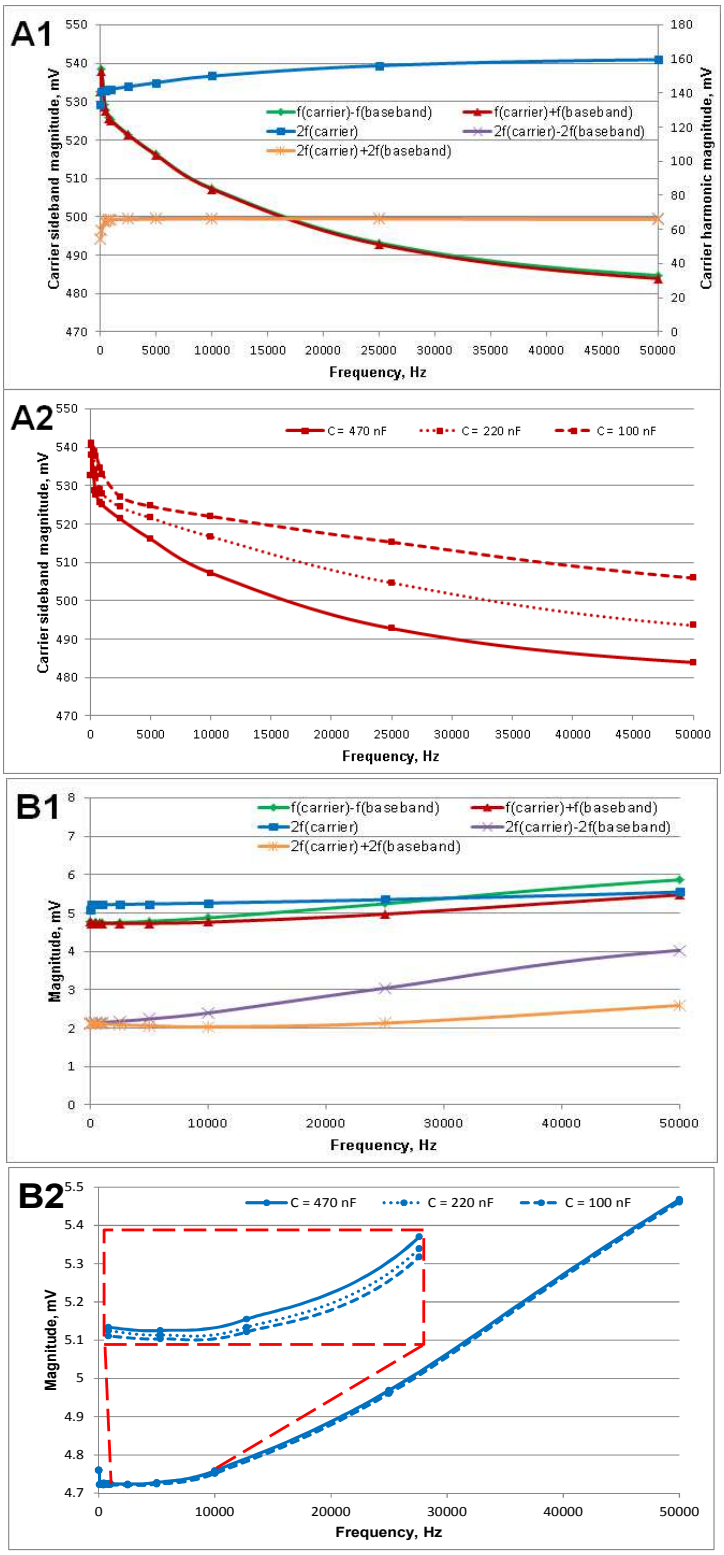

Fig. 26. RC circuit voltage spectra obtained using carrier and harmonic sidebands. (A) Parallel diode configuration, (B) series diode configuration. (1) Measurements done using carrier and carrier harmonic sidebands and harmonic fundamental, (2) measurements using higher frequency sideband of the carrier ($F_{CARRIER} + F_{BASEBAND}$).

II. System performance characterization

Based on the principles discussed in the Methods section, plots of the acoustic power density dependence on driving voltage and of the wirelessly detected voltage RMS on acoustic power density were obtained for two different transducers (Fig. 27). For device output voltage measurements (Fig. 27B) the bridge based device has been used.

Next, device output variability was assessed in case of the wired (Fig. 28A) and wireless (Fig. 28B) detection. In case of wired detection, the data have been recorded at two different

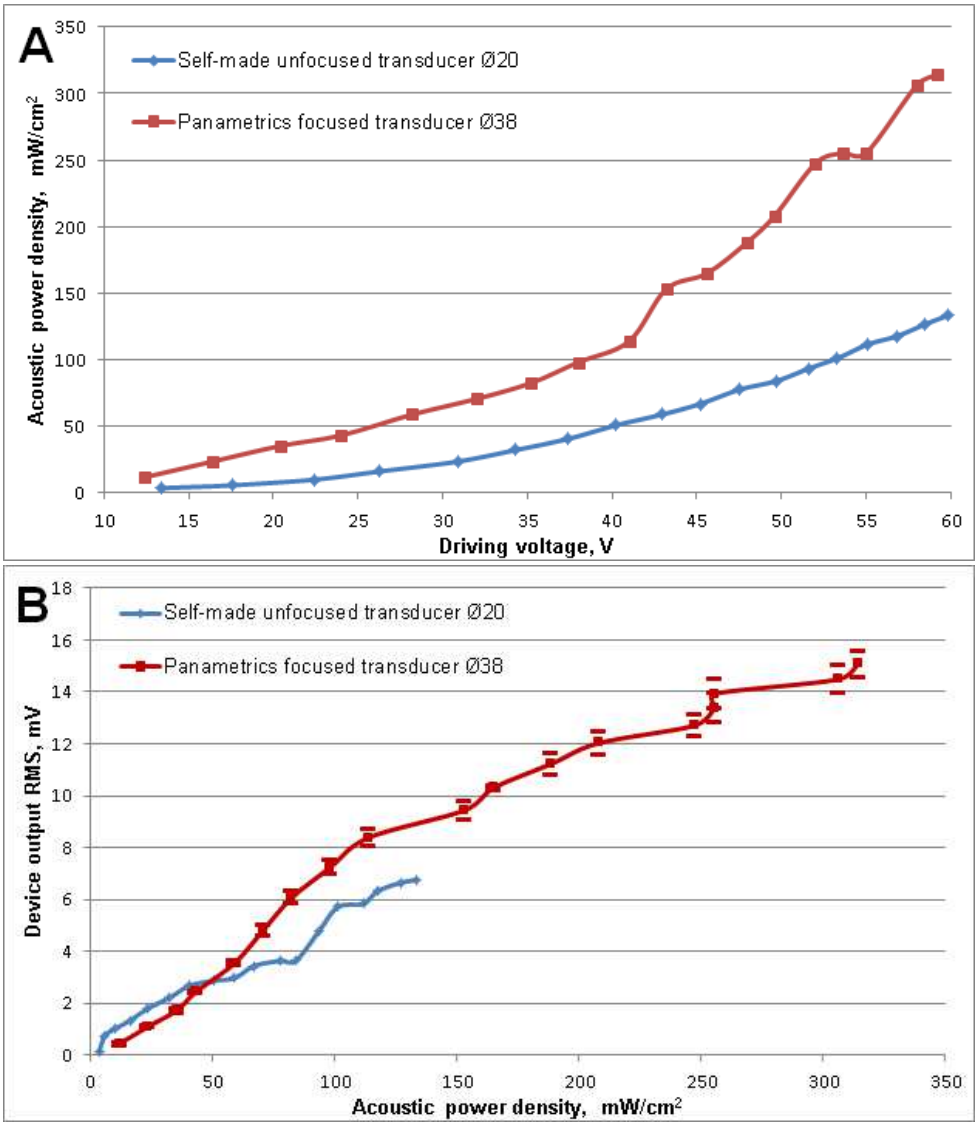

Fig. 27. Plots demonstrating acoustic power density dependence on the driving voltage (A) and device output voltage RMS dependence on acoustic power density (B).

carrier frequencies with the acoustic power density ~98 mW/cm^2. In case of wireless detection, phase and RMS variations were analyzed at two different baseband frequencies at the acoustic power density ~133 mW/cm^2. In this case the maximal possible drive voltage for a given setup was used (~60 V on the self-made transducer). Additionally, cadaveric rat experiment involved two trials performed on different days, where in the second trial the transducer was better fixed relative to the rat to prevent any drift of the transducer over time. For both experiments with results shown on Fig. 28 the bridge based device has been used.

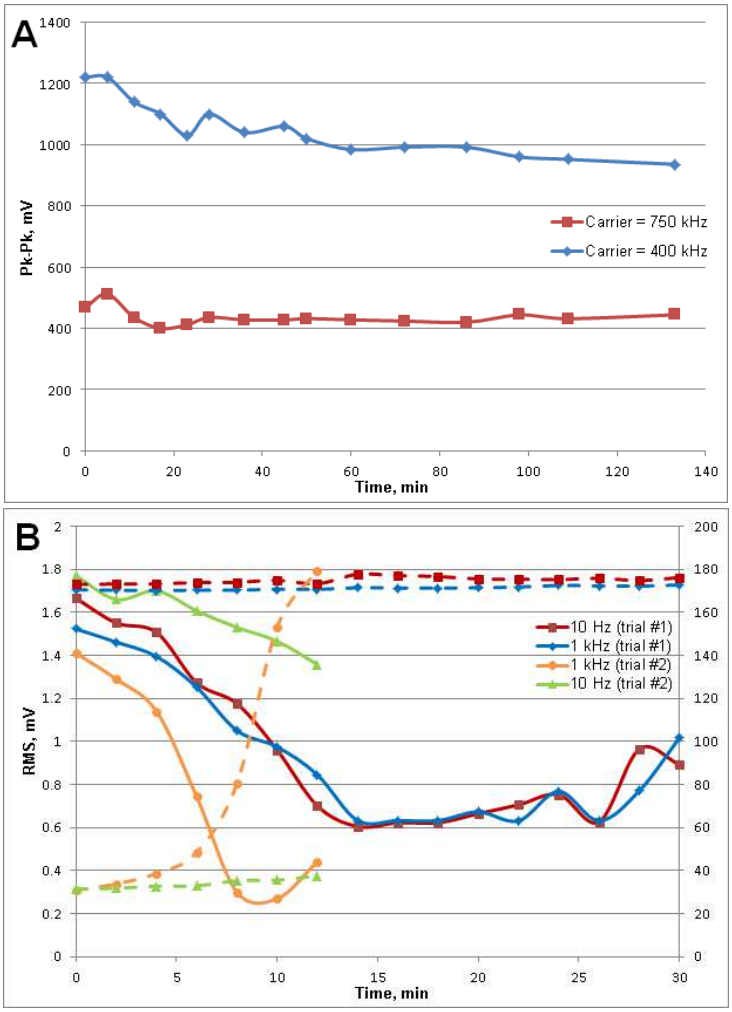

Fig. 28. Device output variability characterization. (A) Plot of variation of the peak-to-peak device output voltage with time at two different carrier frequencies (wired detection). (B) Plot of the phase and RMS variations with time at different baseband frequencies (wireless detection).

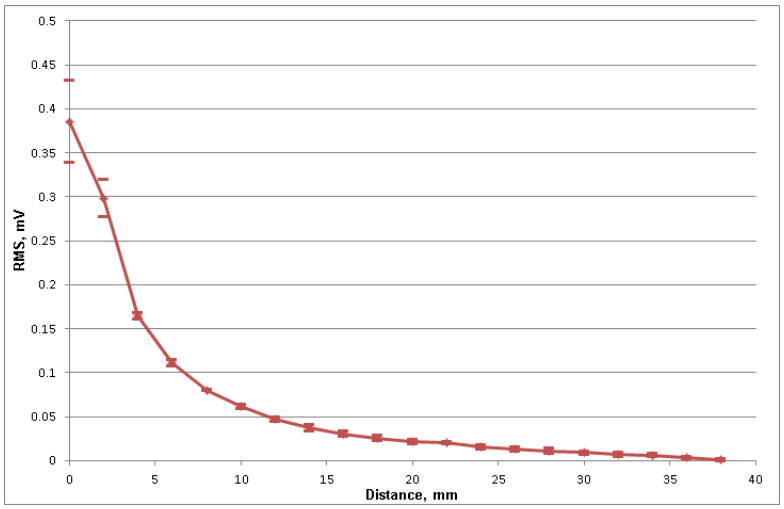

Fig. 29. Wirelessly detected device output voltage RMS dependence on the distance between the electrodes and device (device driven by 43 mW/cm^2 in the solution with conductivity 1950 μS/cm).

Furthermore, Fig. 29 shows average results of the three trials for the dependence of the wirelessly detected output voltage RMS on the distance between the device and the electrodes.

Additionally, the device response to the shock pulse excitation is demonstrated on Fig. 30. This is similar type of excitation used to drive the device for the neurostimulation applications. Fig. 30 shows both actual driving pulse (Fig. 30A), as well as typical device response waveform to the applied excitation (Fig. 30B).

Further, the waveforms and spectra of the output voltage for different types of devices are shown on Fig. 31. This data has been obtained for the simple PZT without the rectifier (Fig.

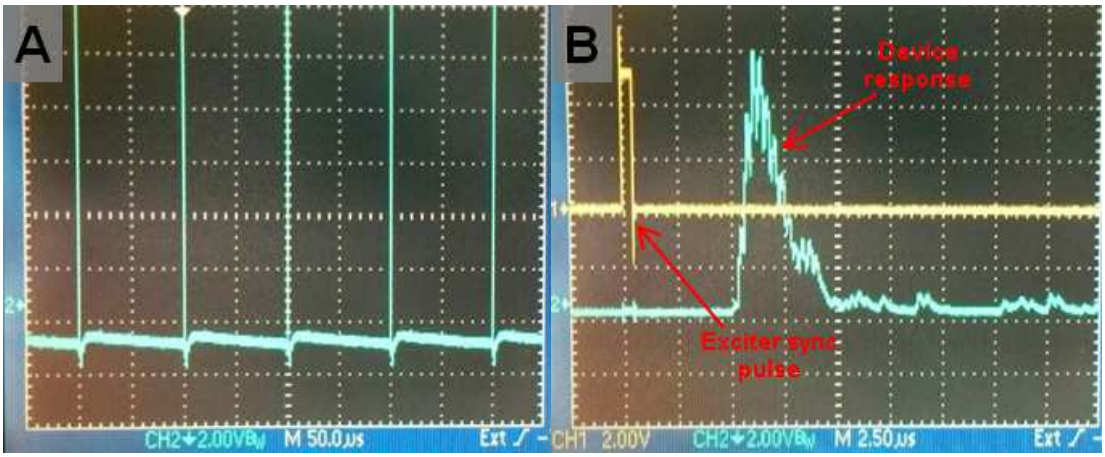

Fig. 30. Device driving using tone burst excitation. (A) Pulse train used for the excitation (peak-to-peak voltage ~ 180 V), (B) Excitation sync pulse (yellow) and device response (cyan).

31A), for the Schottky based device (Fig. 31B), for the bridge based device (Fig. 31C) and varicap diode based device (Fig. 31D). Spectra are shown both for the carrier frequency region (B) and baseband frequency region (B). For these experiments 850 kHz carrier and 1 kHz baseband signal has been used used. In order to maximally mimic the physiological conditions,

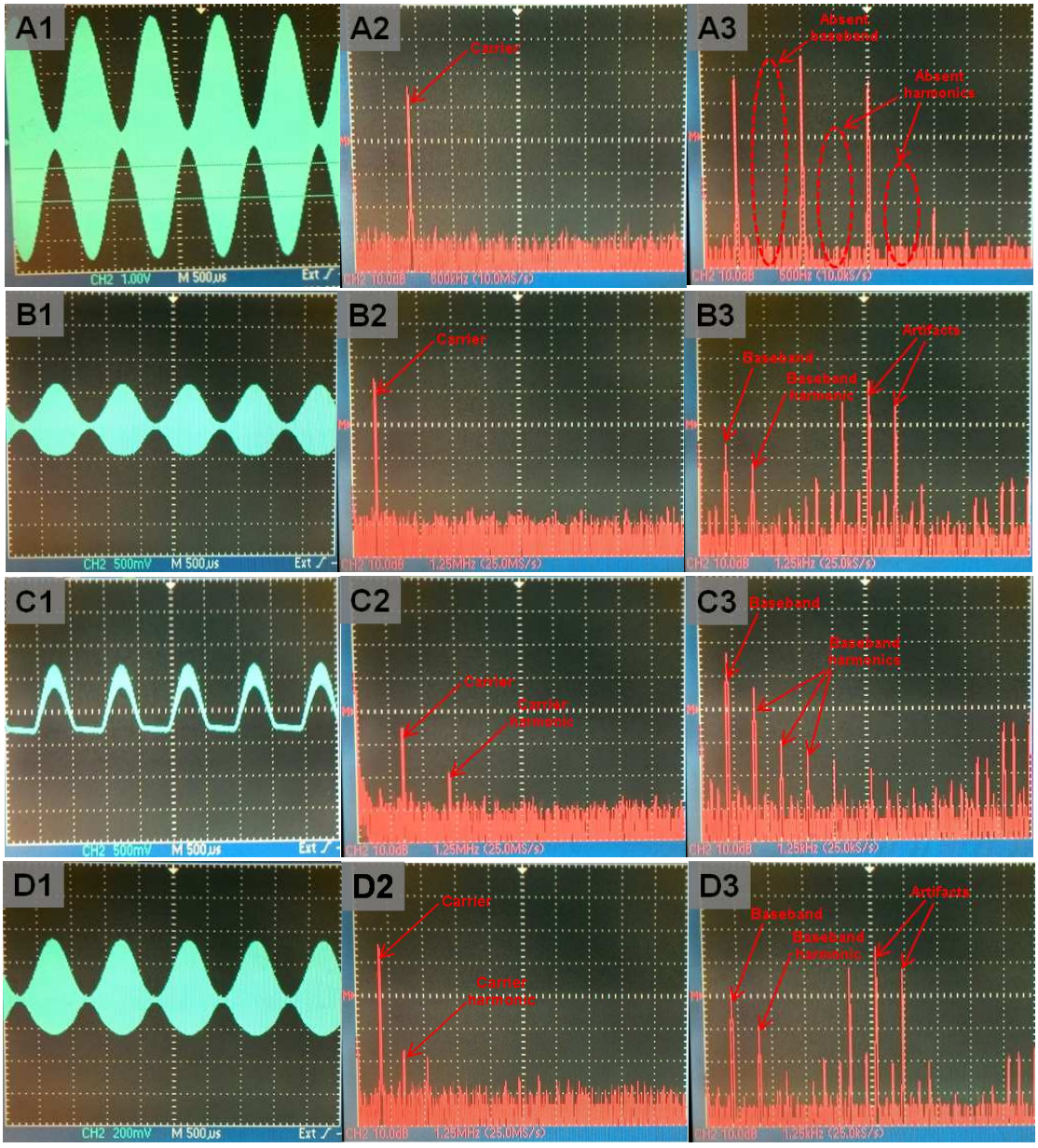

Fig. 31. Photos of the waveforms and Fourier spectra for different types of devices loaded by the solution with conductivity of 880 μS/cm (driven by 43 mW/cm^2 with 850 kHz carrier and 1 kHz baseband). (A) PZT-5A without the rectifier, (B) Schottky based device, (C) bridge full-wave rectifier based device, (D) varicap diode based device.

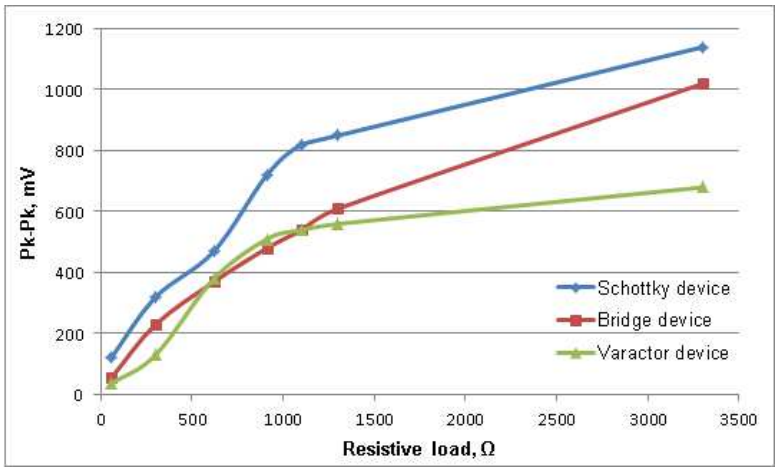

Fig. 32. Device output voltage dependence on the resistive load (wired detection; acoustic power density ≈ 24 mW/cm^2).

the coupling solution with the conductivity from the muscle tissue range has been used to load the devices.

In addition, device output voltage dependence on the load was measured for all three types of devices with devices placed on top of the column of distilled water to prevent loading of the device. Resistive loads were connected in parallel to the devices. Knowing the peak output

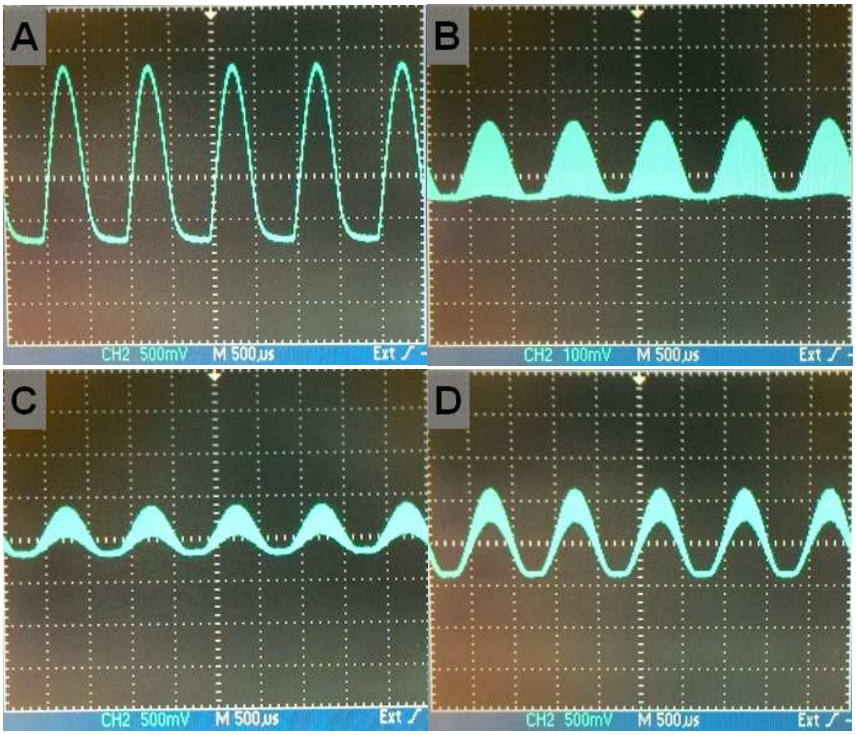

Fig. 33. Bridge full-wave rectifier based device output waveform dependence on the load. (A) Loaded by distilled solution (high load), (B) Load ≈ 300 Ω, (C) Load ≈ 1300 Ω, (D) Load ≈ 3300 Ω.

voltages for every device without any loading attached, Fig. 32 allows estimation of the output port impedances of the given devices. For unloaded Schottky device peak output was 1.52 V, for bridge rectifier device – 2.14 V and for varicap diode device – 1.34 V.

Finally, the changes of waveforms with the load for different devices have been investigated and Fig. 33 demonstrates such results only for the bridge based device.

III. Wired characterization of RC circuits

The results for the experiments involving wired interrogation of RC circuits are shown on Fig. 34, 35 and 36. Fig. 34 presents the results for the RC circuit interrogation using the implant as constant current source (RC circuit has 10 kΩ resistor in series). Spectra for five different cases are presented – four different capacitance values and circuit without the capacitance. Additionally, to be able to assess the accuracy of obtained spectra, the time constant values are marked on the spectra (as 70.7% of the RMS value at 10 Hz).

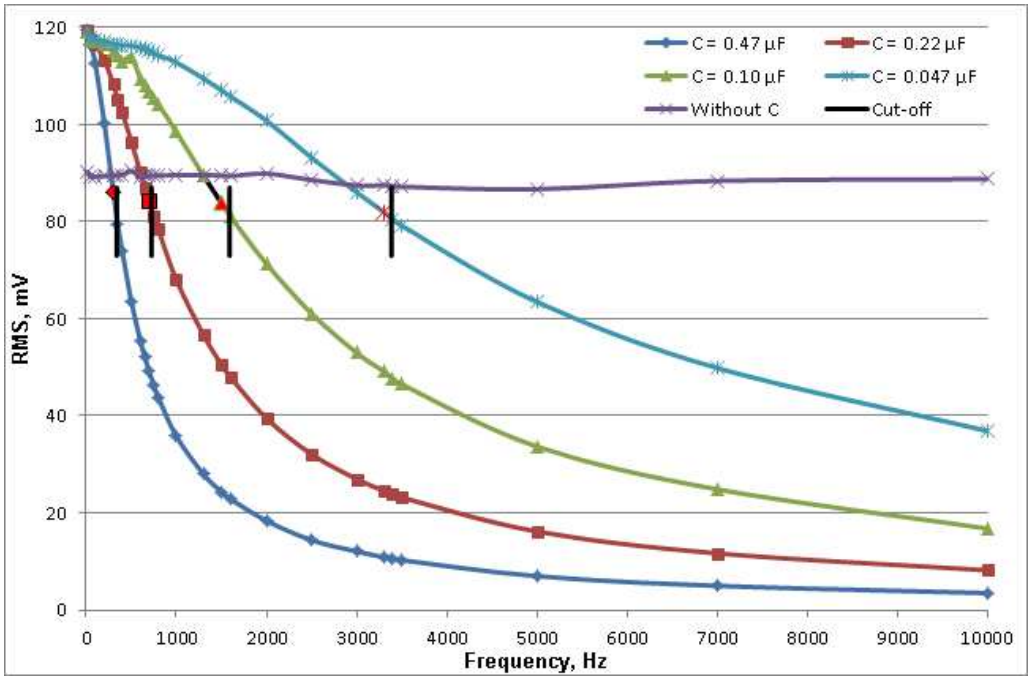

Fig. 34. Voltage RMS spectra for RC circuit with 10 kΩ series resistor (acoustic power density 43 mW/cm^2; wired measurements).

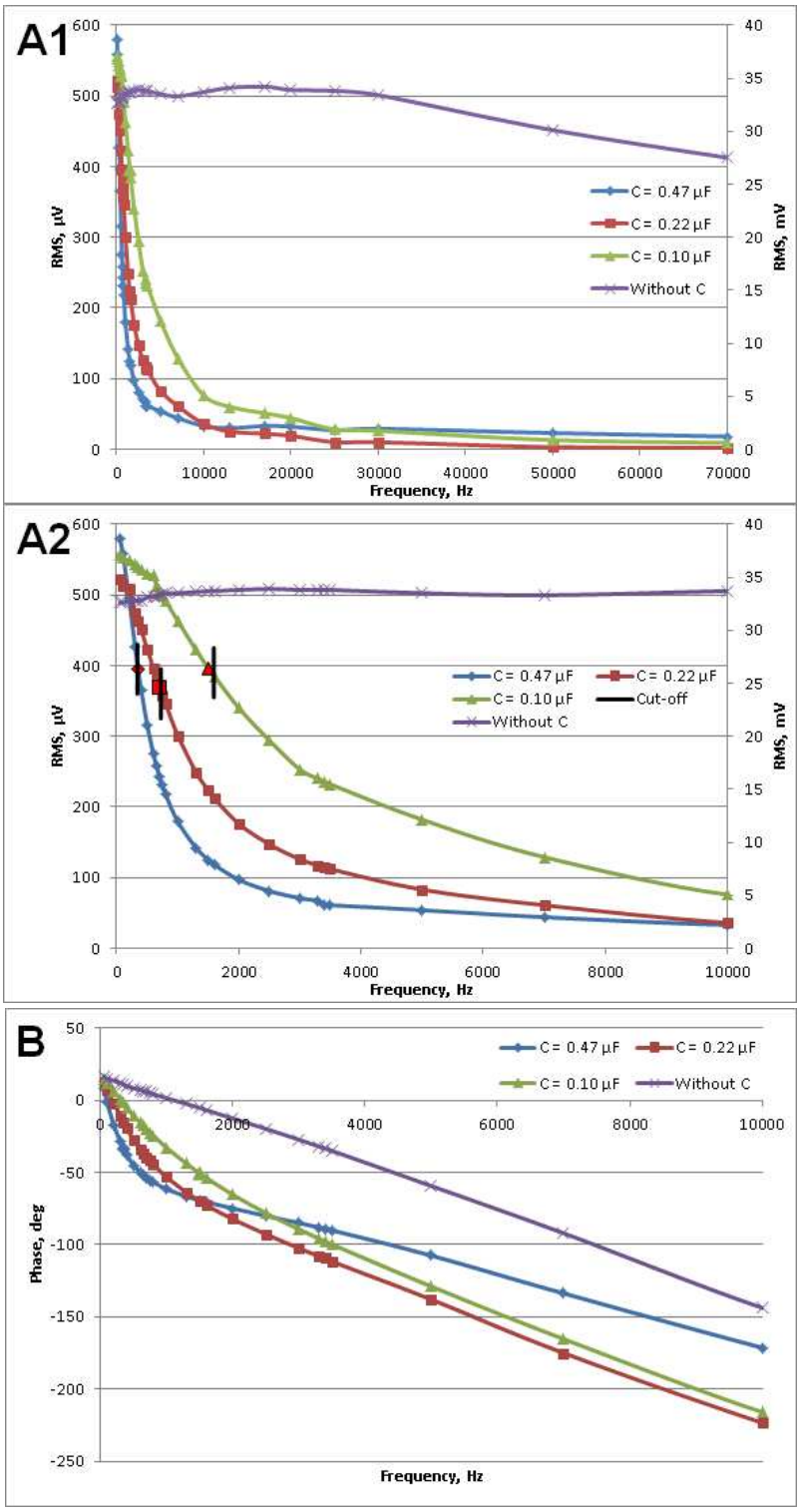

Fig. 35. Phase and voltage RMS spectra for RC circuit experiment (acoustic power density 43 mW/cm^2; wired measurements). (A1) Voltage RMS full spectra for frequency range 10 Hz – 70 kHz, (A2) the same spectra as in (A1) without the higher frequency part (voltages for RC circuit without capacitance on the right Y axis). (B) Phase spectra.

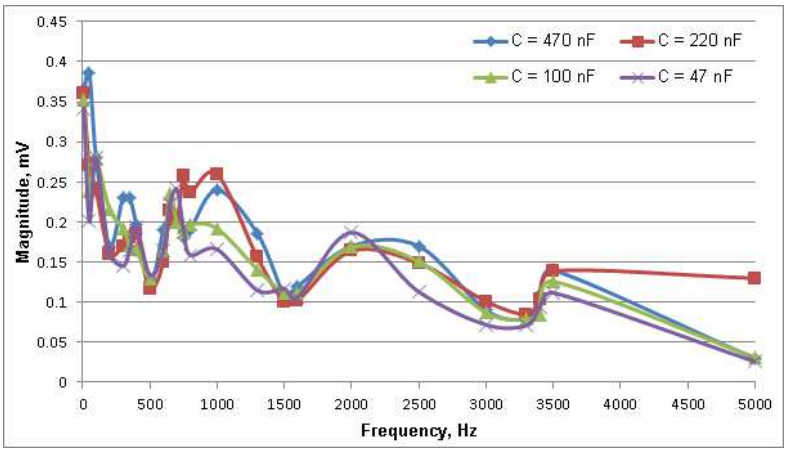

Fig. 36. RC circuit voltage spectra obtained using radio receiver (acoustic power density 43 mW/cm^2; wired measurements through 910 kΩ).

Fig. 35 demonstrates similar results only for the case where neurostimulator is assumed to be the constant voltage source. Fig. 35A1 shows voltage RMS full spectra for all recorded frequencies from 10 Hz to 70 kHz, whereas Fig. 35A2 shows the lower frequency portion of the spectra making possible the analysis of the changes occurring at low frequencies. Additionally, spectra shown on Fig 35A2 have the theoretically estimated and experimentally determined time constants marked on the plots. Fig. 35B shows the phase spectra for the same 4 layouts of RC circuit.

Finally, the results of the RC circuit interrogation experiment using radio receiver are shown on Fig. 36, which shows voltage spectra (up to 5 kHz) for RC circuits with four different capacitance values. The signals of sub millivolt amplitudes shown on Fig. 36 have been detected with device placed on top of the distilled water bath (device output was on the order of 1.5 V).

IV. Wired and wireless characterization of saline solutions

The results of the experiments involving wired and wireless interrogation of the saline solutions with different conductivities are shown on Fig. 37. In case of wired measurements, (Fig. 37A) both phase and magnitude have been recorded at four different baseband frequencies. In case of wireless measurements, only magnitude has been recorded, but measurements for every

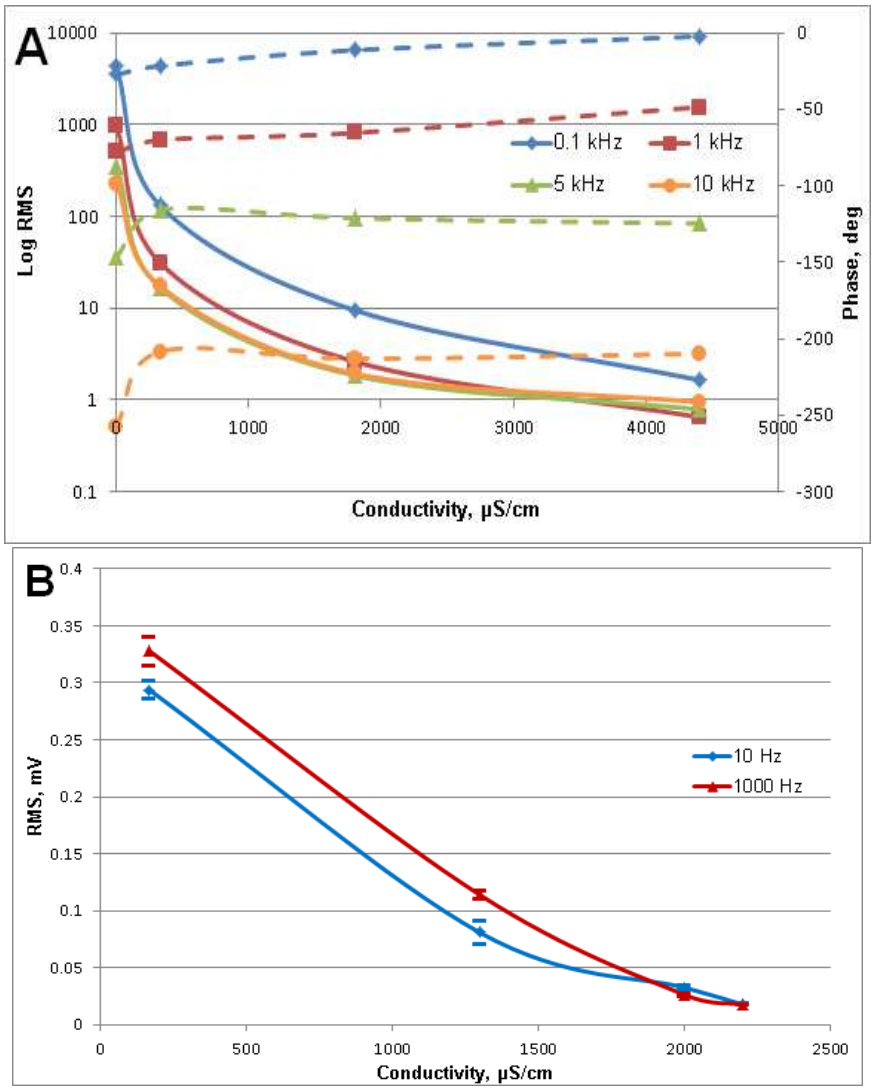

Fig. 37. Results of the wired (A) and wireless (B) characterization of different saline solutions. Solid lines denote voltage RMS, dashed lines – phase.

frequency-conductivity pair have been repeated 25 times to be able to account better for the previously discussed measurement fluctuations characteristic for our system.

V. Wired and wireless characterization of tissue samples

Fig. 38A shows the results of the experiment involving wired characterization of the beef tissue samples with voltage RMS and phase spectra for baseband frequency range of 10 Hz – 7 kHz. Fig. 38B demonstrates the results of the experiment with the same setup, but using remote signal detection.

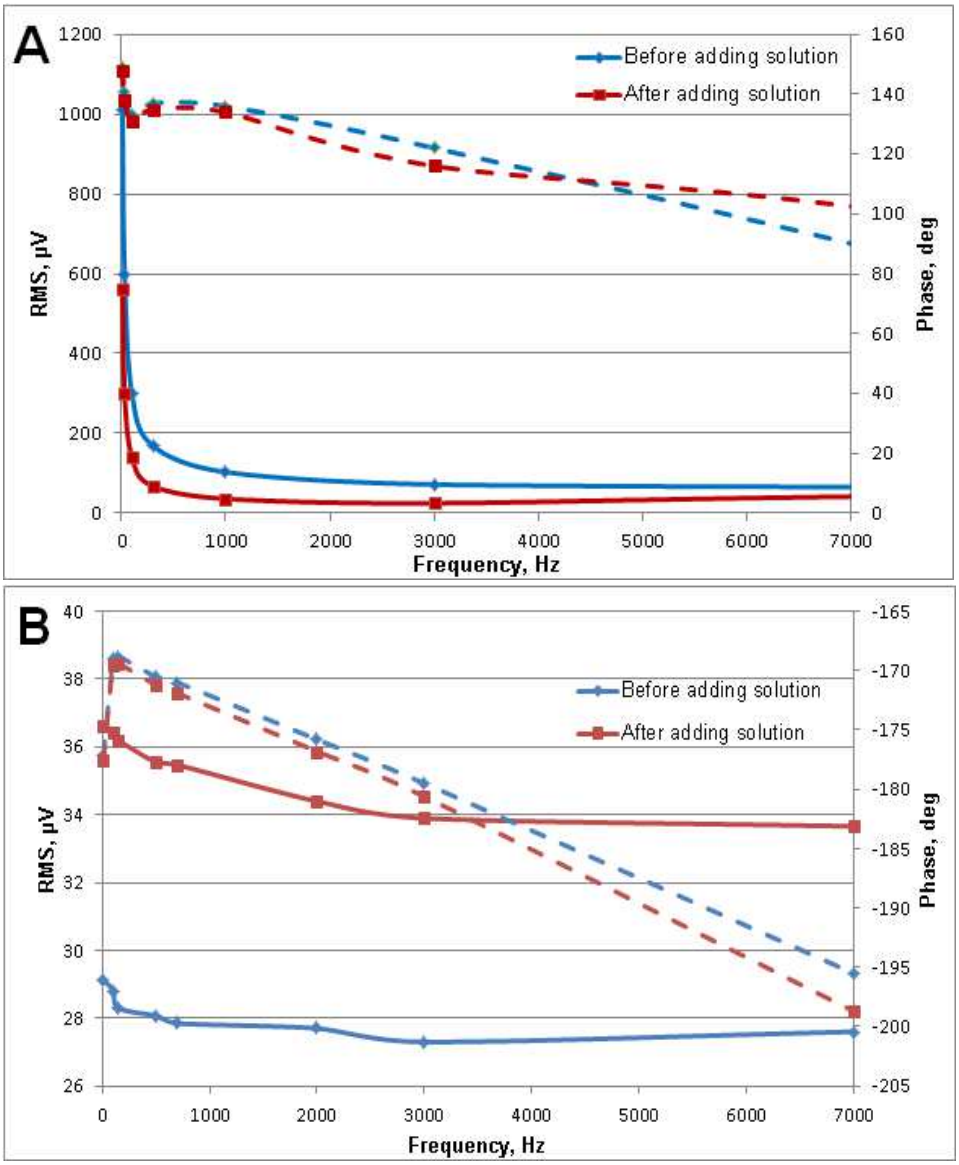

Fig. 38. Wired (A) and wireless (B) magnitude and phase spectra for beef tissue samples (the acoustic power density for wired measurements ~ 40 mW/cm^2, but for wireless measurements ~ 315 mW/cm^2). Solid lines denote voltage RMS, dashed lines – phase.

Furthermore, Fig. 39 demonstrates the results of the two experiments done with device placed into cadaveric rat. The main difference between these two trials done with cadaveric rat is in the number of baseband frequencies used to record the data, which mainly affects the duration of the experiment. Taking into account previously discussed fluctuations of the signal over time, recording duration appeared to be really important in this experiment. Therefore, the second trial

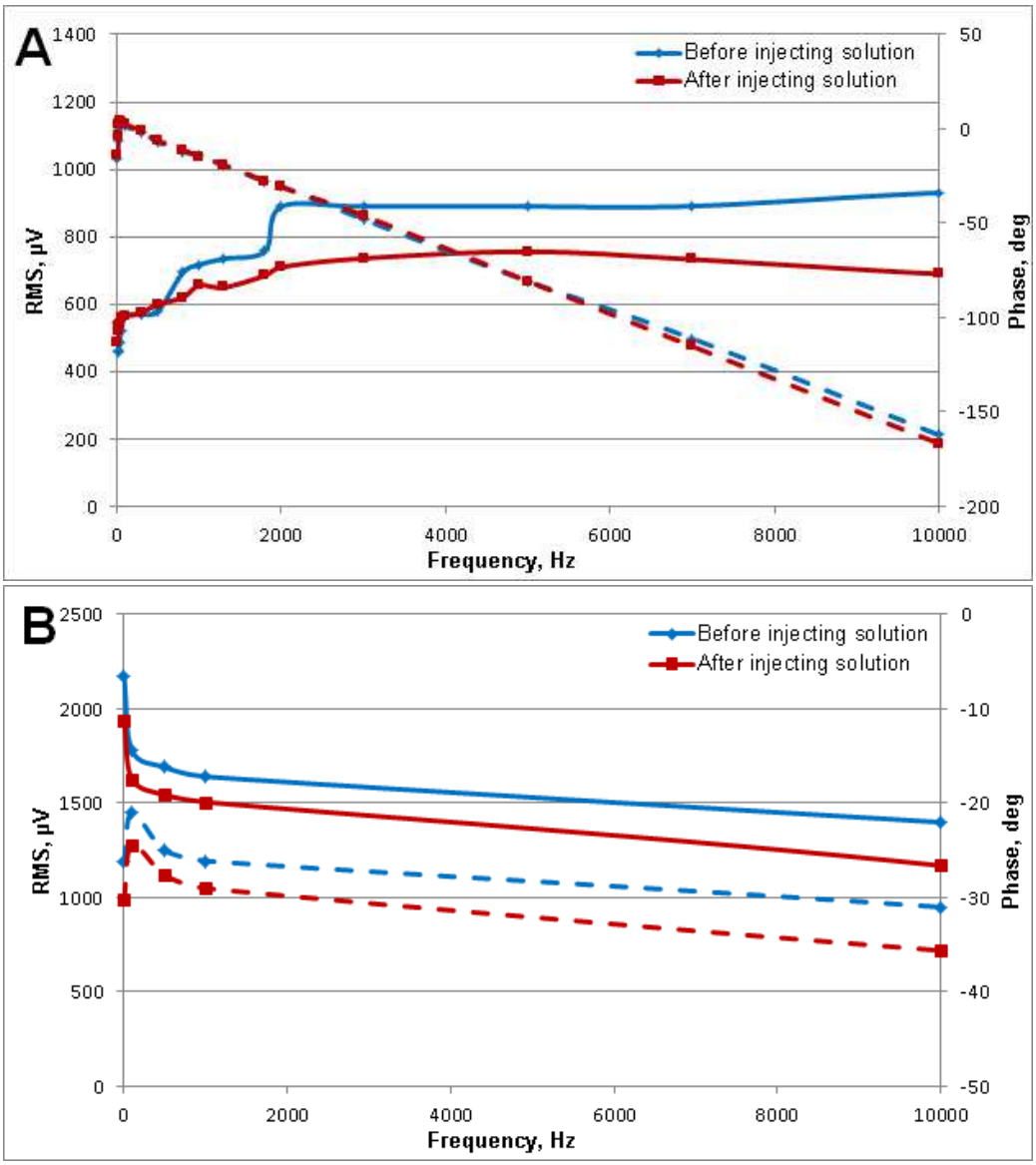

Fig. 39. Phase and voltage RMS spectra for two experiments with device placed into lower limb of the cadaveric rat. Impedance changes have been induced by injection of the saline solutions. Acoustic power density ~133 mW/cm^2. Solid lines denote voltage RMS, dashed lines – phase.

(Fig. 39B) involved recording of the much fewer number of frequencies as the measure of optimization for these fluctuations.

VI. Live animal experiments

As it was discussed in the Methods section, several trials were made in the attempt of getting wireless impedance data from live rat. The first trials involved utilization of highly focused

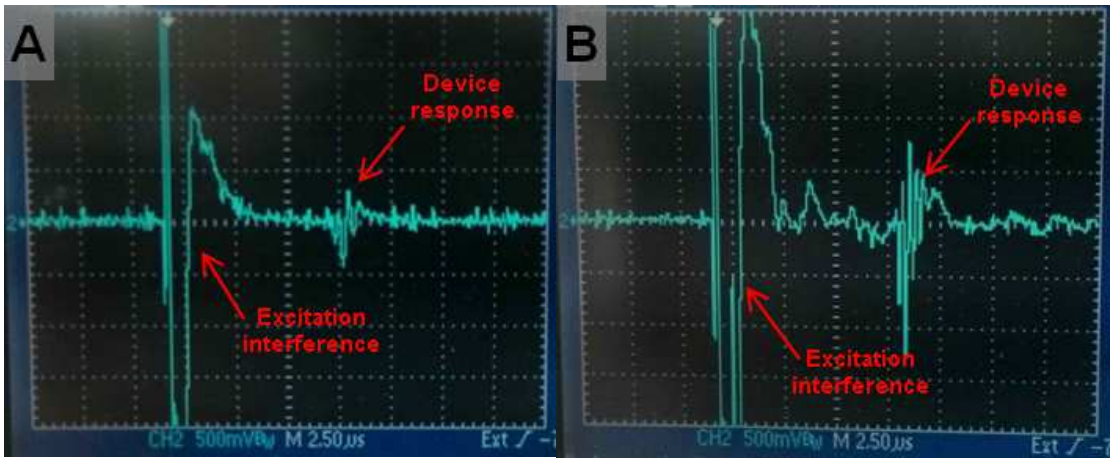

Fig. 40. Photographs of the wirelessly detected responses from the burst excited device implanted in the live rat. (A) Excitation was done using commercial focused transducer, (B) using self-made unfocused transducer.

(focus diameter ~ 7 mm) commercial ungrounded transducer with acoustic power of 315 mW/cm^2. After many attempts as high as 3.3 mV output signal from the device could be wirelessly detected using the surface electrodes and measured with the lock-in amplifier. This signal though was very unstable and the baseline could not be established, which is necessary to be able to do the impedance measurements at multiple frequencies. The details of encountered difficulties will be discussed in the Discussion section.

Following first set of unsuccessful trials rat remained unperturbed for the summer period and next set of trials were done only after 5 months since the implantation (performed using the setup shown on Fig. 19A). The improvements made prior to the new set of trials mainly were aiming at elimination of the crosstalk problem. These improvements mainly involved construction of the new ultrasound transducers (in accordance with structure shown on Fig. 9), as well as introduction of the differential measurement method. Despite the improved measurement setup, baseline could not be established.

These unsuccessful trials have been followed by the measurements performed in accordance with the principles illustrated on Fig. 19B, involving the burst excitation of the device. This approach allowed detection of the output of the device, which is shown on Fig. 40. Signal shown on Fig. 40 is the result of the 60 dB amplification performed by the pulser/receiver, which gives the peak-to-peak magnitude of the signal shown on Fig. 40B to be around 2 mV.

It was important to know whether utilized burst excitation provides sufficient power in accordance with FDA limits and whether power can be increased even further to produce stronger signals. The problem was that previously described method, involving measurements with electrobalance, requires the transducer to be driven using continuous waveform drive, which is not the case with tone burst excitation. Therefore, in order to estimate the acoustic power, additional benchtop measurements have been performed. These measurements involved placement of the device, having very similar characteristics as the one implanted in the rat, in the acoustic beam in the way it is shown on Fig. 12B. The device was first driven using the tone burst excitation, producing 1 V. Next, device was driven using the continuous waveform with drive voltage adjusted in order to achieve the same level of electrical output as in case of the burst excitation. The approximated power density was concluded to be approximately 35 mW/cm^2. The only limitation of this estimation is that determined acoustic power is more indicative of the average power provided by burst excitation, whereas more interesting would be to determine the peak power density (in case of the pulsed excitation, the peak electrical output is mostly defined by the applied spatial peak temporal peak power, but in case of the continuous drive by the spatial peak temporal average power).

CHAPTER 5

DISCUSSION

I. System simulations

Baseband frequency range spectral components. Plots shown on the Fig. 20 and 21 led to the several important observations. One of them follows from the spectra and involves the fact that demodulation produces the baseband signal of the two fold greater frequency than that is produced by the baseband generator. As it was shown in the Results section of System performance characterization, such behavior was not observed on the benchtop. Due to the fact that on the benchtop given specific Schottky diode has not been used, it is possible that this is exactly the way how this type of the diode behaves in real life, but it is also possible that this behavior is just the result of the intrinsic imperfections of the model itself. Still, it must be noted that if this behavior is the case in real world, then it should not have any negative effects on the system performance both in case of neurostimulation and impedance recording. In fact, such behavior can be even beneficial due to the higher interference resistance. Basically, with such behavior of the system we would become shielded against the interference between driving signal and actual output of the device. With our setup such interference was present due to the signal leakage out of the transducer through the sample to the surface electrodes (capacitive coupling), as well as RF (inductive) coupling between the driven transducer and input stage of the detector (lock-in amplifier). The consequence of this is the fact that noise level at the baseband frequency was always higher than at harmonic frequencies. Of course, noise can be dealt with using sophisticated shielding and good grounding, but harmonic utilization for the measurements is much easier approach allowing reduction of the hardware sophistication.

Additionally, as it can be seen from the spectra, demodulation process also results in the generation of the higher order harmonics, which was also observed during benchtop testing. Presence of these harmonics brings additional potential benefit in the form of increased speed of the sample interrogation by applying simultaneously multiple signals of different frequencies and recording responses at all of these frequencies. Of course, as it is done with the conventional impedance measurements, we always can apply complex signal (or even white noise) to begin

with and record full spectrum just from the sample response to this single interrogation signal. The complication here is the fact that we are dealing with really weak signals. As it will be discussed further, the highest signal detected from the live rat was 3.3 mV, meaning that the signal at the harmonic would be below 2 mV (this is an example of the exceptionally good coupling of the highly focused transducer with the implant; on average detected signals were on the order of hundreds of μV and smaller). Basically, the more frequency components we incorporate into interrogating signal, the weaker is spectral power of each component. Therefore, it is really the question of optimization how many frequencies we can simultaneously apply to the sample and still be able to detect signals at each of these frequencies.

In our case, harmonics are always present in case of the demodulation and therefore power is always dissipated, and it makes sense to try to actually utilize this wasted power as much as possible. This is exactly the reason why it was attempted to measure RC circuit spectral response using second harmonic signal. This attempt resulted in the plot shown on Fig. 23C, which is discussed below.

Presence of DC offset. Next observation from Fig. 20 and 21 is presence of the frequency and drive dependent DC offset, which is especially evident in the case of the series diode configuration. As it can be seen from the spectra both on Fig. 20 and 21, DC offset corresponds to the peak at zero frequency, which in some cases has stronger spectral power than the actual baseband (e.g., Fig. 20C2, 20D2 and 21D2). Just as stated before, this leads to the power dissipation and weakening of the signal of interest. As it can be seen from Fig. 21B, 21D1 and 21F, DC offset has time dependent nature. Therefore, by driving the implant using pulsed carrier the DC offset should not present any problems, because any weak DC offset formed during the drive phase would decay when the pulse is turned off.

As it will be discussed further, potentially impedance could be measured also using pulse excitation in contrast to the continuous drive utilized within present work, which would lead to the elimination of the DC offset. Additionally, DC offset can be dealt with by incorporating a capacitor into microdevices, but the problem with this approach lies in the introduction of the higher complexity into device construction and more importantly increase in the device dimensions. This

follows from the fact that in order to allow passage of the baseband signal at least at the frequency of 100 Hz, we would need a capacitor with capacitance of 10 μF (assuming the output port impedance of the device to be around 1 kΩ). Therefore, the most straightforward approach of reduction of the DC offset is utilization of the device construction with the parallel diode configuration.

Diode behavior dependence on the drive. The next observation involves dependence of the level of rectification and overall diode behavior on the magnitude of the driving voltage. In the case of the parallel diode connection, diode starts to provide sufficiently high rectification only at the driving voltage several times greater than the actual diode threshold. Moreover, at the driving voltage level tenfold greater than the diode's threshold the level of rectification with parallel diode configuration is much lower than the level of rectification with the series diode connection driven by the voltage tenfold smaller than the diode's threshold. This is really important, because for neurostimulation and impedance measurement applications we would not want the diode to dictate the level of the power we need to deliver to the device, we want this to be defined only by the threshold level of neural activation and minimal detectable impedance signal still carrying all required information, respectively.

Therefore, the behavior of the diode was further analyzed by looking at the I-V characteristic curves for the diodes (Fig. 22) based on the circuits shown on Fig. 11. From these characteristic curves it can be seen that in case of the diode connection in series, given Schottky diode behaves basically as an ideal diode up until -3 V, i.e., the diode resistance in reverse bias is almost infinite up until -3 V, which exactly corresponds to the reverse breakdown voltage of the used Schottky diode (CDF7621). In case of the parallel diode configuration, diode conducts in both directions at all applied voltages. In this configuration conduction is still greater in the forward direction, but the difference in conducted currents becomes sufficiently high only after reaching voltage levels on the order of several volts. This is exactly the voltage at which rectification was observed in our simulations (Fig. 20). Additionally, the I-V curves were obtained for the different diode loads, but no significant differences in the behavior of the diode were

observed with the changes in the load, as well as with the changes of source output port impedance (results are not shown).

Diode performance dependence on the driving voltage leads to the important conclusion that in the application involving limited voltage supply the diode connection in series might be more beneficial. In case of our microimplants, voltages above 5 V can be easily achieved on the benchtop, but it have not been estimated how high voltages across the device can be achieved in the device implanted in the living subject. Still, the physiological responses, obtained from the live rats as result of the stimulation produced by our implants with the diode in parallel configuration, demonstrate that produced voltages are sufficient to cause rectification and neurostimulation. The problem is though that those results were obtained using the devices with 1 mm thick piezoelectric crystals in them, but for the actual clinical applications such dimensions are a bit on the higher end and we would like to reduce the dimensions down to the 100 μm as discussed in [10] and [11]. With such dimensions achieved voltages can be on the order of magnitude lower than that is achieved with mm size devices and in such cases the diode connection in series can become more favorable than the parallel configuration.

Additional benefit of the series connection also follows from the observation that it basically stops rectifying after reaching certain voltages above 3 V, which would naturally restrict the rectification of applied voltages preventing us from the overdriving the nerves. For the ultimate clinically applicable product such protective control measure would be absolutely crucial in order to obtain an FDA approval.

Finally, there is an additional clearly practical benefit of having the diode in series configuration. Diode connection in series significantly simplifies the construction process of the microimplants by requiring connection only of the one diode's pin to the piezoelectric crystal, whereas parallel connection may require incorporation of the additional wire as is shown on Fig. 6A-2. This becomes even more important when we go down to the smaller dimensions and instead of the packaged rectifiers, used in the present work, utilize the unpackaged die-rectifiers.

It must be noted that all previous work on ultrasonically powered devices has been done using the parallel diode configuration. The reason for that follows from the observations of the

one of the students that this configurations leads to the more efficient performance of the implants, but these observations have not been reported, and any quantitative comparison and analysis have not been performed yet.

RC circuit impedance measurements. Further discussion addresses the results of the RC circuit interrogation using circuits shown on Fig. 10, resulting in the plots shown on Fig. 23, 24 and 26.

Baseband signal based measurements. Fig. 23A shows the results of the RC circuit interrogation by demodulated AM carrier by the diode in two different configurations, as well as circuit interrogation using the output directly from the baseband signal generator. The hypothesis was that sample interrogation using demodulated AM carrier should yield essentially the same spectra as sample interrogation using just the baseband generator.

Such approach of impedance measurements relying on the carrier modulation and consequent sample interrogation using demodulated carrier have not been found anywhere in the literature. Therefore it was essential to demonstrate that this is actually possible. Sample interrogation using just the single generator is essentially the way how this is done in conventional impedance measurements, involving sample electrical impedance spectrum recording by applying one frequency of the interest at the time. In case of the utilization of the high frequency AM carrier, the assumption is that after demodulation sample is interrogated using the baseband signal essentially the same way as it is done in the absence of any carrier.

Consequently, as it can be seen from Fig. 23A, all three plots demonstrate the RC circuit voltage spectra similar to that would be expected from the theoretical point of view, but the plot obtained using AM carrier demodulated by the diode connected in parallel to the source leads to the spectral response, which follows circuit spectral response to the generator excitation much closely than the spectral response obtained in case of the diode connection in series. Discrepancies in both cases can be associated with the different contributions of the circuit loading produced by the diode itself. Used Schottky diode has a Johnson's capacitance of 0.10 pF (at 0 V) and maximal resistance in forward direction of 20 Ω (at 10 mA). Basically, diode is an RC circuit itself and it could be expected that it can distort the actual sample response, because

we are not looking just at the sample response, but at the combinational response of the diode and the sample. Still, as such distortion would be intrinsic quality of the device, it easily could be accounted and calibrated for in real clinical application.

Following better performance demonstrated by the parallel diode configuration, next it was demonstrated how closely RC circuit spectral response to the demodulated AM carrier follows circuit response to the direct interrogation by the generator in cases of the different sample capacitances (100 nF, 220 nF and 470 nF). As it can be seen from Fig. 23B, in all three cases sample spectral responses to the demodulated AM carrier exhibit similar trends to those of the sample response to direct interrogation (e.g., in both cases with decrease in the capacitance the time constant becomes smaller).

Next, as it was discussed before, it was attempted to obtain the RC circuit response using the second harmonic of the baseband signal. As it can be seen from the Fig. 23C, the plot obtained using the circuit with parallel diode configuration demonstrates the reverse trend compared to the expected behavior. Just the fact that this trend is reverse does not imply that harmonic does not carry any impedance information. The only concern is related to the fact that as the baseband is swept, the magnitude changes at the harmonic are much smaller than changes occurring at baseband frequency. In turn, the spectrum obtained from the series diode configuration exhibits signal growth starting from about 7 kHz, similarly as what is observed for baseband signal. This shows that potentially some information about sample impedance could be extracted using the harmonics in case of the parallel diode configuration, but it would require detailed investigation of the trends of impedance plots to be able to account and calibrate for all fluctuations of the signal.

Further, in order to demonstrate that in case of the utilization of AM carrier the demodulation achieved by the rectifier is really necessary, voltage spectra were recorded for the sample interrogation using the AM carrier without demodulation (based on the circuit shown on Fig. 10B). Resulting spectra are shown on Fig. 24 and as it was predicted they do not seem to carry any information about the sample under investigation. Basically, recorded voltages were recorded on the level of system noise, which is simulated in PSpice to make simulations more

realistic. The carrier sidebands though seem to depend on the sample impedance even without incorporating the demodulator into circuit, but voltage differences are at sub-millivolt level, making detection of such changes exceptionally challenging. The benefits and challenges associated with impedance measurements using carrier signal are addressed in the following sections.

Carrier frequency range spectral components. Circuit behavior has been investigated in the carrier frequency region. Fig. 25 shows the Fourier spectra of the absent carrier with sidebands and of the carrier harmonics with sidebands. The absence of the carrier have not been observed during the benchtop testing, but again just as before the reasons for this could be either some unrealistic behavior of the model or more probably this is actually the real behavior of the Schottky diode used in the simulations, which has not been tested on the benchtop.

The absence of the carrier should not have any effects on the performance of the system investigated in this work, which relies on the detection of demodulated baseband frequency volume conducted currents. Still, such behavior would be greatly beneficial for briefly addressed measurement method relying on the signal detection using radio receiver with antenna. Encountered problems associated with radio receiver based detection will be discussed in the section on RC circuit characterization, but the principle is that the carrier emitted from the ultrasound exciter (not the actual microdevice) interferes with radio receiver. Certain techniques might be utilized to eliminate such interference, but having a rectifier with such characteristics as what is observed during the simulations would eliminate this requirement for any further system sophistication. Basically, all the spectral components shown on Fig. 25 are products of the action of the diode, and therefore potentially all of these components can be used for wireless measurements using radio receiver.

Carrier signal based measurements. Consequently, Fig. 26 shows the results of simulation targeting the assessment of the feasibility of wireless impedance measurements using the antenna and radio receiver. The main benefit of this approach is that measurements would become absolutely wireless, eliminating the requirement for having detecting electrodes coupled with the surface of the skin. This could simplify the measurement process for the ultimate user. Additionally, getting rid of the electrodes eliminates the effects of the electrodes on measurement

performance (e.g., changes in electrode coupling with the skin, temperature induced changes of the electrodes). The main question which the results shown on Fig. 26 are trying to answer is if any impedance related changes even occur in the carrier frequency region. Furthermore, additional question is actually related to the spectral component, which would provide the highest measurement sensitivity.

Just as before, the analysis of the high frequency components was done for two circuit configurations and Fourier spectra for both configurations (Fig. 25) exhibit very similar characteristics. The only exception is that the series diode configuration showed to produce stronger higher order sidebands, which ultimately could be used as additional impedance information carriers.

Trying to identify the spectral components providing highest sensitivity, all five main spectral components were used at the beginning (Fig. 26A1 and 26A2). Components exhibiting the gradually changing magnitude with baseband frequency sweep have been chosen to perform the RC circuit analysis. Fig. 26A2 and 26B2 clearly show that despite the opposite changes with frequencies, both diode configurations provide full ability to differentiate between different impedances. Although the parallel diode configuration provides more typical impedance behavior with frequency, if the series configuration would have any additional benefits, we could easily account for the opposite trend of frequency dependence (magnitude increase with frequency versus decrease with frequency). It is important to take into account how big are signal changes with impedance in case when measurements are done using baseband signal and using the carrier-frequency range signals. By looking at results from Fig. 23 and Fig. 26, if capacitance is changed from 470 nF to 100 nF then the magnitude changes, for example, at 1 kHz are the following:

- doubled baseband (2 kHz) signal with series configuration – 29.5%;
- carrier sideband (1 MHz + 1 kHz) signal with series configuration – 0.06%;
- doubled baseband (2 kHz) signal with parallel configuration – 22.6%;
- carrier sideband (1 MHz + 1 kHz) signal with parallel configuration – 1.6%.

These values clearly illustrate that the highest sensitivity can be achieved by measuring the baseband frequency range signals and this sensitivity drops more than by the order of magnitude if we move to the carrier frequency range. Still, it is possible that some circuit alterations can improve system sensitivity and radio receiving based impedance measurement method demonstrates the potential for being useful.

Summarizing points. Some of the conclusions of the simulation experiments are:

- based on the fact that parallel diode configuration demonstrated ability of characterizing the sample impedance in more similar way to sample characterization using just the baseband generator, much stronger baseband signal with this configuration, as well as taking into account the fact that all work previously done in our lab involved devices constructed with parallel diode configuration, for the present study only devices with parallel Schottky diode-to-source configuration have been used (as well as devices with bridge full-wave rectifier and varicap diodes);
- further reduction of the implant dimensions would require maximal optimization of the system, which would also require quantitative benchtop testing of the performance of devices with different diode configurations;
- RC circuit impedance characterization proved to be possible using carrier sideband signals, but further system improvements might be required to improve measurement sensitivity.

II. System performance characterization

Acoustic power dependence on the drive. From the results presented on Fig. 27A it can be seen that, just as it was expected, there is square law relationship between the transducer driving voltage and the acoustic power density produced by this transducer. It can be seen that the highest acoustic power density achieved with the used setup being driven by continuous waveform is still more than two fold smaller than the FDA approved safety limit for the spatial peak temporal average power density. In every instance when specific acoustic power density

used in the experiment is mentioned in this work, it follows from the results presented on the Fig. 27A.

Fig. 27B demonstrates the dependence of the wirelessly detected output voltage RMS on the acoustic power density or essentially the driving voltage of the transducer. Again, as it could be expected, this relationship is fairly linear. It demonstrates our good ability to control the actual currents delivered to the nerves by controlling the acoustic power applied to the implant.

Analysis of signal variability. Results shown on Fig. 28 give insights into instabilities associated with our devices. Of course, the time duration investigated in the experiment, which produced the results shown on Fig. 28A and involved wired signal detection directly from the device, is a bit to the higher end than what would be used in real life for impedance measurements. Still, the additional clinical application of the devices discussed within present work is pain relief, which might require as long stimulation times as 10 minutes. In the case of wired detection after 10 minutes, the output voltage of the device dropped by about 7%. Additionally, with stimulators presently available on the market for pain relief, patients actually have an option of leaving them on for all the time and often times this preference is dictated by the patient readiness to tolerate the buzzing sensation instead of the pain. Furthermore, it must be emphasized that in both experiments producing the results shown on Fig. 28 the device was remained absolutely undisturbed and firmly fixed in the focus of the transducer. This would not be the case with the patients and actual clinical applications, because no matter how well you would fix the external exciter, the relative motion of the exciter and implant still will be present, especially if we are talking about the applications on the extremities. This fact highlights the importance of the continuous feedback for the stimulation applications, which will be reinforced later in the discussion. This feedback would allow continuous adjustment of both the beam focus and driving voltage, ensuring the stable output of the stimulatory currents.

In case of the wireless detection from the cadaveric rat (results on Fig. 28B), variability of the output RMS is even higher than in case of the wired detection. The highest observed change of 80% was observed after 10 minutes during the trial #2 with 1 kHz baseband signal. This can be associated with the fact that we moved to the more realistic testing setup, in which the relative

positioning of the device and transducer cannot be controlled so well as during the experiments with saline solutions. There is a number of factors which can contribute to such variations of output:

- changes in the coupling between the transducer and device (despite all the attempts to prevent motion of the system components, some microdrift still could be present);
- the heating of the sample (although, in this cases care has been taken to prevent overdriving of the transducer, causing the heating of the transducer itself, which then can be transferred to the sample; additionally, despite the fact that some time was spent letting the cadaveric rat body to warm up after getting it out of the fridge, some internal temperature fluctuations still could be present; heating caused by the ultrasound itself is not considered here due to the low power density levels utilized to perform the experiments);
- the fluctuations (including temperature induced ones) in the equipment used to drive the transducer;
- variations in the sample or device electrode impedance (this definitely was the case in the experiment involving wired output detection, because the hydrolysis of the water around the device electrodes could be observed; this is also related to the previous discussion of temperature changes). Impedance variations is the most probable contributor to observed changes mainly due to the fact that it was attempted to eliminate and account for all other factors, but it is difficult to account for impedance variations due to the changing nature of the impedance. Therefore, it can be argued that this experiment demonstrates the impedance sensitive behavior of the microdevices.

The notion of hydrolysis leads to the important problem of charge balancing, which would need to be dealt with before our devices can become clinically applicable. The most straightforward solution involves incorporation of the charge-balancing capacitor into the device, which must be selected carefully to prevent significant increase in the dimensions of the devices, as well as retain the ability of tissue interrogation at very low baseband frequencies.

Additional observation from Fig. 28A is the fact that the carrier frequency producing weaker output also results in the lower fluctuations of the output over time. This was often observed during the experiments performed in the process of this work, where reduction in the output voltages of the devices was also typically associated with less distorted waveforms than that was observed in the cases of higher outputs (results not presented).

Moreover, from Fig. 28B it can be noted that overall the variations of the phase over time are weaker than variations of RMS values (except the trial #2 at 1 kHz, for which both RMS and phase exhibited significant changes). This observation can suggest that the main cause for the fluctuations lies in the impedance changes of the device electrodes or the sample, because as it could be noted from [50] the highest phase changes occur in the high frequency region (with peak around 90 kHz), whereas the magnitude sensitivity to the changes starts to roll off exactly around the 100 kHz. If this assumption of the reasoning for output fluctuations is correct, then it provides the first insights into very high sensitivity of these microdevices to the impedance changes (although of course it is not known how close are all the impedance changes occurring during these experiments to the actual impedance changes associated with the physiological events).

Final remark about the results of the output variability over time emphasizes the importance of these results for all the rest of the experiments performed within this work. As it can be seen from Fig. 28B, basically obtained curves for a single frequency have very similar trends to the actual impedance spectra and precautions must be taken to prevent misinterpreting the data and accepting the spectral plots demonstrating the falling trend as the real impedance characteristic curve. It can resemble a problem especially in some experiments lasting for tens of minutes due to the lack of the recording automatization (all the numbers were typically recorded by hand), as well as additional time required for the lock-in amplifier to lock into new baseband frequency (required time depends on the selected time constant defining the range around the baseband frequency we lock into). As the matter of precaution, many measurements, results for which are shown within this work, involved continuous referral to one specific frequency to make sure that the output at this reference frequency have not change during the time while data was collected for the other frequencies (for example, experiment can start by looking into voltage at 1

kHz, then data can be collected for 5 other frequencies and 1 kHz frequency is checked again. This pattern repeats after looking into each set of 5 different frequencies). For example, in case of the experiment aiming at the analysis of waveform characteristics, as well as device output dependence on the load (results shown on Fig. 31, 32 and 33), the “cheating” approach was used. It was desired to maintain the outputs at the same level throughout the experiment, but too significant output fluctuations were observed (on the order of 10% within 1-2 minutes). Therefore, for many measurements the position of the device relative to the transducer was continuously adjusted (typically by ~ 1 mm in X, Y or Z direction) to maintain the output stable.

Volume conducted electrical response detectability dependence on the distance. Fig. 29 presents the results of the assessment of signal detectability depending on the distance between the implant and detection electrodes. Of course, the applicability of these results is fairly limited because measurements have been done in the water bath, offering us full control over the acoustic coupling between the implant and transducer (e.g., with such setups in cases of too low output it typically can be easily corrected by rotating the device, whereas with live subjects such control measures are much more restricted). Still, it can be seen that even in the case of good acoustic coupling between highly focused transducer and device, the detected output voltages at baseband frequencies are on the order of sub-millivolts (in reality detected voltages were much higher due to the crosstalk between the transducer and detection electrodes resulting in the 0.29 mV of background noise, which was subtracted from all measurements before plotting them). Despite fairly weak signal, it still was detectable up to 36 mm. Taking into account that in reality applied acoustic power could be increased by more than 15 times, as well as with live subject electrode-device relative positions could be better suited for more efficient detection (as it can be seen from Fig. 13, the detection electrodes were oriented perpendicularly to the device electrodes, which is not perfect orientation in case of the detection at long distances, it is perfect orientation only at 0 mm distance when the electrodes are on the same line with the electrodes), the maximal achievable distance still allowing detection should be easily increased even further. Still, even the depth on the order of 36 mm is fairly close to that is required for the applications in PVD (as it was stated in [2], the sciatic nerve in humans in lower limb is 50 mm or less away from

the surface). Finally, this was the first experiment where the crosstalk between the transducer and electrodes started to be considered.

Burst pulse excitation. Fig. 30A presents the tone burst pulse train. This excitation pattern can be used for neurostimulation in a similar way as it is shown on Fig. 7B (as well as on Fig. 19B). Fig. 30B illustrates the response of the bridge device to such type of excitation. The response waveform detected using the wired pickups clearly exhibits the ring-up and ring-down phases, with the ring-down phase longer than the ring-up phase, which is defined by the quality factor of the receiver. In this case, the ring-down of the device is fairly short, indicating that the piezoelectric receiver in the implant is highly damped by the solution and epoxy. Fig. 30B also illustrates the important benefit of the pulse excitation versus the excitation using the continuous waveform. In case of the pulsed excitation there is a transient time delay between the excitation induced crosstalk and the actual response of the implant. This is caused by the fact that it takes much less time for the electrical signal to pass to the detection electrodes (or in this case the wired pickups) than what it takes for the acoustic waves to reach the implant, perform piezoelectric conversion and reach the detector. This driving modality allows clear separation between device output and excitation artifact, making it very desirable to use similar type of pulsed excitation also for the impedance measurements.

Characterization of different device types. Fig. 31 demonstrates a set of waveforms and spectra of these waveforms, produced by the different types of devices, being loaded in the similar way to that we expect them to be loaded while being implanted in tissue.

Piezoelectric material without rectifier. Fig. 31A illustrates the case of simple piezoelectric material (PZT-5A) without any rectifier attached. Just as it would be expected, on the spectra we can see the carrier (without sidebands due to the low modulation frequency of just 1 kHz and broad frequency span of 5 MHz) and no signs of baseband. There are some fairly strong peaks in the baseband frequency region, but they probably are caused by the system imperfections. As these artefacts are not present at the same frequencies for other types of devices, they must be caused by the piezoelectric material itself, probably due to the fact that piezoelectric material does not perfectly recreate the supplied driving waveform. One of the reasons for that is the fact

that the water bath used to obtain these waveforms (Fig. 12A) contains a lot of reflections, meaning that the piezoelectric receiver actually receives the more complex waveform than what is produced by the exciting transducer. This fact could be easily confirmed by observing how the waveform changes while the device is moved around the ultrasound beam. For instance, the level of modulation could change from 100% down to 50% simply by moving the device by several millimeters. Fortunately, this is just the imperfection of the used setup, which we must be aware of, but in the tissue we would not have such reflection problems.

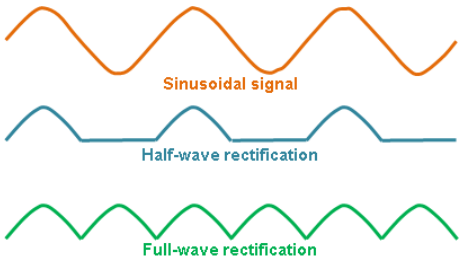

Fig. 41. Half-wave and full-wave rectified sinusoidal signal in case of the ideal rectification.

Schottky diode based device. Fig. 31B presents the waveform and spectra obtained for the Schottky diode based device with the parallel diode configuration. This time spectra show not only the carrier at 850 kHz, but also the demodulated baseband signal at 1 kHz, as well as the harmonic at 2 kHz. Baseband frequency region also contains a lot of the other spectral components, which represent the natural artifacts caused by both the reflections discussed above and the actual rectification produced by the diode (rectification deform the waveform and we cannot expect it to contain just the carrier and baseband with harmonics). All these additional spectral components basically dissipate the power, leading to the weaker baseband signal of interest. Therefore, we would like to achieve as perfect rectification as possible. The ideal half-wave rectified waveform what we would like to obtain using Schottky based device is shown on Fig. 41. It must be noted that even the waveforms obtained using the PSpice simulations (Fig. 20) did not exhibit perfect rectification; instead waveforms observed during the simulations fairly closely repeat the waveforms observed in the experiments. Furthermore, the level of rectification achieved using the Schottky diode is significantly dependent on the load. The most perfect rectification maximally close to what is shown on Fig. 41 was observed for the devices placed into distilled water without any load attached (results are not shown, but the level of rectification is very similar to the shown on Fig. 33B).

Bridge full-wave rectifying device. Fig. 31C presents the waveforms and spectra obtained for the full-wave rectifying bridge based device. In this case the high frequency portion of the spectrum contains not only the carrier, but also the harmonics of the carrier, which as it was discussed in the simulations section, potentially can carry the impedance information in its side-bands and be detectable using the radio receiver. The baseband frequency region in this case also contains much greater number of harmonics (at least three harmonics are present). As it can be seen from the actual waveform, the level of rectification in this case is much higher than in case of the single Schottky diode. This was absolutely expected, because we basically have four Schottky diodes instead of the single one. Therefore, the strength and number of harmonics potentially can be associated with the strength of the signal produced by the device and the level of rectification. This correlates with the observations previously done, but never reported by another student in our lab, who proposed to use the surface electrodes detected harmonics for the estimation of device output in the tissue.

Additionally, from the spectrum on Fig. 31C3 it can be noted that the strength of the artefacts is much weaker than what was observed for the simple piece of PZT or Schottky based device, which again can be linked to the better rectification achieved by bridge full-wave rectifier. Moreover, by comparing the simulations results (Fig. 20 and 21) with the results obtained from benchtop testing of the bridge device (Fig. 31C), it can be noted that the waveform produced in case of the full-wave bridge rectification, is very similar to that was observed for the series diode configuration. There is even more important similarity between the simulation results for the series diode configuration and experimental results for the bridge devices. In both cases fairly good rectification was still present even at voltages significantly below the threshold, which is especially surprising for the bridge diode, because taking into account the fact that bridge rectifier contains actually several diodes instead of the single one, it would be expected to be required to reach higher voltages to get any rectification. Such behavior was observed both for the bridge devices with attached resistive load and devices loaded only by the solution. Even at voltages below 200 mV the bridge was providing much higher rectification than the single Schottky, which at such voltage barely provides any rectification at all.

Fig. 33 demonstrates the waveforms produced by the bridge based device at various loads. The load of 300 Ω drops the voltage below 200 mV, but rectification remains almost 100%. It was also observed that by dropping the voltage down to 50 mV by adding the 56 Ω resistive load, the level of rectification still remains almost 100%, with slight deformation of the waveform (results are not shown). Overall, before performing any experiments the full-wave bridge rectifier was considered the perfect choice offering the best rectification characteristics, having the main disadvantage of much higher dimensions, as well as higher construction complexity and expected higher threshold. After performed testing, additional benefit of the full-wave bridge rectifier was observed in the form of its good rectification characteristics even at the voltages below its threshold. Still, the dimensions remain serious problem and taking into account similarities between the behavior of the single Schottky diode in series configuration observed in the simulations and benchtop testing results for the bridge devices, it would be useful to look both into benchtop behavior of the series diode configuration and behavior of the full-wave bridge rectifier in the simulations.

Varicap diode based device. Fig. 31D demonstrates the rectification performance of the varicap diode based device. As it can be seen the varactor diode demonstrates weaker rectification than the Schottky diode, the same spectral content in the baseband frequency region and for unclear reasons slightly noisier carrier frequency region. Potentially the varicap diode with better rectification characteristics could be found, but even observed level of rectification demonstrates the potential for varactor based device to incorporate triple functionality – neural recording, neurostimulation and impedance measurements. The idea of neural recording using varicap based devices relies on the capacitance dependence of the varactor on applied bias. Therefore, the capacitance of the varactor should depend on the presence or absence of the neural spikes. Changes in capacitance cause the changes in the tuning of the device. Consequently, such device can be shock excited by tone burst with consequent recording of its decaying response. Depending on the tuning of the device, this decaying response will change, i.e., number of ring-down pulses will vary depending on the presence or absence of neural activity. During this work only the RF powered varactor devices have been tested with minimal

detected signal of 5 mV (results not shown), which potentially could be reduced even lower by eliminating all the sources of noise and improving the detection methods (e.g., using highly tuned antenna with radio-receiver).

Alternatively, varactor based devices could be used to convert the amplitude and phase carrying impedance signal into-ring down signal, which is more desirable due to the amplitude dependence on many different factors (e.g., surface electrode coupling with the skin, relative position of the surface electrodes, implant and ultrasound exciter coupling). Basically, the perfect system would involve excitation of the varactor based implant using chopped AM carrier, which generates tissue interrogating currents passing around the device. These currents would change the capacitance of the device itself in accordance to their amplitude, which is again dependent on tissue impedance. Then the next excitation wave comes in only in the form of tone burst. The resulting ring-down signal then would be dependent on the currents produced by the device itself, which in turn are dependent on tissue impedance. Ultimately, the ring-down signal now would contain the impedance information and this signal would be immune to the factors affecting measurements of the AM signals. The key difficulty would be to make such recordings possible using the single one device, but having two devices placed relatively close together (e.g., one with simple Schottky and another varicap based) would make such measurements much easier, but introduction of simultaneously multiple devices would be acceptable only if they can be made sufficiently small, preventing undesirable damage of the tissue.

Device performance with loading. In addition to the previously discussed waveform changes associated with device loading (Fig. 33), the actual dependence of the device output peak-to-peak voltage on the resistive load was investigated with the results shown on Fig. 32. For the Schottky and bridge based device the relationship is fairly linear. For the Schottky and varactor based devices the curves exhibit the breaking points around the output port impedance of the devices (both for varactor and Schottky based devices it was estimated to be around 1 kΩ), but for the full-wave rectifying device the output port impedance was estimated to be around 3.3 kΩ (the breaking point for the bridge device is not shown because the highest resistive load used in the experiment was 3.3 kΩ). The importance of the output port impedance follows from the fact

that it defines the load a specific device is capable to drive and we would like to have the output port impedance of the device to be as close as possible to the tissue (load) impedance, because although voltage is shown to be increasing with the increase in resistive load, what we are interested in is actually the power produced by the device. Therefore, despite the fact that we would like our devices to be as simple as possible, if there would be a really significant benefit of having higher load on the device, it is possible to incorporate the resistor into device.

Summary on system performance characterization. Some key observations, findings and conclusions of this section on System performance characterization are the following:

- the acoustic power density produced by the ultrasound transducer exponentially depends on the transducer driving voltage;
- the relationship between the acoustic power density and device output voltage is almost linear;
- device output measured on the benchtop exhibited significant (as high as 80% within 10 minutes) fluctuations over time. These fluctuations arguably can be considered associated with impedance changes and must be mainly taken into account while performing measurements using given specific setup utilized in this work;
- even at acoustic power densities more than 15 times smaller than approved FDA limit, the signal from the device is still detectable as far as 36 mm in homogenous media made of saline solution;
- device pulsed excitation is associated with additional benefits both for the stimulation and monitoring applications – it allows achieving higher spatial peak powers while maintaining the same level of temporal average power and it allows separation of the crosstalk and actual signal of interest;
- the full wave bridge rectifier provides the best rectification characteristics, whereas the varactor diodes – poorest rectification;
- varicap diode based device exhibit the potential for triple functionality – neural recording, neurostimulation and impedance monitoring;

- full bridge rectifier demonstrates the performance similar to that was observed during the simulations of the circuit with single diode series connection configuration. Taking into account benefits associated with usage of the single diode, diode series configuration would need to be further investigated;
- the output port impedance and impedance of the tissue the device will be implanted to must be carefully considered to ensure their approximate equivalence for maximally efficient power delivery to the tissue.

III. Wired characterization of RC circuits

RC circuit characterization using constant current source. Voltage RMS spectra shown on Fig. 34 demonstrate the ability of the neurostimulator to interrogate RC circuits in case of the wired signal detection and constant current source. As criterion of accuracy the cut-off frequency was used. The device allowed estimation of the cut-off frequencies with the maximum error of 6.1%. Additional important observation is the stability of the device output in case when it is loaded only with resistive load. The maximal change of the voltage RMS across the frequencies is 4%, which can be associated with previously discussed naturally occurring output fluctuations over time. This implies that device the capacitance of the device itself (the electrodes, the PZT, the diode) do not have significant contribution to the load created by the sample.

RC circuit characterization using constant voltage source. Fig. 35 demonstrates the voltage RMS and phase spectra for the case when device is assumed to be the constant voltage source. Just as before, device clearly demonstrates the ability to differentiate between different RC circuits, as well as obtain the spectral characteristics of the circuits. In this case the maximal error for the estimation of cut-off frequency was on the order of 5% (the fact that the measurements are done starting not from the 0 Hz, but from the 10 Hz, makes slight contribution to this error). In this experiment in the case of absence of the capacitor in RC circuit the voltage RMS exhibited as high as 15% drop. Still, as this happens only when we go to the frequencies above 50 kHz, this must be associated with the limited bandwidth of the transducer. No matter how broad bandwidth the transducer has, as the driving frequency moves away from the central

frequency the transducer is tuned to, the output of the transducer will gradually roll off. In our case, the carrier remains unchanged having the same frequency maximally close to the frequency the transducer is tuned to, but the modulation caused sidebands move further away from the carrier as we sweep the baseband frequency. Therefore, as these sidebands move further away, the acoustic output of the transducer at these sideband frequencies (carrier frequency +/- baseband frequency) also decreases, leading to the decreased electrical response of the implant at these frequencies. We are essentially measuring the output of the device at demodulated sidebands and if device response to these sideband frequencies decreases, our readings at demodulated baseband frequencies will also change.

As PZT in the implant is also essentially the ultrasound transducer, it's tuning curve also have a bell shape and essentially its output can roll off as the excitation frequency moves away from the frequency the PZT is tuned to. Basically, the limited baseband of the piezoelectrics in exciter and receiver limits the frequency range we can work with. In the case of the used exciter-receiver (transducer-device) combination this range is essentially limited to about 10 kHz, which can be absolutely sufficient for the magnitude measurements of the impedance, because above this frequency theory predicts mainly phase changes with low magnitude sensitivity to physiological events.

Additionally, we could argue that knowing specific baseband characteristics of the piezoelectrics being used, we can account and calibrate for these changes. Of course, in such case for effective calibration it would be necessary to account for the fact that device will be damped by the tissue, which actually should make the baseband of the device only broader.

Finally, it also must be noted that in the experiments it was observed that piezoelectrics also exhibit harmonic behavior, i.e., the output is highest at certain resonance frequency of the transducer and at harmonics of this frequency. As efficiency of the device drive and therefore the output of the piezoelectric depends on the coupling between exciter and receiver, it could be observed that depending on the receiver position in the beam, the highest electrical output will be obtained at different carrier frequencies. For instance, in some cases the highest output could be obtained just as expected at the resonance frequency of the transducer, but after moving the

receiver into slightly different position the peak output could move actually to the harmonic frequency.

In case of the phase, it can be seen that significant changes occur in case of the absence of capacitor in the circuit, but still by looking at the phase spectra, different RC circuits can be easily differentiated.

RC circuit characterization using radio receiver based detection. Finally, a number of unsuccessful trials have been made to obtain impedance spectra for RC circuits using radio receiver for signal detection. From Fig. 36 it can be noted that, just as in the case of simulations, the carrier sideband signals measured using radio receiver exhibit the typical falling trend expected for frequency dependent impedance, but signal contains too many fluctuations to be able to differentiate between different RC circuits. The key problem identified in the process of measurements was associated with used radio receiver. WinRadio G305e incorporates such function as automatic gain control, which provides stable demodulated signal (stable sound) despite any variations in the amplitudes of the sidebands. In our case we are specifically interested in the changes in amplitudes of the sidebands, because these changes are associated with impedance changes. From Fig. 36 it can be clearly seen that the falling trends of voltage spectra contain many jumps in magnitude, which can be associated with automatic gain control trying to maintain the stable level of decreasing sideband magnitudes. Being unable to switch off the automatic gain control, chosen radio receiver cannot be used for such types of measurements.

Additional difficulty was associated with differentiation between the signal from the device and crosstalk. In this context the best performance was observed in case of the full-bridge rectifier based devices, which produce strong carrier harmonics. The crosstalk level at the carrier is much stronger because the transducer is driven by high voltage at carrier frequency, whereas the crosstalk at carrier harmonic frequency is associated only with imperfections of the used amplifier driving the transducer. The harmonics produced by the driving amplifier could be filtered out, allowing detection of the clean harmonic using radio receiver.

The problem is of course that in the simulations the Schottky diode connected in parallel showed weak system sensitivity with carrier harmonic and harmonic sidebands. Simulations also demonstrated the ability of the Schottky diode to eliminate the carrier. The same elimination could also be attempted to achieve by feeding the carrier reference into radio receiver and subtracting it from the carrier measured from the device. Finally, it must be noted that during performed experiment the unturned antenna has been used to determine that the output of the device generating 1.5 V could be still detected as far as 120 mm away (mainly by listening to the sound produced from demodulated sidebands), providing μV level signal. This demonstrates high sensitivity of radio receiver based approach, but in a real situation having the microdevice implanted in the body such distances would probably not be achievable.

Summarizing points. The main observations made from the RC circuit analysis experiment can be summarized in the following points:

- acoustically powered neurostimulator demonstrates the same ability to perform impedance spectral characterization of the RC circuit as the circuits simulated in PSpice, meaning that if impedance characterization will show to be not possible at further stages of the work, this must be associated with the limitations introduced by wireless detection;
- both magnitude and phase spectral curves obtained using neurostimulator demonstrate the trends predicted by theory;
- neurostimulator showed to be able to differentiate between different RC circuits both by phase and magnitude;
- the capacitance of the neurostimulator itself does not have significant contribution to the sample under investigation, leading to the stable device voltage output under resistive load;
- it has been shown that the neurostimulator based constant current source does not have advantages over constant voltage source. Whereas the benefits of having a constant voltage source include the more simple device construction (no need in resistor) and higher currents delivered to the tissue;

- impedance measurements using a radio receiver for wireless signal detection have been shown to be potentially feasible, but further investigation is required using radio receiver without automatic gain control, as well as additional measures for carrier crosstalk suppression must be employed;
- the bandwidth characteristics of the piezoelectric exciter and receiver must be taken into account when analyzing the spectral response of the sample.

IV. Wired and wireless characterization of saline solutions

Wired characterization of saline solutions. In case of the wired measurements (Fig. 37A) it can be seen that device can easily differentiate between the solutions of different conductivities using the magnitude information, whereas phase has shown to allow differentiation between different conductivities, but results are not consistent. The magnitude measurements showed the ability of differentiation at all 4 analyzed frequencies, having the expected falling trend with increase in the conductivity of the sample, as well as voltage undergoes a decline with an increase in baseband frequency. This trend of frequency dependence is broken if we look at the results at 5 kHz and 10 kHz, because voltages at 10 kHz were slightly higher than at 5 kHz, but overall they are very similar just as would be expected. Based on the previously mentioned theory and shown results, as the frequency goes up impedance magnitude differences for different samples become really small. In case of the phase, at 0.1 kHz and 1 kHz the trend was that phase was increasing with increase in conductivity, whereas at 5 kHz and 10 kHz this trend was broken and less consistent dependence can be observed. This result can follow from the fact that as it was mentioned before the sensitivity of the phase to the impedance changes becomes greater with the increase in frequency and frequencies below 10 kHz might be not sufficiently well suited for the phase-based monitoring of impedance changes. Still, the observed phase and magnitude trends clearly illustrate the system sensitivity to the electrical characteristics of the media the device is placed into, with the highest sensitivity observed at the lower ranges of conductivities below 1000 μS/cm. The conductivity of a 1000 μS/cm is exactly approximate beginning of the range of conductivities characteristic for the muscle tissue, which is of the

interest in case of the peripheral vascular disease. As it was discussed earlier, the sensitivity of the device would be dependent on the output port impedance of the device, which could be set to desired range depending on our application by incorporating the resistor or changing the characteristics of the device electrodes (dimensions and material).

Wireless characterization of saline solutions. In case of the wireless measurements almost the same trends have been observed, including voltage RMS decrease with the increase in conductivity, highest sensitivity at lower range of conductivities (in this case in the range below 1500 μS/cm) and some inconsistencies in the results at higher conductivities. The difference between the results shown at Fig. 37A and 37B is in the fact that in case of the wireless measurements the voltage RMS appeared to be increasing with the increase in baseband frequency. This can be somehow caused by the contribution of the Ag/AgCl electrodes used in the experiment, but if this would be a known characteristic of our system we still would be able to account and calibrate for it. This experiment also involved repeated measurements at every condition to account for the output variations over time. Basically the results showed that despite all the fluctuations the changes in output occurring with the baseband frequency sweep are still greater than the fluctuations present in the system.

The key summarizing points of this experiment are the following:

- wired and wireless interrogation experiments with saline solutions showed system sensitivity to the electrical parameters of the media surrounding the device;
- the output port impedance showed again to be important in defining the highest sensitivity region of the neurostimulator.

V. Wired and wireless characterization of tissue samples

Wired characterization of the beef tissue samples. The results obtained from the experiments involving wired impedance analysis of the beef tissue samples (Fig. 38A) exhibit the trends similar to the discussed earlier. The magnitude is characterized by the slow decay with frequency, as well as highest sensitivity to the induced impedance change at low frequencies. Frequency dependent behavior of phase in this case does not allow differentiation between

different conditions. The nature of the phase changes induced by the actual physiological events (e.g., increase or decrease in perfusion) would actually need to be carefully examined through animal studies and the only thing that can be concluded from these results is that our devices are sensitive to changes in electrical characteristics of the sample under investigation.

Wireless characterization of the beef tissue samples. The results of the same experiment with beef samples only involving wireless detection (Fig. 38B) also exhibit similar trends, but with significant distortions, which could be expected as now we are basically dealing with more than 20 times weaker signals on the order of tens of microvolts and these weak signals are achieved using fairly high acoustic power on the order of 315 mW/cm^2, leaving not so much space for further increase in power before reaching an FDA limit. Basically, what can be seen is that voltage RMS drops with increase in frequency just by about 2 μV, but the change in RMS as result of the introduction of solution are about 3 times greater (20% at 10 Hz). As soon as we can detect such changes it can be absolutely sufficient for monitoring of the physiological events. In case of the phase the detected change is around 1.6% at 7 kHz, but taking into account the expected trend of the phase to have greater change at higher frequencies, which is evident also from our results, the phase change and consequently the usability of the phase information is expected to increase with the increase in bandwidth of the baseband frequencies.

Wireless measurements in cadaveric rat. In case of the cadaveric rat experiments much higher detected voltages could be achieved (Fig. 39) than in case of the experiments with beef samples (Fig. 38B), which might be associated with better acoustic coupling of the transducer with device in cadaveric rat. It must be noted that in case of the experiments with cadaveric rat achieving good coupling was more difficult than in the case of the beef samples stacked in the column because in case of the cadaveric rat there is no visual feedback about the exact position of the device and it was localized by looking at the readings on the lock-in amplifier.

The experiment with cadaveric rat involved two stages. The first stage involved many unsuccessful trials and the results of the one of the most successful trials are shown on Fig. 39A. Basically, the problem encountered in these experiments was associated with much higher reading fluctuations than observed before. The most contributing factors to observed fluctuations

were transducer drift relative to the implant and crosstalk. Despite the fact that in the experiment with beef samples used acoustic power density and consequently driving voltage was much higher, which always is associated with higher crosstalk, in case of the experiments with cadaveric rat, the surface electrodes are placed right next to the transducer. In the experiments with beef samples the electrodes and transducer are separated by 40 mm high stack of beef. As could be expected, the level of crosstalk showed to be very significantly dependent on the separation distance between the detection electrodes and exciting transducer. Consequently, these fluctuations led to many results which look like that is shown on Fig. 39A, where the behavior of the RMS signal looks more similar to the noise.

It can be argued that phase information was successfully detected and it even demonstrates change in phase on the order of 2% with solution injection. The problem with this argument is the fact that in the experiment with RC circuits even in the case when the capacitance was removed from the circuit, the phase still exhibited similar frequency dependent behavior as is observed in the experiments with tissue samples (Fig. 35B, Fig. 38A, Fig. 39A). Basically, this is an additional factor that would need to be accounted and calibrated for before we could start making any conclusions about the tissue based on the phase information. The simple correction by subtraction of the known phase curve characteristic for the specific device can be complicated by the fact that over time after the implantation device can change its characteristics (especially characteristics of the electrodes) and this would consequently lead to the degradation of measurement performance.

Going back to the experiments with cadaveric rats, Fig. 39B illustrates the results of the more successful trial. The main improvement introduced into the experiment leading to the more reasonable results was significant reduction in the number of frequencies used to record the spectra. Basically, this ensured that any significant output fluctuations simply did not occur in the process of the experiment. This led to the spectra with similar trends that were observed in the experiment with beef samples (Fig. 38B). The impedance change caused by the injection of the solution is well detectable, although the RMS change appeared to be much greater at high frequency than at low frequency (64% at 35 kHz versus 11% at 10 Hz; results for high

frequencies are not presented in this work). The deformation of the curve at 20 kHz after solution injection might suggest that some not-impedance related fluctuations occurred even in the process of this experiment, producing distorted results. In case of the phase, detected change at 35 kHz is ~ 4%.

Reference measurements. It must be noted that for all performed experiments with tissue samples it would be very useful to incorporate reference impedance measurements performed in parallel to the device based measurements using the conventional impedance measurement technique (e.g., using the tetrapolar technique with impedance bridge). The problem with such reference measurements is that the stimulation electrodes must not only be placed into the same location as device, but also have the same dimensions and material to produce comparable measurements. The problems of doing such reference measurements simultaneously with device based measurements lies not only in the separability of two signals (this probably could be done by using two different baseband frequencies used to modulate the carrier and drive the reference stimulation electrodes), but the problem would also involve high risk of ground crosstalk (we basically have 4 or even 5 grounds being in contact with the sample simultaneously). It must be admitted that in case of the live animals such reference measurements would be even more difficult to perform, because it would require the powering wires to be tunneled under the skin delivering wired stimulation to the same location where the device is placed.

Summarizing points. Overall, the main points and observations of these experiments can be summarized in the following statements:

- wired measurements showed satisfactory results with the biological samples. This observation allows to conclude that all limitations of the proposed technique identified after transition to wireless detection can be associated with the efficacy of wireless signal transmission and detection, as well as information encoding to begin with (other encoding techniques such as FM modulation would be immune to many factors causing all the variability in the measurements);

- in addition to the previous observation from magnitude measurements, the results of the phase measurements discussed here showed the importance of the accounting for the frequency response characteristics of the device itself;
- device proved to be sensitive to the induced impedance changes in biological samples, but it must be noted that changes induced on the benchtop are not equivalent to the changes occurring *in vivo* with physiological events. Additionally, any evidences of the ability of system to extract the absolute impedance values have not been observed yet, leaving the potential only for the monitoring of impedance relative changes;
- reference impedance measurements are very desirable at least in such types of benchtop experiments, but to make such measurements possible a number of additional technical issues would need to be addressed;
- measurement instabilities became really appreciated during the experiments with biological samples. This leads to several important improvements, which would need to be realized in the ultimate system: spectral data collection for the sample impedance characterization at given specific instance must be performed as fast as possible (recording automatization, reduction in the number of frequencies, excitation using pulsed waves instead of the continuous), measures must be taken against the crosstalk (shielding, grounding, time delays between excitation and recording), reduction of the directional sensitivity must be achieved (all of these factors will be further addressed in greater detail in the section on Live animal experiments and final summary of the study).

VI. Live animal experiments

First trials with highly focused transducer. As it was stated in the Results section, first trials done using big aperture highly focused transducer showed the signal detected from the surface of the skin to be as high as 3.3 mV. According to the experiments done on the benchtop such level signal would be absolutely sufficient to perform the measurements. The problem was in the exceptionally high directional sensitivity of the device. Basically, in order to get the signal on the order of millivolt about an hour long search of the peak coupling window around the rat's

limb was required. After finding the right location, the signal would cease away too rapidly not allowing impedance spectrum recording. This ceasing could not be prevented by simply restraining the rat and fixating the transducer. First trials were concluded to have multiple problems in the setup: too highly focused transducer with too high mass and dimensions; high crosstalk level. In this case the highly focused commercial transducer had good shielding, but due to the high drive (~60 V) the resulting level of the crosstalk was still too high, preventing differentiation between noise and weak outputs produced by weak acoustical coupling.

Introduced system improvements. To solve just discussed problems it was decided to use the unfocused transducer. Commercial unfocused transducers available in the lab were shown not capable of producing sufficiently high output from the devices, therefore it was decided to build the transducer using PZT-5H characterized by relatively good quality factor and therefore suitability for being used as the transmitter. First set of transducers were built simply by isolating the piezoelectric material with epoxy. This design was tested on the cadaveric rat and demonstrated unacceptably high level of crosstalk on the order of multiple millivolts. This crosstalk is mainly caused by the capacitive coupling of transducer with the rat and consequent signal leakage to the surface electrodes placed in vicinity of the transducer. It was determined that the nature of crosstalk is capacitive by placing the transducer at different parts of the rat. As soon as transducer touches the rat, the reading on the lock-in amplifier starts to increase and the closer transducer is located to the electrodes, the greater is level of interference. Basically, we have two conductors (nickel coated piezoelectric material and cadaveric rat) separated by the layer of epoxy forming a capacitor. It was attempted to use a higher column of acoustic coupling gel, which is supposed to have relatively low conductivity, but as the drive goes up the crosstalk becomes too high. The level of severity of the crosstalk problem follows from the fact that we are applying as high as 60 V driving voltages to the ultrasound exciter and are trying to measure mV or even sub-mV level signals using the electrodes placed about 10 mm away from the exciter. Basically, the ratio of the driving signal and measured signal occurring in the same location is greater than 10^4.

Consequently, further improvements into transducer design were introduced to reduce the level of crosstalk as much as possible. The design of the final version of transducers is shown on Fig. 9. The main introduced improvements include shielding by the grounded copper tubing and the mesh, as well as incorporation of the spacer made out of the steatite. Additionally, instead of the simple measurements done using a pair of surface electrodes, a differential measurement system was employed (shown on Fig. 19A).

Trials with improved setup. Despite these improvements the level of noise in live rat was observed to be as high as 100 μV, whereas on average it was in the range of 20-30 μV, which depended on the exciting transducer relative position to the detecting electrodes. While moving the transducer around the implantation sight any distinct peaks could not be observed. It was also attempted to look into signal at the baseband harmonic, which with differential measurements produced 0 μV crosstalk, but again any output from the device could not be detected. This can be caused by the fact that device was producing voltages below diode's threshold, although during benchtop testing bridge rectifiers demonstrated very good rectification performance.

Next, in order to differentiate between the crosstalk and actual signal from the device at the baseband frequency, it was decided to introduce the carrier frequency sweeping. The level of crosstalk is not supposed to change by changing the carrier frequency (it was confirmed by benchtop testing), but the output signal from the device is highly dependent on the carrier frequency (as it was mentioned earlier, this is associated with the resonance frequencies of exciting and receiving transducers). The highest reading change that could be observed from live rat with frequency sweeping was on the order of 10% (basically 90% of signal was just the interference), but even these 10% was difficult to associate with actual output of the device because these changes can also be associated with micromotion of the exciter or receiver. Therefore, due to not being able to establish the baseline any impedance measurements could not be conducted.

Burst excitation of the implanted device. Finally, measurements were done using the burst excitation (Fig. 19B) to identify if the experienced problems during the impedance measurements were caused by the device itself. The implant has been in the rat for 5 months and

can be expected not to function properly anymore. As it is shown on Fig. 39, it was possible to detect the signal from burst excited implant. Six different transducers were tried again and only two of them allowed obtaining the signals shown on Fig. 39 with maximal peak-to-peak magnitude of 2 mV. Based on the previous experience the signal of such magnitude would be absolutely sufficient for impedance measurements. Additionally, based on the reading from the oscilloscope this signal was fairly stable. Still, it could be identified that the coupling window of the device was very narrow (on the order of 10 degrees).

Ultimate planned proof-of-feasibility experiment. The ultimate planned experiment, which would demonstrate if proposed system really has a potential for becoming a clinical tool, is illustrated on Fig. 42. Fig. 42 shows the ultimate experiment involving a number of introduced improvements, which, based on the observations from the experiments, would make the performance of the system more similar to what is expected from the ultimate clinical instrument.

The idea behind envisioned rat experiment shown on Fig. 42 relies on the phenomenon called reactive hyperaemia, which involves the significant increase in the tissue perfusion as the consequence of having it exposed to the ischemia. The experiment would involve occlusion of the femoral artery supplying rat's lower limb. This would produce the decrease in blood flow with consequent overshooting after the pressure is released. The blood flow was planned to be measured using the laser Doppler flowmeter (as in the previous work on blood flow modulation [2]), whereas the implant would be expected to show the opposite trend in impedance.

As an alternative way of blood flow modulation the irritation of tissue using the capsaicin was considered. This relates to the additional application considered for the investigated technique, which involves monitoring of the blood supply and health of the nerves rather than muscles or other non-nervous tissue. This would require precise device placement right along the nerve or with sufficient size reduction even inside the nerve. Such measurements would be useful in case of neuropathy, for instance, caused by obesity or drugs used for pain relief (e.g., capsaicin) [58].

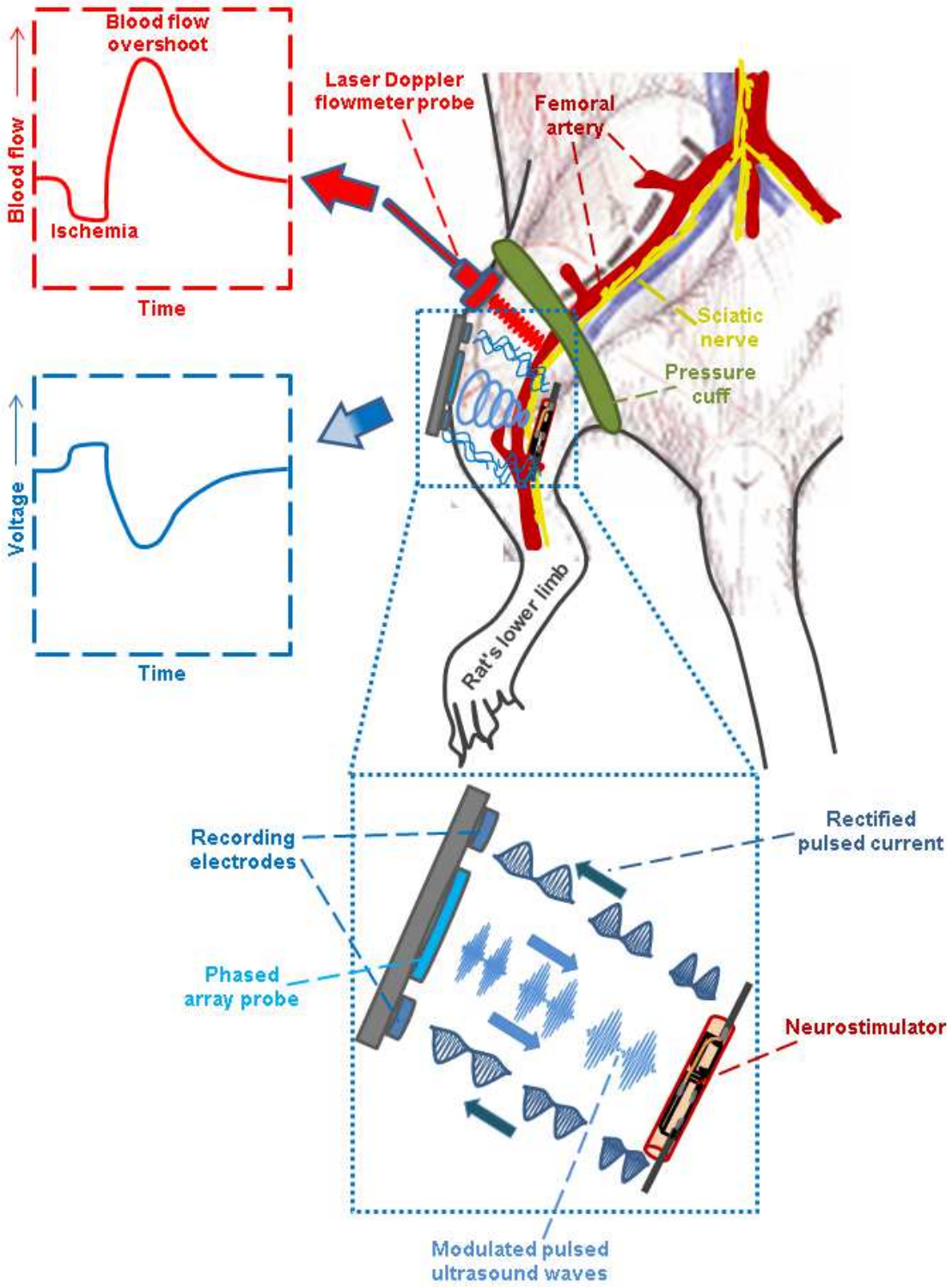

Fig. 42. Schematic of the ultimate live rat experiment for testing the sensitivity of microdevices to the changes in blood flow.

Main identified problems. During the animal experiments the main identified problems are considered to be the directional sensitivity and crosstalk. The directional sensitivity though is considered to be more severe problem because it fundamentally degrades our ability to perform any measurements. Even if we could manage to record impedance data at several frequencies by stabilizing the output for 10s of seconds, we still would not be able to perform the envisioned experiment shown on Fig. 42 because it involves too many simultaneous interactions with the rat, all of which can serve as perturbations to the acoustic coupling. In the parallel project, smaller dimension devices showed to be less directionally sensitive and this something that must be systematically evaluated to identify if simple size reduction can reduce the directional sensitivity down to the level where it would be well tolerated by the patients and clinicians, making investigated system clinically applicable and attractive. Ultimately, elimination of directional sensitivity and ability to maintain stable acoustic coupling would make crosstalk problem less severe simply because the output signal from the device would become sufficiently greater than the crosstalk.

Additional approaches for fighting directional sensitivity problem would involve:

- injection of the multiple randomly oriented micrometer size devices into the same area so that the supplied excitation pulses would always activate at least a fraction of the implants;
- driving the excitation transducer with a complex waveform, for instance, white noise (as it was noted from the experiments, the carrier frequency providing highest output from the device is dependent on the position and orientation of the device in acoustic beam. Hence, it could be expected that by sending in the more complex waveform you would get the output at bigger number of positions, although the overall peak output in such case would be decreased);
- utilization of the multi-element array exciting transducer, potentially involving selection of the combination of the elements providing highest output from the device at given instance of time and space (the strength of the power generated by the implant would be estimated using the surface detected potentials, although alternatively the acoustic echo

analysis could also potentially provide similar feedback, but echo detection and analysis would require additional system sophistication and increase in the cost).

Besides directional sensitivity, the problem of the data recording automatization plays an important role. In the clinical situation we would like to have all the data collected as fast possible before any perturbations can be introduced (e.g., tissue or transducer motion). Ideally even within a second data could be collected at multiple frequencies by using pulse excitation instead of the continuous waveform. Each pulse can consist of a single period of the baseband signal (Fig. 42), which would also eliminate the crosstalk problem by introducing time delay between the excitation and recording. Alternatively, the data extraction process could potentially be made even faster by using complex baseband waveform excitation, involving sample interrogation simultaneously at multiple baseband frequencies. Moreover, the data in such case could be analyzed using the computerized system, involving the signal analysis similar to what is done using the lock-in amplifier.

Taking into account all the problems discussed, the initially planned experiment involving microdevice actuation by single element transducer using continuous waveform drive seems to be almost unfeasible, mainly because it involves multiple simultaneous interactions with the rat: placement of three recording electrodes, application of the ultrasound and laser probes, and application of the cuff for the blockage of blood flow. Basically, performance of all of these manipulations without even slightest movements of the animal is almost impossible, but even if the coupling of the exciter and receiver could be maintained stable in such experiment, the system would still remain clinically inapplicable until all discussed problems would be addressed.

Summary of the animal experiments. Overall, animal experiments allowed identification of many limitations of the proposed system, which would need to be dealt with before final proof of feasibility of proposed system for wireless impedance measurements. Findings of the animal experiments can be summarized in the following key points:

- the implant was proven to maintain functionality over as long time period as 5 months after the implantation;

- in case of the continuous waveform drive, the carrier frequency sweeping has shown to allow differentiation between noise and device output signal;
- the utilization of the highly focused ultrasound transducer demonstrated the high efficacy of power delivery to the implant, providing easily detectable signal from the skin surface, but the directional sensitivity with focused transducer and PZT receiver of dimensions on the order of 1 mm was observed to be unacceptably high (sensitivity window narrows down to a few degrees);
- the issue of directional sensitivity of the ultrasonically powered microdevices must be addressed in order to make these devices potentially clinically applicable and to make possible the proof-of-feasibility of the investigated wireless impedance measurement technique;
- the data collection must be automatized in order to reduce the effects of the transient environmental factors (e.g., motion induced changes in transducer or electrode coupling);
- high drive on the transducer exceeding the detected signal by about 10^4 times results in high crosstalk level, characteristic for the continuous waveform driving;
- implant excitation must be optimized to allow faster data collection. The transition from continuous excitation to pulsed excitation should reduce the time required for spectral recording, as well as elimination of the noise, allowing clear separation of the interference and the signal of interest. Alternatively, it would be preferable to perform the transition from amplitude encoding of the impedance information to other forms of encoding, not so dependent on relative positioning and coupling.

CHAPTER 6

SUMMARY AND CONSIDERATIONS FOR FUTURE WORK

Proposed and investigated technique aims at wireless tissue electrical impedance measurements using ultrasonically powered microdevices. This work serves as the first step towards proving feasibility and clinical applicability of this technique. Benchtop testing and preliminary animal experiments allowed identification of the key problems, which must be addressed before proposed technique can be concluded as feasible for wireless tissue impedance monitoring based clinical applications.

A number of questions have been identified in the process of this work, requiring further investigation. For efficient neurostimulation and impedance measurements, full system optimization would be necessary:

- rectification optimization (requires systematic analysis of the different types of rectifiers and their connection configurations). As an example of attractive rectification approach can be considered the rectification produced by the electrodes themselves (by using appropriately selected materials);
- external exciter optimization (consideration of the transducer physical parameters, including the resonance frequency, bandwidth, focusing, excitation mode, number of the elements in array, acoustic impedance matching). The attractiveness of the pulse excitation for impedance measurements has been highlighted in this work, allowing separation of the signal of interest from the crosstalk, as well as higher power delivery to the implant. Array transducer would have the advantage not only in its ability to reduce the directional sensitivity of the implants, but through beam steering it also has a potential for multi-channel functionality. Furthermore, based on the approach discussed in [8], beam steering would allow much more efficient localization of the implant. Knowledge of the geometry of system components (implant relative position to the surface electrodes) and tissue impedance, could allow more precise estimation of the currents produced by the implant;

- implantable receiver optimization (receiver dimensions, loading, type of piezoelectric material);
- data recording, post-processing and analysis optimization (requires fast data collection and automated analysis). Data analysis would also need to deal with the interference produced by the electromyographic activity present in the baseband frequency range. The potential problems associated with muscular activity make the radio receiving approach more attractive, as it would be insensitive to these types of interference because the signals used for data extraction are in the carrier frequency region;
- stimulation optimization (selection of the right driving waveform parameters, charge balancing, electrode material and dimensions);
- detection optimization (deeper analysis of the surface electrodes based detection versus wireless detection using the antenna and radio receiver).

The safety concerns associated with ultrasound and application of the electrical currents to the tissue have not been discussed in great details throughout this work, but these questions would be of the key importance if investigated technique would ever reach the FDA approval process. One of the briefly discussed questions is related to the control of the current applied to tissue. Simulations have shown the natural ability of the Schottky diode connected in series to piezoelectric element to provide limitation of the stimulatory currents. This is achieved by reduced rectification efficiency with increase in applied voltages. If the same device would be used both for neurostimulation and impedance measurements, an important issue would be an efficient control of the impedance measuring currents, which due to the rectification are capable to cause nerve excitation. The only factor that would prevent stimulation by impedance measuring currents is restricted magnitude of these interrogative currents, which must be maintained below neural stimulation threshold.

One of the critical questions relates to the biological processes occurring after the implantation. The key process would be the scar tissue formation as result of the introduction of the foreign body into tissue. It is not known yet if formation of the scar tissue encapsulation around the implant would make it insensitive to the physiological changes occurring outside the

region of scar tissue. Previously explanted devices (after the year since the implantation) of the type and scale used in the present work have not shown evidences of the formation of extensive masses of scar tissue. Additionally, as it was discussed in [10], the tissue response is highly dependent on dimensions of the implant and as the dimensions become smaller, tissue response decreases proportionally. Moreover, this issue could also be addressed by using special coatings, which can reduce tissue response and potentially lead to the reduced scar tissue formation (e.g., PEG coating).

Another potential long-term issue can be related to the impedance changes of the implant's electrodes. It is difficult to estimate the course of such impedance changes and at this point it does not seem possible to correct for such changes. Therefore, as possible solutions different electrode materials and dimensions can be explored to mitigate this issue.

Alternative impedance measurement techniques would need to be considered if the problems associated with technique investigated in this work cannot be mitigated down to the acceptable levels. For instance, as an alternative wireless tissue bioimpedance measurement technique can be considered the approach based on the utilization of epidermal high frequency currents as discussed in [32]. In its basic form this technique can involve implantation of the microrectifiers serving for signal demodulation, current injection using surface electrodes, and consequent detection of the rectified currents using the same electrodes. The key potential benefits of such approach would include elimination of the orientation and position sensitivity problems associated with acoustic powering. This approach would also allow to get rid of the requirement for physical coupling, as well as would simplify device structure by eliminating need for piezoelectric material. This approach might be overlooked as the more complicated and more invasive version of the conventional impedance measurement technique, but the key benefit would involve the ability to perform more chronic and more localized impedance measurements at specific location of interest in the tissue.

In addition to exploration of the alternative wireless impedance measurement approaches, it is important to think about complementary potential applications for investigated technique, besides the discussed peripheral vascular disease. The most attractive application

seems to be the monitoring of the neural activity, discussed in greater details in [56-57]. Extensive work has been done on neural activity monitoring using the electrical impedance tomography (EIT). At this point, this application still is considered to be feasible, and it offers a potential for reaching the “holy grail” of monitoring neural activity non-invasively with a time and spatial resolution of about 1 ms and 1 mm respectively. EIT based neural activity monitoring technique still involves many challenges and these challenges would become only magnified if we try to apply presently investigated wireless impedance measurement technique for neural activity monitoring. Some of the problems would be associated with the fact that this application is considered to require interrogative currents of the sub-threshold magnitude on the order of 1-10 μA. In our experiments generated currents have not been exactly estimated, but from previous work [2] the maximal currents generated by our devices were estimated to be on the order of 1 mA. Therefore, currents used in all the experiments in this work must be much greater than 10 μA. Still, even with higher currents wireless signal detection using surface electrodes proved to be challenging. Additionally, so far reported resistance changes with action potentials are around 1% or even lower, and some of the researchers used signal averaging over as long periods as 1 minute to perform such measurements. Both of these factors emphasize the severity of the baseline variability problem widely discussed in this work. Even with conventional EIT measurements the encountered baseline variability can be on the order of 1-2%, resulting in SNR of 2-3 [57]. These issues present even in the sophisticated multi-electrode EIT measurement systems are indicative of how challenging wireless extraction of neural activity related impedance information can be.

Ultimately, the feasibility study of the single device allowing triple functionality (neurostimulation, impedance measurements, neural recording) would need to be done. The idea of the triple functionality of the single wireless microimplant is very attractive due to the high benefits for the patients. These benefits can include reduced injury and pain, as well as absence of the tethering wires allowing not only the more unconstrained patient motion, but also leading to the better stability and quality of neurostimulation and recording. Present work suggested two potential approaches for wireless neural recording. One approach relies on structural device

modification, involving rectifier replacement with varicap type rectifier. The second approach relies on the measurements of transient impedance changes associated with neural events.

At the present stage ultrasonically powered implantable microdevices clearly demonstrate the potential of being applicable for wireless bioimpedance measurements. These devices have shown to be sensitive to impedance changes of the media surrounding them. Still, final conclusion about the feasibility and clinical applicability of investigated technique would depend on its ability to extract physiologically relevant information in reliable, safe and convenient way. Present work provides the insights into questions, which would need to be addressed in the future studies, and can be considered as a first step in development of the new clinical tool for wireless bioimpedance monitoring.

REFERENCES

[1] Phillips, W.B.; Towe, B.C.; Larson, P.J. (2003). "An ultrasonically-driven piezoelectric neural stimulator," *Engineering in Medicine and Biology Society, 2003. Proceedings of the 25th Annual International Conference of the IEEE*, vol.2, no., pp.1983,1986 Vol.2.

[2] Towe, B.C., Graber, T., Gulick, D., Herman, R. (2013). "Wireless microstimulators for treatment of peripheral vascular disease". In *Neural Engineering (NER), 2013 6th International IEEE/EMBS Conference on*, pages 1485–1488.

[3] Towe, B.C., Larson, P.J., Gulick, D. (2012). "A Microwave Powered Injectable Neurostimulator", 34th Annual International Conference of the IEEE EMBS, San Diego, Ca, USA.

[4] Larson, P.J., Towe, B.C. (2011). "Miniature Ultrasonically Powered Wireless Nerve Cuff Stimulator", 5th International IEEE Conference on Neural Engineering 2011, pp. 265-268.

[5] Abbaspour-Tamijani, A, Farooqui, Muhammad F., Towe, B.C., Junseok Chae (2008). "A miniature fully-passive microwave back-scattering device for short-range telemetry of neural potentials,"*Engineering in Medicine and Biology Society, 2008. EMBS 2008. 30th Annual International Conference of the IEEE* , vol., no., pp.129,132.

[6] Towe, B.C., Larson, P.J., Gulick, D.W. (2009). "Wireless ultrasound-powered biotelemetry for implants," *Engineering in Medicine and Biology Society, 2009. EMBC 2009. Annual International Conference of the IEEE* , vol., no., pp.5421,5424.

[7] Towe, B.C. (2007). "Passive Backscatter Biotelemetry for Neural Interfacing," *Neural Engineering, 2007. CNE '07. 3rd International IEEE/EMBS Conference on* , vol., no., pp.144,147.

[8] Gulick, D.W., Towe, B.C. (2012). "Method of locating ultrasound-powered nerve stimulators," *Engineering in Medicine and Biology Society (EMBC), 2012 Annual International Conference of the IEEE* , vol., no., pp.887,890.

[9] Towe, B.C. (2005). "Piezoelectric contrast materials for ultrasound imaging," *Ultrasonics, Ferroelectrics, and Frequency Control, IEEE Transactions on* , vol.52, no.9, pp.1483,1488.

[10] Seo D., Carmena J.M., Rabaey J.M., Alon E., Maharbiz M.M. (2013) "Neural Dust: An Ultrasonic, Low Power Solution for Chronic Brain-Machine Interfaces,"arXiv: 1307.2196.

[11] Dongjin Seo, Jose M. Carmena, Jan M. Rabaey, Michel M. Maharbiz, and Elad Alon (2014). “Model validation of untethered, ultrasonic neural dust motes for cortical recording,” *Journal of Neuroscience Methods*.

[12] Bertrand A., Seo D., Maksimovic F., Carmena J. M., Maharbiz M.M., Alon E., Rabaey J.M. (2014). "Beamforming Approaches for Untethered, Ultrasonic Neural Dust Motes for Cortical Recording: a Simulation Study". International IEEE/EMBS Conference.

[13] Denisov A. and Yeatman E. (2010). "Ultrasonic vs. inductive power delivery for miniature biomedical implants," in *Body Sensor Networks (BSN), 2010 International Conference on,* pp. 84-89.

[14] P.N.T. *Wells. PNT, Biomedical Ultrasonics, Academic Press.*

[15] Ozeri S. and Shmilovitz D. (2010). "Ultrasonic transcutaneous energy transfer for powering implants," *Ultrasonics,* vol. 50, pp. 556-566.

[16] Borna, A.; Najafi, K. (2011). "A low-power, low-voltage, user-programmable, wireless interface for reliable neural recording", *Biomedical Circuits and Systems Conference (BioCAS), 2011 IEEE*, vol., no., pp.77-81.

[17] Biederman, W.; Yeager, D.J.; Narevsky, N.; Koralek, A.C.; Carmena, J.M.; Alon, E.; Rabaey, J.M. (2013). "A Fully-Integrated, Miniaturized (0.125 mm²) 10.5 μW Wireless Neural Sensor," *Solid-State Circuits, IEEE Journal of* , vol.48, no.4, pp.960,970.

[18] Rabaey, J.M.; Mark, M.; Chen, D.; Sutardja, C.; Chongxuan Tang; Gowda, S.; Wagner, M.; Werthimer, D. (2011). "Powering and communicating with mm-size implants," *Design, Automation & Test in Europe Conference & Exhibition (DATE), 2011*, vol., no., pp.1,6.

[19] Hannan M.A., Mutashar S., Samad S.A., Hussain A. (2014). "Energy harvesting for the implantable biomedical devices: issues and challenges," *BioMedical Engineering OnLine*, 13:79.

[20] Sahin M., Pikov V. (2011). "Wireless microstimulators for neural prosthetics". *Crit. Rev. Biomed. Eng.* 39 63–77 10.1615/CritRevBiomedEng.v39.i1.50.

[21] David S. Freedman, Mesut Sahin, Bruce C. Towe (2014). "Wireless Microstimulators," *Encyclopedia of Computational Neuroscience (Online), Springer*, 1:11.

[22] John S. Ho, Alexander J. Yeh, Evgenios Neofytou, Sanghoek Kim, Yuji Tanabe, Bhagat Patlolla, Ramin E. Beygui, and Ada S. Y. Poon (2014). "Wireless power transfer to deep-tissue microimplants," PNAS 2014 111 (22) 7974-7979.

[23] Ho, J.S., Sanghoek Kim, Poon, AS.Y. (2013). "Midfield Wireless Powering for Implantable Systems," *Proceedings of the IEEE*, vol.101, no.6, pp.1369,1378.

[24] Yakovlev A, Kim S, Poon A. (2012). "Implantable biomedical devices: wireless powering and communication". IEEE Commun Mag 2012;50(4):152-9.

[25] Poon, AS.Y., O'Driscoll, S., Meng, T.H. (2010). "Optimal Frequency for Wireless Power Transmission Into Dispersive Tissue," *Antennas and Propagation, IEEE Transactions on* , vol.58, no.5, pp.1739,1750.

[26] Sodagar A.M., Amiri P. (2009). "Capacitive coupling for power and data telemetry to implantable biomedical microsystems". *IEEE EMBS 2009 Conf* 411-4.

[27] Hao Jiang, Jun Min Zhang, Shy Shenq Liou, Fechter, R., Hirose, S., Harrison, M., Roy, S. (2010). "A high-power versatile wireless power transfer for biomedical implants," *Engineering in Medicine and Biology Society (EMBC), 2010 Annual International Conference of the IEEE* , vol., no., pp.6437,6440.

[28] Talary, M.S., Dewarrat, F., Huber, D., Falco-Jonasson, L., Caduff A. (2007). "Non-Invasive Impedance based Continuous Glucose Monitoring System". ICEBI 2007, pp.636-639.

[29] Abdo A., Sahin M., Freedman D.S., Cevik E., Spuhler P.S., Unlu M.S. (2011b). "Floating light-activated microelectrical stimulators tested in the rat spinal cord". J Neural Eng 8:056012.

[30] Abdo A., Ersen A., Sahin M. (2013). "Near-infrared light penetration profile in the rodent brain". J Biomed Opt 18:075001.

[31] G. E. Loeb, R. A. Peck, W. H. Moore and K. Hood (2001). "BION™ system for distr. neural prosthetics," *Med. Eng. Phys.,* vol. 23, pp. 9-18, 1.

[32] Becerra-Fajardo L., Ivorra A. (2014). "Towards Addressable Wireless Microstimulators Based on Electronic Rectification of Epidermically Applied Currents". International IEEE/EMBS Conference.

[33] Kim, H.-H., Mano, N., Zhang, Y., Heller, A. (2003). "A miniature membrane-less biofuel cell operating under physiological conditions at 0.5 V", J. Electrochem. Soc. 150 (2) A209–A213.

[34] González, J.-L., Rubio, A., Moll, F. (2001). "A prospect on the use of piezoelectric effect to supply power to wearable electronic devices". Fourth Int. Conf. Mater. Eng. Resources, ICMR, pp. 202–206.

[35] Clark GM. Cochlear implants: fundamentals and applications. New York: Springer-Verlag; 2003.

[36] US Department of Health and Human Services, Food and Drug Administration, Center for Devices and Radiological Health. Information for Manufacturers Seeking Marketing Clearance of Diagnostic Ultrasound Systems and Transducers. Washington, DC: US Department of Health and Human Services, Food and Drug Administration, Center for Devices and Radiological Health; 2008.

[37] Nelson, T.R., Fowlkes, J.B., Abramowicz, J.S., and Church, C.C. (2009). "Ultrasound biosafety considerations for the practicing sonographer and sinologist". J Ultrasound Med 28, 139–150.

[38] Jaksukam, K., Umchid, S. (2011). "Development of ultrasonic power measurement standards in Thailand," *Electronic Measurement & Instruments (ICEMI), 2011 10th International Conference on*, vol.3, no., pp.1,5, 16-19.

[39] Huber, Stanford J., Vaglienti, Richard M., Huber, Joan S. (2000). *Spinal Cord Stimulation in Severe, Inoperable Peripheral Vascular Disease*, International Neuromodulation Society Volume 3, Number 3, 131-143.

[40] Park, Rae Joon et al. (2011). *The Effect of Microcurrent Electrical Stimulation on the Foot Blood Circulation and Pain of Diabetic Neuropathy*, Journal of Physical Therapy Science 23: 515-518.

[41] Khalil, Zeinab, Merhi, Merhi (2000). *Effects of Aging on Neurogenic Vasodilator Responses Evoked by Transcutaneous Electrical Nerve Stimulation: Relevance to Wound Healing*, Journal of Gerontology, Volume 55A, Number 6: 257-263.

[42] Seoane, F., Lindecrantz, K., Olsson, T., Kjellmer, I., Flisberg, A., Bagenholm, R. (2004). "Brain electrical impedance at various frequencies: the effect of hypoxia", *Engineering in Medicine and Biology Society, 2004. IEMBS '04. 26th Annual International Conference of the IEEE*, vol.1, no., pp.2322-2325.

[43] Seoane, F., Lindecrantz, K., Olsson, T., Kjellmer, I., Flisberg, A., Bågenholm, R. (2005). "Spectroscopy study of the dynamics of the transencephalic electrical impedance in the perinatal brain during hypoxia". Physiol. Meas. 2005;26:849–863.

[44] Atefi, S.R., Seoane, F., Thorlin, T., Lindecrantz, K. (2013). "Stroke Damage Detection Using Classification Trees on Electrical Bioimpedance Cerebral Spectroscopy Measurements," *Sensors*. 2013; 13(8):10074-10086.

[45] Schwartzman, D., Chang, I., Michele, J.J., Mirotznik, M.S., Foster, K.R. (1999). "Electrical impedance properties of normal and chronically infarcted left ventricular myocardium", Journal of Interventional Cardiac Electrophysiology, 3, 231-224.

[46] Yufera, A, Rueda, A, Munoz, J.M., Doldan, R., Leger, G., Rodriguez-Villegas, E.O. (2005). "A tissue impedance measurement chip for myocardial ischemia detection," *Circuits and Systems I: Regular Papers, IEEE Transactions on*, vol.52, no.12, pp.2620,2628.

[47] Mellert, F., Winkler, K., Schneider, C., Dudykevych, T., Welz, A., Osypka, M., Gersing, E., Preusse, C.J. (2011). "Detection of (Reversible) Myocardial Ischemic Injury by Means of Electrical Bioimpedance", *Biomedical Engineering, IEEE Transactions on*, vol.58, no.6, pp.1511,1518.

[48] Khalil, S.F., Mohktar, M.S., Ibrahim, F. (2014). "The Theory and Fundamentals of Bioimpedance Analysis in Clinical Status Monitoring and Diagnosis of Diseases", *Sensors*.; 14(6):10895-10928.

[49] Aberg, P., Nicander, I., Hansson, J., Geladi, P., Holmgren, U., Ollmar, S. (2004). "Skin cancer identification using multifrequency electrical impedance-a potential screening tool," *Biomedical Engineering, IEEE Transactions on*, vol.51, no.12, pp.2097,2102, Dec. 2004.

[50] Kun, Stevan, Ristic, B., Peura, R.A., Dunn, R.M. (2003). "Algorithm for tissue ischemia estimation based on electrical impedance spectroscopy", *Biomedical Engineering, IEEE Transactions*, vol.50, no.12, pp. 1352-1359.

[51] Songer, J.E. (2001). “Tissue ischemia monitoring using impedance spectroscopy: Clinical evaluation,” M.S. thesis, Worcester Polytechnic Inst., Worcester, MA.

[52] Martinsen O.G. and Grimnes S. (2008). Bioimpedance and Bioelectricity Basics, Second Edition. Academic Press, 2nd edition.

[53] Sauter, A.R., Dodgson, M.S., Kalvøy, H., Grimnes, S., Stubhaug, A., and Klaastad, Ø. (2009). “Current Threshold for Nerve Stimulation Depends on Electrical Impedance of the Tissue: A Study of Ultrasound-Guided Electrical Nerve Stimulation of the Median Nerve,” *Anesth. Analg*., vol. 108, no. 4.

[54] Kalvøy, H., Frich, L., Grimnes, S., Martinsen, Ø. G., Hol, P. K. and Stubbhaug, A. (2009). “Impedance based tissue discrimination for needle guidance”. *Physiol. Meas*.

[55] Suyoung Bang, Changik Lee, Jinwoo Park, Min-Chang Cho, Young-Gyu Yoon, SeongHwan Cho. (2009). "A pulse transit time measurement method based on electrocardiography and bioimpedance," *Biomedical Circuits and Systems Conference, 2009. BioCAS 2009. IEEE*, vol., no., pp.153,156.

[56] Gilad O., Ghosh A., Oh D., Holder D.S. (2009). “A method for recording resistance changes non-invasively during neuronal depolarization with a view to imaging brain activity with electrical impedance tomography,” J Neurosci Methods 180:87–96.

[57] Holder D.S. (1989). “Impedance changes during evoked nervous activity in human subjects: implications for the application of applied potential tomography (APT) to imaging neuronal discharge,” Clin Phys Physiol Meas. 10:267–74.

[58] Herman R.M., Brower J.B., Stoddard D.G., Casano A.R., Targovnik J.H., Herman J.H., Tearse P. (2007). “Prevalence of somatic small fiber neuropathy in obesity,” International Journal of Obesity. 31:226–235.

[59] Celinskis, D., Towe, B.C. (2014). "Wireless Impedance Measurements for Monitoring Peripheral Vascular Disease," *Engineering in Medicine and Biology Society (EMBC), 2014 Annual International Conference of the IEEE*.

BIOGRAPHICAL SKETCH

Dmitrijs Celinskis graduated with a BS in Medical Physics and Physical Technologies in Medicine from Riga Technical University. During his undergraduate studies through European exchange program he studied at Norwegian University of Science and Technology. In his final year of undergraduate education he participated in the European Union project on Development of the Telemedicine Screening Complex and project on Development of the Pauls Stradins Clinical University Hospital.

After graduation Dmitrijs worked in healthcare, industry and research with consequent award of Fulbright scholarship. In the framework of Fulbright program, he has undertaken MS studies at Arizona State University. During his studies at ASU, the main focus of his work was on wirelessly powered microdevices with potential for neural stimulation, recording and tissue electrical impedance monitoring. Along the lines of his interests in neuroscience and neural engineering, he also participated in the studies on ultrasound induced neuromodulation for the treatment of diabetes, neuromuscular control of hand movements and neural mechanisms contributing to falling in stroke survivors.